INNOVATIVE DESIGNS FOR LOW PROFILE ANTENNA SYSTEMS FOR MIMO 5G/V2X AND GNSS COMMUNICATIONS

by

AHMAD MAZIN YACOUB

A dissertation submitted in partial fulfillment of the
requirements for the degree of

DOCTOR OF PHILOSOPHY IN ELECTRICAL AND COMPUTER ENGINEERING

2022

Oakland University
Rochester, Michigan

Doctoral Advisory Committee:

Daniel N. Aloi, Ph.D., Chair
Aycil Cesmelioglu, Ph.D.
Jia Li, Ph.D.
Guangzhi Qu, Ph.D.

Many thanks are due to
ALLAH (God),

To my lovely wife and son
Naglaa *and* Sanad

To my brother and sisters,
Dr. Lina Yacoub, Dr. Rawan Yacoub, Razan Yacoub, Raghad Yacoub
and Mohammad Yacoub

and my parents
Dr. Mazin Yacoub
and Laila Abdullah

ACKNOWLEDGMENTS

I would especially like to thank my advisor, Professor Daniel N. Aloi for supporting and guiding me through my research work, and for giving me the opportunity to work and research in my field of interest.

I would also like to express my thanks to my doctoral advisor committee, Dr. Aycil Cesmelioglu, Dr. Jia Li, and Dr. Guangzhi Qu for their efforts, willingness to be part of my committee, and their guidance and feedback in reviewing my research that helped improving my work.

My deepest gratitude goes to my wife and my son who supported me through my journey and helped me accomplish my goals.

Many thanks to my parents, brother, and sisters who encouraged me to pursue my research work and helped me stay focused throughout my studies.

Ahmad Mazin Yacoub

PREFACE

The drive and motivation of this research is to participate in developing smart wireless automotive technologies that will help improve the driving experience and make it safer. Automobile accidents and congested traffic can be fatal and cause high delays that could waste drivers' time. Recently, the most upcoming standards that are implemented for vehicle wireless systems are 5G and V2X communications (via DSRC or C-V2X) protocols. These technologies will significantly improve driving experience and have a vital role in developing autonomous vehicles as well as increase traffic safety. In this work, I have developed antenna wireless solutions with unique, compact, and easily manufactured designs to be implemented for 5G and V2X technologies that will improve the wireless performance of these technologies on vehicles.

Size limitation is one of the many challenges addressed for 5G and V2X that will restrict the volume occupied by the antennas which would require innovative designs to compensate for the size reduction, especially at lower frequency bands. In addition, many wireless applications co-exist within the same housing that could cause mutual coupling between the elements and reduce the electrical performance of each application. Therefore, advanced, and creative designs are needed to overcome these challenges, especially with the rapid growth of wireless technologies in bandwidth and radiation performance.

Finally, I would like to thank my family and friends for their continuous blessing and support throughout my journey. In addition, many thanks to my advisor Professor

Daniel Aloi and my doctoral committee for their mentorship and valuable help on my work. My deepest gratitude to all of you for your complete support.

ABSTRACT

LOW PROFILE ANTENNA SYSTEMS FOR MIMO 5G/V2X AND GNSS APPLICATIONS

by

AHMAD MAZIN YACOUB

Adviser: Daniel N. Aloi, Ph.D.

The research in this dissertation shows the analysis and development of designing antenna elements and MIMO antenna systems that can be implemented in the automotive industry and have a significant role in an autonomous driving system. The antennas presented in this research cover 5G-sub-6GHz bands which have much more extended bandwidth compared to previous LTE network, in addition to covering Vehicle-to-Everything (V2X) frequency band. The design work presented in this research followed a scientific method that included simulating the antenna element using 3-D electromagnetic solver (HFSS) on 1-meter ground plane. The antenna was then fabricated using properly cut metal sheet, measured on 1-meter rolled-edge ground plane, and measured on a vehicle's roof inside an anechoic chamber for practical measurements. The design guidelines and measurements are discussed in detail throughout this work.

The first two sections of this research begin with presenting a novel wideband low-profile Planar Inverted F-Antenna (PIFA) that covers a wide frequency range (617MHz-6000MHz) that includes cellular 5G bands and V2X band while having reasonable rejection for Global Navigation Satellite System (GNSS) frequency bands.

Then, Multiple MIMO configurations based on the novel PIFA design are studied by using spatial diversity, rotational diversity, and orthogonal diversity to increase the total throughput and data rate of the system. The performance of each element in the MIMO system is analyzed and discussed to evaluate the functionality of the system.

The third section of this work introduces a 2x2 MIMO antenna system for vehicular application in the sub-6GHz 5G systems that operates in the middle and high frequency bands from 1.71GHz to 5GHz. The design consists of two novel raised printed monopoles on Flame Retardant 4 (FR4) dielectric material with Partial Ground Plane (PGP) structure to improve bandwidth impedance and achieve higher isolation across the operating frequency range. The design is an excellent candidate to be implemented in a shark-fin housing due to its low-profile characteristics and good electrical performance.

Eventually, in the fourth section of this work, a fully integrated low-profile antenna systems for MIMO 5G and global navigation satellite system (GNSS) for L1/L5 frequency bands is presented. The designs can be used on the vehicle's roof inside a low-profile housing due to its physical parameters and RF performance.

TABLE OF CONTENTS

TABLE OF CONTENTS—Continued

LIST OF TABLES

LIST OF FIGURES

LIST OF ABBREVIATIONS

1G	First Generation
2G	Second Generation
3G	Third Generation
4G	Fourth Generation
5G	Fifth Generation
ADS	Advanced Design System
DAB	Digital Audio Broadcast
DCS	Digital Communication System
DG	Diversity Gain
DSRC	Dedicated Short-Range Communication
ECC	Envelope Correlation Coefficient
EM	Electromagnetic
fc	Center Frequency
FM	Frequency Modulation
FR4	Flame Retardant 4
GHz	Giga Hertz
GNSS	Global Navigation Satellite System
GND	Ground Plane
GSM	Global System for Mobile Communication
HFSS	High Frequency Structure Simulator

IMT	International Mobile Telecommunications
IoT	Internet of Things
LAG	Linear Average Gain
LTE	Long Term Evolution
MHz	Mega Hertz
MIMO	Multiple-Input Multiple-Output
OEM	Original Equipment Manufacturer
PCB	Printed Circuit Board
PCS	Personal Communications Services
PIFA	Planar Inverted-F Antenna
RF	Radio Frequency
SADRS	Satellite Digital Audio Receiver System
V2I	Vehicle-to-Infrastructure
V2P	Vehicle-to-Pedestrian
V2V	Vehicle-to-Vehicle
V2X	Vehicle-to-Everything
VLP	Vertical Linear Polarization
VSWR	Voltage Standing Wave Ratio
WLAN	Wireless Local Area Network
XPR	Cross Polarization Ratio

CHAPTER ONE

INTRODUCTION AND WORK CONTRIBUTIONS

1.1 Introduction

Over the past two decades, the automotive industry has changed drastically. The vehicle's design does not only consist of simple mechanical parts, but is now loaded with sensors and wireless systems which has transformed the automobile into a smart device. Recently, the most significant standards that are implemented for vehicle wireless systems are 5G and vehicle-to-everything (V2X) communications via the dedicated short-range communications (DSRC) or the cellular vehicle-to-everything (C-V2X) protocols. These technologies will significantly improve the driving experience, have a vital role in developing autonomous vehicles, and increase traffic safety. Traffic congestions from and to the cities have increased rapidly due to the high growth of urban areas which has increased the number of car accidents, and causes drivers to spend a lot of unnecessary hours on the road which has led to some serious socioeconomic issues. Vehicle-to-X (V2X) communication allows the car's system to communicate with other vehicles, pedestrians, and infrastructures in order to optimize traffic safety, improve the self-driving experience, and establish connection with Internet of Things (IoT) to different nodes across the network. 5G network and DSRC are two upcoming technologies that can interwork with each other to provide solutions for V2X communication. The cellular network can be used as a backup to the short-range communication while also providing internet access which can provide information far beyond the DSRC range [1].

The 5G network has an increased frequency band compared to the previous LTE system by adding the frequency band (617MHz to 698MHz) and sub-6GHz bands (3.4GHz to 5GHz) in addition to millimeter waves (mmWaves). The system is expected to have data rates up to 10Gbps at peak, very low latencies up to 1msec, and up to 100 times power consumption efficiency by using smart allocation of RF resources to user nodes [2].

DSRC frequency band in the USA is allocated between 5850 MHz and 5925 MHz. The short-range signals improve the vehicle communication with its surroundings and provide various road warnings for traffic safety and public services [3]. The DSRC network as specified by the Department of Transportation in the USA should be able to operate in a short range of 300 meters (detection range) which can allow spectrum reuse for different nodes and limit the interference between them. It should also have a fast message delivery up to 6 megabytes per second, operate in high-speed vehicle scenarios, and be resilient to severe weather conditions such as rain, snow, and fog [4].

The antenna design on vehicles suffers from size limitation and coupling between different elements since usually many applications come in a single package. For instance, Cellular, Global Navigation Satellite Systems (GNSS), Satellite Digital Audio Radio Systems (SDARS), and AM/FM in one restricted-size package which raises the issues of antenna size, passive isolation between elements, and bandwidth of each application because the antenna bandwidth depends on the physical volume that it occupies [5, 6]. The motivation and challenges for this work, literature review, work contributions, and dissertation organization are discussed next in this chapter.

1.1.1 The Growth of Cellular and V2X Wireless Communications

In the late 1970s, the first commercial cellular network was created, with fully official standards being established during the 1980s. The radio signals utilized by 1G are analogue, which means that instead of being encoded to digital data, the voice of a call is analogue modulated to a higher carrier frequency. 1G provided speed of 2.4Kbps with coverage area limitations. In the early 1990s, the second generation (2G) saw the adoption of GSM (Global System for Mobile Communication) standards with speed up to 64Kbps. It introduced roaming across different operators for the first time and allowed digital speech and data to be transferred across the network. Many of the core services that we still use today were launched with the advancement in technology from 1G to 2G, such as Short Text Messages (SMS), call hold, internal roaming, and billing based on services, such as rates for long distance calls and real-time billing. In the time between 2000 and 2003, a technological improvement launched the packet network, which provided internet access and higher packet data rate and was dubbed as 2.5G. General Packet Radio Service (GPRS) and Enhanced Data Rates in GSM (EDGE) are two standards introduced in 2.5G. The goals of third generation mobile communication (3G), which went on sale in 2001, were to provide more voice and data capacity, support a larger range of applications, and enhance packet data transmission at a smaller cost. It increased speed rates up to 256Kbps and allowed streaming of videos and Voice over Internet Protocol (VoIP).

The fourth generation (4G), which began in 2010, is an all-IP network infrastructure. Its goal is to provide consumers with high-speed/quality, high-capacity phone and data services, multimedia, and internet over IP while enhancing security and lowering costs. It enhanced the data rates to 1Gbps and made high speed applications like high-definition video streaming and online-gaming possible. 5G is developed to greatly increase internet connectivity which provides data rates up to 10Gbps and can support the rapidly growing demands for higher speeds and reliability for applications such as IoT, smart environment connectivity, and future autonomous driving systems in vehicles. In addition to significantly increasing the speed, 5G reduced the latency to a maximum of 1msec, network capacity was increased up to 10,000 more traffic, and power consumption was reduced for both cell towers and user devices by smartly allocating RF resources based on user usage.

5G is being developed in the automotive industry to provide high connectivity speeds and strong reliable connections for autonomous driving systems and IoT nodes. 5G network will have a vital role in autonomous driving to provide a safer driving experience, reduce traffic congestions, and connect different nodes across the network. In order to meet 5G network characteristics, the frequency bandwidth has greatly increased compared to its previous LTE technology to involve a new B71 band that goes from 617MHz-698MHz, new high frequency bands from 3.3GHz-5GHz in addition to millimeter waves (mmWaves). The extended frequency range makes it challenging to design multi-wideband antenna to cover the entire bandwidth from 617MHz-5GHz given size limitation and RF performance requirements.

V2X communications use two technology standards: WLAN V2X (DSRC) and cellular V2X (C-V2X). The main goal of V2X technology is to establish wireless communications between the vehicle and any object that may affect it which will help in increasing road safety, reducing time wasted by traffic, and increasing energy saving [7].

Toyota was the first carmaker in the world to deploy V2X-equipped vehicles in 2016. These vehicles are only available in Japan and employ DSRC technology. GM was the second carmaker to introduce V2X in 2017. In the United States, GM sells a Cadillac model vehicle that includes DSRC V2X. V2X standards based on LTE technology were issued by 3GPP in 2016. To distinguish itself from the 802.11p-based V2X (DSRC) technology, it is commonly referred to as "cellular V2X" (C-V2X). C-V2X provides long range wireless communication over the LTE/5G network in addition to direct communication (V2V, V2I) (V2N) for short range. In the United States, the frequency spectrum allocated for DSRC is from 5850MHz-5925MHz with 75MHz bandwidth, while in Europe DSRC is allocated from 5875MHz-5905MHz with 30MHz bandwidth. Therefore, designing a low-profile wide-band antenna that works for 5G sub-6GHz and V2X frequencies would be challenging to cover the entire range from 617MHz-6GHz while having excellent radiation performance.

1.1.2 Automotive Antennas

Recently, automotive antennas have evolved to provide many applications on the vehicle such as: AM/FM/DAB radio, SDRAS, GNSS, WiFi/Bluetooth, cellular 5G, and V2X communications. Vehicular antennas should grow more reliable as they become more advanced. An automobile's antenna is exposed to intense temperatures of up to 125 degrees Celsius. The mechanical and electrical features of an antenna can also be influenced by road structure, vehicle's speed, and various electrical/mechanical components. Automotive antennas must go through many tests to ensure their capability of having good RF performance under different conditions, such as: vibration testing, thermal shock, high temperature exposure, thermal cycling, and pre-and post-stress validations. Electrical performance is checked after each of these tests within minor tolerance values to ensure stability and long-life duration of the antennas. Cellular 5G and V2X communications need to have omnidirectional coverage around the vehicle which means that at certain lower elevation angles, the antenna should be able to receive the signal from any azimuth angles surrounding the car. A Multiple-Input Multiple-Output (MIMO) antenna system could be used to ensure omnidirectional behavior, increase the coverage area around the element that will increase the total throughput of the system providing low correlation between the antennas. If one antenna is not enough to satisfy the requirement, then two or multiple antenna elements forming an antenna array must be considered.

Furthermore, to avoid attenuation caused by increasing cable length, antennas should be placed within minimum distance to the receiver. Moreover, the surrounding environment around the antenna may affect its performance significantly and hence, materials and physical spaces around the antenna must be carefully analyzed. As a rule, antennas that operate at lower frequencies need more clearance than high frequency antennas since lower frequency waves support longer wavelengths that require additional space. This makes its more challenging to design wide-band antennas that operate across low and high frequency bands. In addition, noises and interference caused by vehicle engine and battery management system (BMS) on electric cars can also affect the received signal to the antenna, so placing the antenna in a clear spot as far as possible from these noise sources is vital. The polarization of 5G and V2X antennas is usually Vertical Linear Polarization (VLP) which means the antennas need to be perpendicular to the surface of the ground or vehicle’s roof. However, the polarization of GNSS patch antenna is Right Hand Circular Polarization (RHCP) and for SDARS patch is Left Hand Circular Polarization (LHCP) which shows that for every application, polarization of each automotive antenna is extremely important.

In conclusion, for automotive antennas, several requirements come to play such as: mechanical validations (vibration, thermal, stress), omnidirectional coverage around the vehicle, RF cable length, noise and interference from surrounding environment, and antenna polarization. For a successful vehicular antenna design, all these aspects must be considered.

1.1.3 Different automotive antenna topologies

There are multiple antenna topologies that can be used on vehicles depending on physical location on the car, size/height limitation, required antenna polarization, and frequency bandwidth of the desired wireless application.

1.1.3.1 Monopole

Most vehicle manufacturers mount antennas on the roof of their cars. The reason for this is that the roof of the car is highest point above ground and unobstructed, allowing for good signal reception from all directions. Monopole antennas are a very common automotive antenna type since they are simple to handle, easy to construct, easy to install on a vehicle, and are inexpensive. A monopole antenna is made up of an antenna base pin and a long rod. To mount the antenna on the vehicle's roof, all that is required is a hole in the metallic framework to accommodate the antenna base and cable. The rod can be a quarter wavelength ($0.25*\lambda$) or longer stiff metallic stick. Monopoles are useful in a wide range of frequency bands, from VHF applications to 5.9 GHz car-to-car communication. The monopole can be mounted in the middle of the roof, on a roof edge or frame, or even on the front/back bumper. This antenna technology may be quickly installed almost any place on the vehicle. Monopoles are the top choice in the automotive sector since they offer very cheap pricing due to speedy development and ease of manufacturing. The monopole antenna is highly dependable on direct contact to the ground, which is the vehicle's metallic structure. When the ground is small in proportion to the wavelength, the monopole will not work well. To reduce effects on performance, the ground plane must be at least ($0.25 * \lambda$) in radius, having a larger size ground plane would enhance performance. Monopole antennas have good omnidirectional behavior at lower elevations which make them good candidates for 5G/V2X antennas specially if they are placed on the vehicle's roof, however, height restriction could be an issue specially at low frequency bands, hence, a lower-profile topology might be needed.

1.1.3.2 PIFA

Planar Inverted F-Antenna (PIFA) consists of a horizontal plane bent over to run parallel to the ground plane beneath it. It has the advantage of an Inverted L-antenna and monopoles combined by reducing height as in the Inverted L-antenna while still having good impedance to match the feeding circuit. In the automotive industry, the Planar Inverted-F antenna (PIFA) is becoming more popular for low-profile applications. The antenna has a quarter-wavelength resonant frequency thus reducing the required space needed compared to patch antennas. The PIFA name comes from the fact that this antenna looks like an inverted F but with a horizontal plane on top to increase the operating bandwidth. The general structure of a PIFA antenna is shown in Figure 1 [8]. The feed distance to the short pin (D) can be used to alter the PIFA's impedance. The impedance decreases as the feed gets closer to the shorting pin, while it increases as the feed gets further away from the short edge.

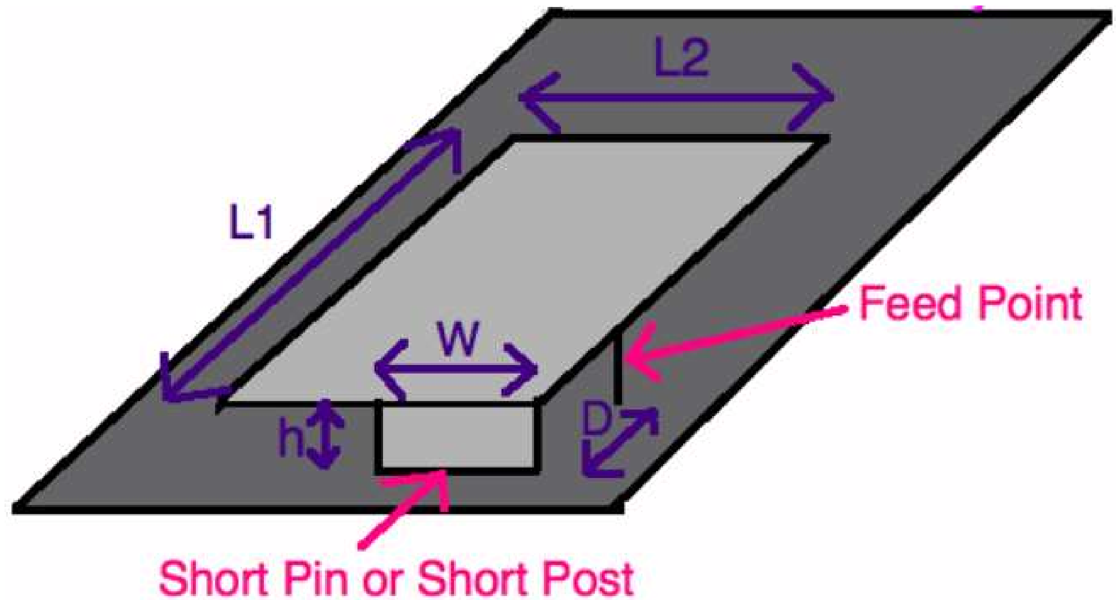

Figure 1.1. General structure of PIFA antenna with shorting pin.

PIFAs are popular for vehicular applications especially for 5G/V2X communications because of their low profile, omnidirectional pattern at low elevations, easily manufactured, and their low production cost.

1.1.3.3 Patch Antenna

A patch antenna is essentially a flattened monopole. A patch antenna's main construction is shown in Figure 1.2 [9]. A half wavelength (0.5* λ) metallic plate is put over a ground plane, which is separated by air or a low loss dielectric substance. The RF should be delivered directly to the radiating patch through the excitation pin or coupling mechanisms. In automotive antennas, patch antennas are becoming increasingly widespread. Originally used mostly for high-frequency applications beyond 1 GHz, such as GNSS for RHCP at 1.5 GHz or SDARS radio for LCHP at 2.3 GHz, but now patch antennas are being used more for wireless communications such as: WLAN at 2.4GHz/5GHz, and V2X Communication at 5.9GHz, and cellular bands. However, patch antennas are usually narrow band antennas with around 5% operating bandwidth which makes them unpractical for broadband applications.

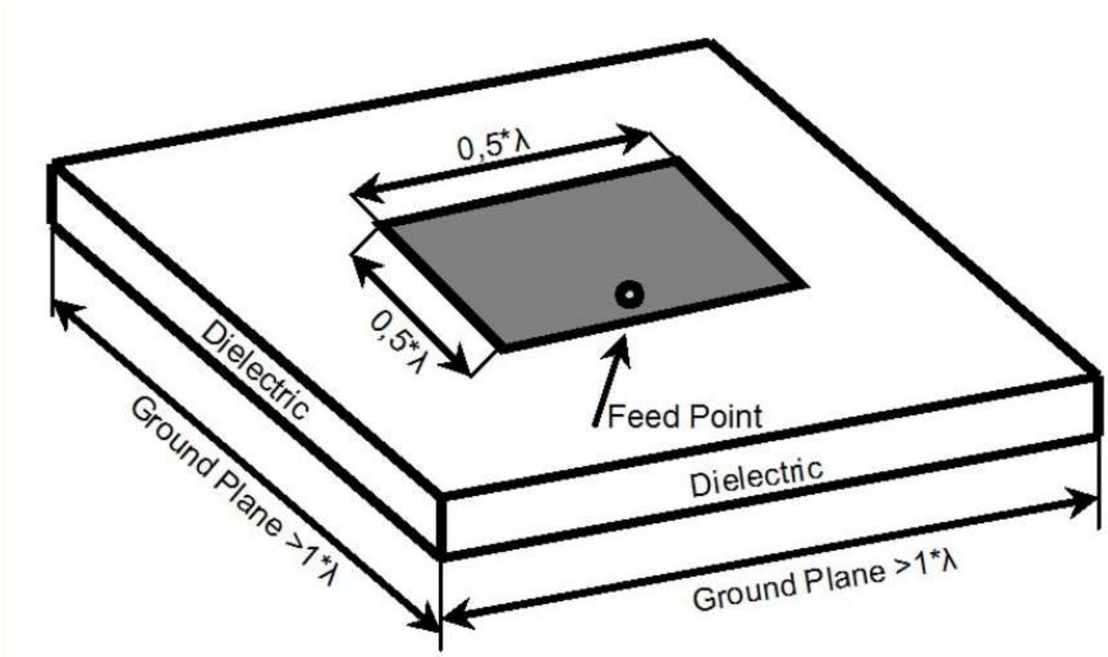

Figure 1.2. Patch antenna main layout.

Because this antenna is flat and unobtrusive, it can be incorporated into the vehicle's structure, such as on a vehicle’s roof, or beneath a fender or bumper. Patch antennas require a big metallic ground plane that is preferably flat and measures at least one wavelength in diameter.

1.1.3.4 On-glass antenna

In the 1980s, as automotive antenna design became more important, this antenna type became popular in the luxury vehicle sector. With on-glass antennas, a number of antennas can be hidden from the average user's view. Antenna topologies can be installed in the glass windows of most vehicles in the front/back windshields or side glass. The slot antenna theory is the most straightforward antenna technology for on-glass. The antenna becomes part of the metallic car construction, and the glass (windshield, side glass, or rear window) serves as the slit in the vehicle's metal structure. When this slot is connected to a thin conductor, it resonates and becomes an antenna. It is important to consider the feeding posture. Different modes can be engaged by carefully selecting the feeding position, which can aid in the excitation of specific polarity or radiation pattern direction.

In conclusion, automotive antennas can have different topologies such as: dipoles, monopoles, PIFAs, patches, helical antennas, or on-glass antennas. Depending on the required application, specified size, operating bandwidth, antenna polarization, certain antenna topology can be preferred over the others. 5G/V2X antennas can be implemented on the vehicle's roof (in a shark-fin housing), fender/bumper, spoiler, trunk, or hidden in the dashboard. Due to the broad band bandwidth of 5G communication, dipoles, monopoles, and PIFAs are the most successful solution for such technologies. However, for a vertical polarization antenna, monopoles and dipoles would require extended height dimension especially at lower frequency bands which could not be possible due to style and size restrictions. Hence, for a low-profile design, PIFA elements could cover the 5G/V2X bands with lower height dimension and good RF performance, if designed properly, which is the main goal of this research. Placing the antennas in a shark-fin housing on a vehicle's roof has proven to be most efficient for RF performance since the elements are isolated from other noise/interference sources on the vehicle and can provide omnidirectional radiation behavior without being blocked by any metallic structure on the car. In addition, shark-fin antennas have shown to be useful in improving the aerodynamics efficiency of the vehicle, making automobiles more fuel efficient [10].

This research shows the design of a low-profile wideband PIFA in addition to a novel raised printed monopole antenna to cover 5G/V2X communications. The antennas can be placed inside a shark-fin or low-profile housing on a vehicle's roof or hidden in the spoiler for best performance. Vehicular roof antennas usually consist of multiple applications inside the same housing such as: GNSS, SDARS, 5G Cellular, WiFi/Bluetooth, and even AM/FM/DAB in some designs, which raise isolation concerns between elements, antenna size restriction, and makes it very challenging to design such antennas.

1.2 Motivation and Challenges

In this section, multiple challenges that face automotive antennas for 5G/V2X are discussed whether it is a single element design or multiple applications integrated in one housing.

- 5G network has much more extended bandwidth compared to its previous LTE technology covering a broad range of operating frequencies, including low-band (617MHz- 960MHz), middle band (1710MHz- 2700MHz) and high-band (3.3GHz- 5GHz). With such a wide variety of frequencies, designing a wide band antenna with appropriate performance characteristics is a difficult task especially when low-profile design is required. In fact, covering low band frequencies of 5G is a design barrier since the antenna dimensions are restricted within the housing style, whether it is shark-fin or low-profile, and it is usually significantly smaller than the operating wavelength of the antenna which makes it very challenging to cover the required bandwidth while getting good RF radiation performance. Aside from achieving strong 5G cellular performance, antenna element cost, and manufacturability are critical parameters to the antenna product's economic success.

- Vehicle roof antennas (in shark-fin or low-profile housing) usually have multiple antenna elements for various applications implemented in the same module such as: cellular 5G, V2X, GNSS, SDARS, Wi-Fi, Bluetooth, Remote Key Entry (RKE), and AM/FM/DAB, which could raise integration issues including shadowing and blockage, mutual coupling between elements, and degradation in radiation performance especially with wideband antennas. Shadowing and blockage occur from the geometric structure of each antenna in respect to each other which causes the radiated RF signal to be blocked or reflected, and this can be seen as nulls (minimum points) in the radiation pattern of the antenna. Coupling between antennas can happen between elements that share the same operating frequencies or different frequency bands. Filtering can be used to reduce the coupling between antennas on different bands, but for same-band antennas (as in 5G MIMO system), other techniques can be analyzed to increase isolation such as: spatial, rotational, or polarization diversity. Mutual coupling could significantly reduce the radiation efficiency of the antenna since the transmitted RF signal is not being normally received by the required antenna, but some of the energy gets coupled to another element. Coupling between antennas, shadowing, and blockage could result in reducing the coverage area around the antenna and degrading the omnidirectional behavior of the radiation pattern by introducing nulls in certain azimuth angles and reducing the total gain. Hence, this research presents a low-profile antenna design with unique structure that has an acceptable rejection for GNSS L1/L5 frequencies which makes it suitable for integration with navigation systems having minimal effect on RF performance.

- MIMO antenna system for 5G communications is needed to meet the high speed, low latency, enhanced throughput requirements. MIMO system increases the total throughput of the system by increasing the number of antenna elements that operates on the same frequency bands and having independent Tx/Rx channels which would increase the transmission capacity. Envelope Correlation Coefficient (ECC) and Diversity Gain (DG) are two main parameters in the MIMO system. ECC measures the correlation between the antenna elements to have independent transmission channels as best as possible. Correlation depends on the distance between the elements and the radiation pattern shape (amplitude and phase) of each antenna. Size limitation on a vehicle's roof antenna makes it difficult to design a 5G MIMO antenna system with multiple elements especially at low frequency bands to have low correlation between antennas. Hence, MIMO antennas need to be carefully designed and placed in locations that will consider spatial distances and radiation pattern of each element to reduce the correlation of the system.
- For V2X technology, it is important for the antenna to have high radiating performance (especially at front/rear side of the vehicle), good coverage around the car without any severe nulls (minimum points) in the radiation pattern, and

operate below the horizon up to six degrees in elevation. V2X communications work at frequency band (5.85GHz-5.925GHz) in the US and hence, antenna size would usually be relatively small at that frequency. However, integrating the V2X antenna in the same housing with other antennas from different applications might result in blockage of V2X signal from larger size antennas that operate at lower frequencies. This might result in severe nulls in the radiation pattern and reduce the coverage around the vehicle at certain azimuth angles. The work in this research presents a 5G/V2X antenna element that has good radiation coverage for V2X communications, without extreme nulls in the radiation pattern which provide good overall V2X system performance.

1.3 Literature Survey

In this section, comparison to existing work in the literature is presented for automotive antennas regarding 5G/V2X applications for low-profile designs, printed monopole designs, and MIMO antenna systems.

1.3.1 5G/V2X low-profile automotive antenna

The antenna in [11] is a low-profile novel compact 3D cellular antenna that covers the band from 790MHz till 2.69 GHz. However, 5G bands require much wider bandwidth that could cover from 617 MHz to 5 GHz. The design in [12] is a low-profile nefer antenna that covers a broad frequency range for 5G/V2X from 698MHz-6GHz, but the dimensions of the element are bigger than the proposed design in this work, in addition, it doesn’t cover the extended lower frequency band from 617MHz-698MHz which would require bigger volume. In [13], the authors present a low-profile top loaded monopole antenna for cellular applications that has good performance at lower elevations, but it only operates on the frequency range (700MHz-3GHz) and the occupied volume of the element is bigger than the proposed design in this work. The antenna designs from [14] to [19] are monopole-based elements with larger physical height values and they do not cover the whole 5G/V2X bands from 617MHz-6GHz.

1.3.2 5G printed monopole automotive antenna

Compared with our work in [23], [24], [25], [26], and [27], the proposed printed antenna design in this research provides a smaller footprint by using Flame Retardant (FR4) as dielectric material to reduce the overall occupied volume of the radiating element while maintaining a very good RF performance. In [28], and [29], the authors presented printed antenna elements with a bit bigger dimension, however, the designs operate from 3GHz to 6GHz and do not cover the lower frequency bands starting from 1.71GHz which would need a bigger volume occupied by the antenna.

1.3.3 5G/V2X MIMO Antenna Systems

The 2x2 MIMO systems in [30, 31] and [32] consist of low-profile elements, but the frequency band covered by these systems are narrow and do not cover the extended 5G/V2X bands from 617 MHz-6 GHz. In [33], the authors present a 2x2 nefer antenna MIMO system that operates from 700MHz to 6GHz, but the physical dimensions of the elements are too large, and the system doesn't cover B71 frequency band (617 MHz - 960 MHz) that will make it more challenging in terms of antenna size and volume. In [34, 35, 36], and [37] the MIMO systems present printed antenna elements on dielectric materials, however, they still don't cover the wide frequency range from 617 MHz - 5 GHz and the physical dimensions of the antennas are larger. The authors in [38] present a 2x2 MIMO system with transparent monopole antennas designed on glass material, but the elements do not cover the low and middle 5G frequency bands which will introduce the challenge of bigger volume of the antenna and degraded passive isolation.

1.4 Work Contributions and Dissertation Organization

This section provides an overview of the research's main contributions on low-profile automotive roof antennas, which are summarized in the following paragraphs:

- Chapter 2 shows the design process for low-profile PIFA antenna for vehicular 5G/V2X applications that is capable of operating across wide frequency ranges from 617MHz-6GHz while having acceptable rejection for GNSS bands which makes it an excellent candidate to be used in a roof antenna housing integrated with other applications. The proposed antenna design enables coverage of the 5G low-band frequencies (617MHz-960MHz) with a relatively small footprint/volume that is easily contained within a low-profile housing or automobile shark-fin. In addition to enhancing overall antenna module performance by minimizing coupling effects, the designed antenna features an inherited GNSS rejection for L1/L5 bands. This removes the need for additional filtering at the PCB board level and lowers the total cost of the antenna system. The antenna design is made to be small and does not require printing on dielectric material, which lowers the cost of the design even more. The antenna's physical structure and slots allow it to cover the entire 5G sub-6GHz bands with a VSWR of less than 3.3:1. The height of the antenna is reduced to 28mm only instead of the standard monopole height of around 120mm (λ/4 of the lowest frequency) with relatively small length and width to cover the entire band, which enables the antenna design to be packed into low-profile antenna module.

- Chapter 3 presents multiple 2x2 MIMO antenna configurations which have been analyzed for automotive applications in the 5G and V2X frequency bands. The first configuration consists of two low-profile PIFA antennas separated by a spatial distance on the vehicle's roof. The second configuration has two PIFAs within the same printed circuit board (PCB) with different rotational positions. The third configuration has a compact wideband monopole antenna and a PIFA within the same PCB to analyze the ECC between the horizontal current introduced by the PIFA and the vertical current introduced by the monopole. Both antennas have suitable physical dimensions and operate in the sub-6GHz 5G and V2X frequency bands (617MHz-6GHz) with reasonable rejection to GNSS bands which makes the proposed MIMO systems suitable to be deployed with other applications within the same package. The MIMO systems presented in this work cover the extended sub-6GHz 5G bands from 617MHz to 5GHz in addition to the V2X band at 5.9GHz with reasonable physical dimensions and unique features of the proposed antennas. The 5G/V2X MIMO systems also have acceptable filtering for GNSS bands which make it compatible with different navigation systems under the same housing. Furthermore, this research provides data comparisons between ground plane and vehicle measurements in terms of different MIMO parameters such as: ECC, diversity gain, combined radiation pattern, and port efficiencies.
- In Chapter 4, a novel wide band raised printed monopole with partial ground plane structure has been developed for vehicular applications that has unique shape and physical dimensions which makes it suitable for placement inside a shark-fin module on the car's roof. The proposed design can cover wide frequency bands

from 1.71GHz-5GHz with reasonably small dimensions because of its unique shape in addition to using slots, partial ground plane (PGP) structures. A 2x2 MIMO antenna system is also analyzed to achieve the high-performance requirements for 5G communications. The proposed MIMO system was able to achieve good performance and isolation between elements by using ground plane structure on the back side of the monopole that improves passive isolation without increasing spatial distance between the elements specially at lower frequency bands.

- In Chapter 5, low-profile antenna systems have been developed for vehicular applications in the sub-6GHz 5G and L1/L5 GNSS frequency bands to be used in low-profile housing on the vehicle's roof. The first system integrates MIMO 5G with upper L-band from 1559MHz to 1610MHz (L1-band) while the second system covers the lower L5 band from 1164MHz to 1189MHz.
- Chapter 6 concludes the work done in this research and makes recommendations for potential future works.
- The Appendix provides a tabular overview of the literature review that was analyzed during the research project.

CHAPTER TWO

WIDE BANDWIDTH LOW-PROFILE PIFA ANTENNA

2.1 Introduction

With the cellular communications and V2X sectors developing quickly, communication services such as 2G, GSM, 3G, 4G, LTE, Personal Communications Services (PCS), Digital Communication System (DCS), Broadband Radio Services (BRS), International Mobile Telecommunications (IMT), C Band, and V2X/DSRC have added a significant increase in number of frequency bands (listed in Table 2.1). This wide selection of frequency bands has made it necessary to design wideband antennas for these applications. These antennas must have a small size, an omnidirectional radiation pattern, low cost, linearly polarized, and easily fabricated in order to be useful and practical in real applications. Hence, a PIFA element design can be an excellent candidate for these requirements. Unfortunately, standard PIFA is a narrow band antenna with around 15% bandwidth which makes it very challenging to design a low-profile element that covers the entire 5G/V2X bands and more advanced design techniques need to be implemented to gain broadband performance. A successful 5G/V2X antenna requires an omnidirectional design, affordability, excellent matching attributes, good gain performance, low-profile or shark-fin compatibility, and simplicity of manufacture. Table 2.2 lists key design objectives and performance criteria that Original Equipment Manufacturers (OEM) in the automobile sector frequently demand. The designed low-profile PIFA architecture will be analyzed next in this section.

Table 2.1. Frequency bands of 5G sub-6GHz and DSRC

Cellular Band	Frequency Range (MHz)
Digital Dividend (US)	617-698
Lower and Upper SMH/ Lower 800 (Japan)	699-875
Extended GSM	880-960
DCS	1710-1880
PCS	1850-1990
IMT	1920-2170
WCS	2350-2360
C Band	3300-5000
DSRC (US) DSRC (EU)	5850-5925 5875-5905

Table 2.2. 5G/V2X Design Goals and Requirements.

Parameter	Value
Polarization	Vertical Linear Polarization (VLP)
VSWR	3.3 VSWR for 5G bands 2.5 VSWR for V2X bands
Efficiency	40% at low 5G bands 60% at high 5G/V2X bands
LAG	-4 dBi across θ = 75-87 degree for 5G bands -2 dBi across θ = 80-96 degree for V2X bands

2.2 Low-Profile PIFA Antenna Design

2.2.1 Work Overview

The objective of this research is to create a 5G/V2X antenna that operates in the frequency range of 617MHz to 6GHz while having reasonable rejection for GNSS bands, has an omnidirectional behavior, and performs well for the requirements listed in Table 2.2. The antenna is simulated using HFSS software and measured on a 1-meter rolled edge GND plane inside an anechoic chamber. Then, a vehicle level measurement was conducted with the antenna placed on the backside center of the roof. The antenna was first simulated using HFSS software on a 1-meter GND. Next, the discussion of antenna parameters, design process, and antenna positioning follows.

2.2.2 Design Guidelines and Parameters

The newly extended 5G band has made it challenging to design a reasonable low-profile antenna especially at the low band where the operating frequencies have shifted lower, and the bandwidth has increased to cover 617 MHz–960 MHz. The conventional monopole would require a radiating height of approximately 95mm to operate at the center frequency of 788 MHz which is not practical. A top loaded monopole as presented in [20] can be used to reduce the height to 30mm at the expense of increasing the length and width dimensions to 80mm. The proposed design in the paper is derived from a PIFA by introducing distinct physical dimensions and slots that would lower its low band operating frequency and increase its bandwidth with smaller occupied volume than those in existing literature. The proposed antenna is made of a metal sheet with dimensions of 28mm (height) × 55mm (length) ×50mm (width), and it is mounted on FR4 board material. The space between the horizontal top plate and the board material is filled with free space (air). Figure 2.1a. and Figure 2.1b. show the antenna dimensions from side and top views with its distinct features and variables. The location of the wide feeding plate is placed at the edge of the horizontal plane which is important for the middle and high bands to create folded monopole structures with the slots. A shorting pin is also placed at a specific distance W_d from the feeding plate to control the resonance frequency of the low band. Table 2.3 shows various geometric parameters of the antenna with their optimized values. The proposed design introduces two new structures containing slot 1 and slot 2 which will create two resonance frequencies at middle and high frequency bands.

First, the low frequency band is determined by the physical dimensions of the element in addition to the shorting and feeding pins. Equation (2.1) approximates the resonance frequency on the low band using the values of Table 1 (*fc* = 790 MHz) [21]:

$$f_c = \frac{c}{3W + 5.6L + 3.7H + 3W_f - 3.7W_s - 4.3W_d - 2.5L_b} \tag{2.1}$$

where *c* is the speed of light ($c = \lambda f$); *W*, *L*, and *H* are width, length, and height of the antenna; *Wf* is the width of the rectangular feeding plate; *Ws* is the width of the shorting pin; *Wd* represents the width distance between the shorting pin and the rectangular feeding plate; and *Lb* is the length distance between the shorting pin and the edge of the horizontal top plate. The volume occupied by the antenna determines the bandwidth of the low frequency band which operates from 617 MHz to 960 MHz. The vertical arm of length *Hb* is added to further reduce the resonance of the low band to around 750MHz to balance the VSWR values without increasing the total volume.

Secondly, Structure 1 consists of a rectangular feeding plate and up to slot 1. It acts as a folded monopole that has a radiating length of 31.25mm which is ($\lambda/4$) of 2.39 GHz. The width of the rectangular feeding plate and width of slot 1 determine the bandwidth of the middle band that operates in the frequency range (1.71GHz–3.8GHz). Tuning the low band with the proposed element dimensions along with Structure 1 dimensions and gap will filter out the GNSS bands that reside between low and middle cellular frequency bands.

Structure 2 consists of a feeding plate and up to slot 2. It acts as a folded monopole with a center frequency of 5.5GHz. Slot 2 changes the current path across the horizontal plane that creates the resonance for the high bands (3.8GHz–6GHz). The location of the shorting pin is not only vital for the low frequency band, but also important for the DSRC frequencies to avoid getting severe deep nulls (minimum points) in the radiation pattern that will affect the coverage area around the antenna element at the azimuth angles where the shorting pin is located.

The antenna's geometrical parameters are shown in Figure 2.1, and Table 2.3 lists their ideal values. Future sections will go into greater detail about certain value selections. Figure 2.2 demonstrates how the antenna has been symmetrically positioned toward the back of the vehicle's roof in preparation for chamber measurements. The next part discusses the equivalent circuit model of the antenna, simulation outcomes, ground plane measurements, and vehicle-level measurements.

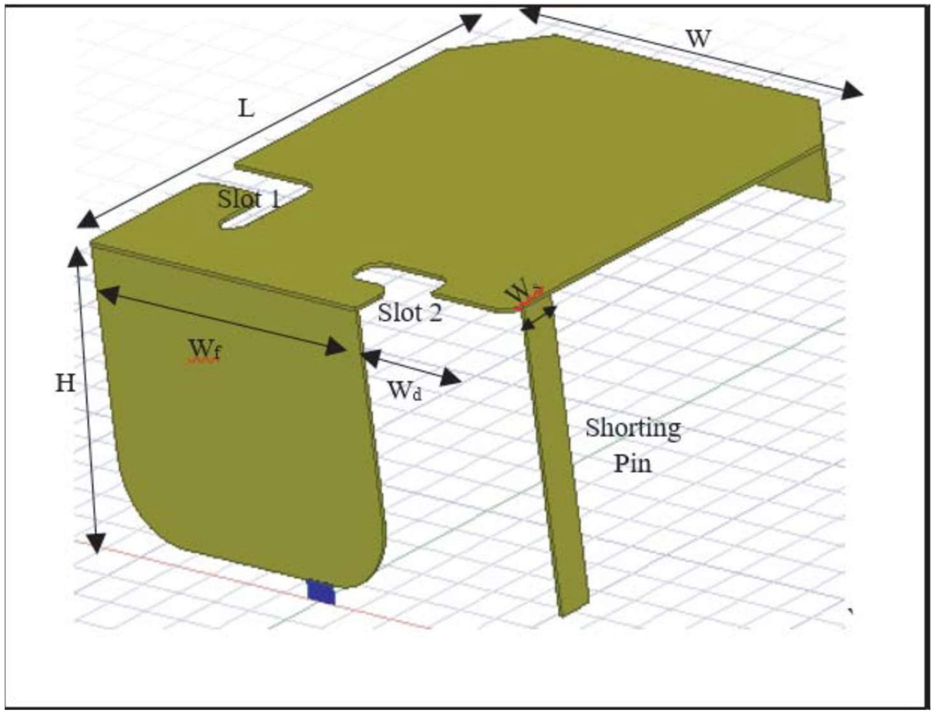

(a)

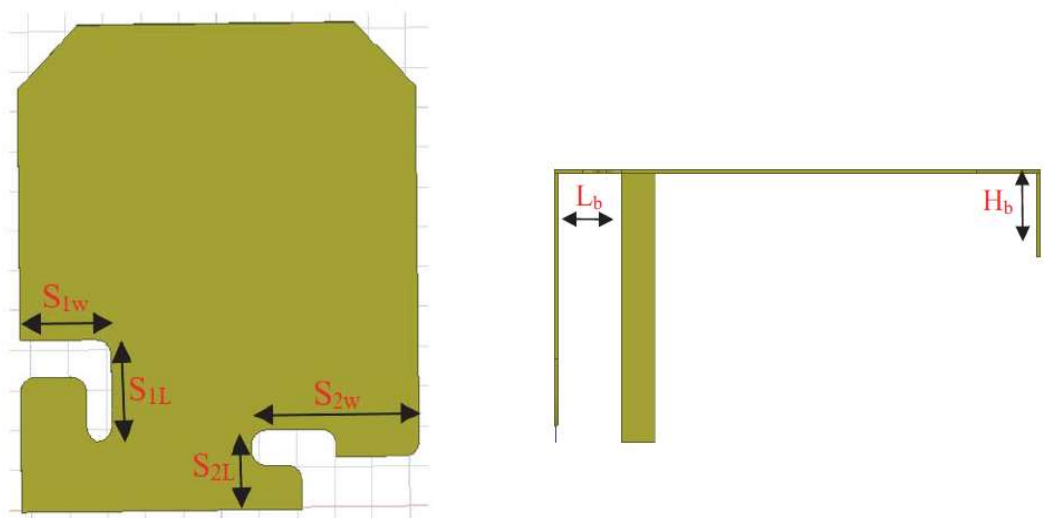

(b)

Figure 2.1. Cellular 5G/V2X PIFA antenna in (a) front and side view of the simulated antenna; and (b) top and right-side view of the antenna with the slots and shorting pin structures.

Table 2.3. Geometrical parameters Values of the designed antenna.

Parameter	Value (mm)
H	28
L	55
W	50
S_{1w}	12.1
W_s	6
L_b	7.5
S_{1L}	12.5
S_{2w}	22.25
S_{2L}	10
W_f	29.5
H_b	8.5
W_d	17.5

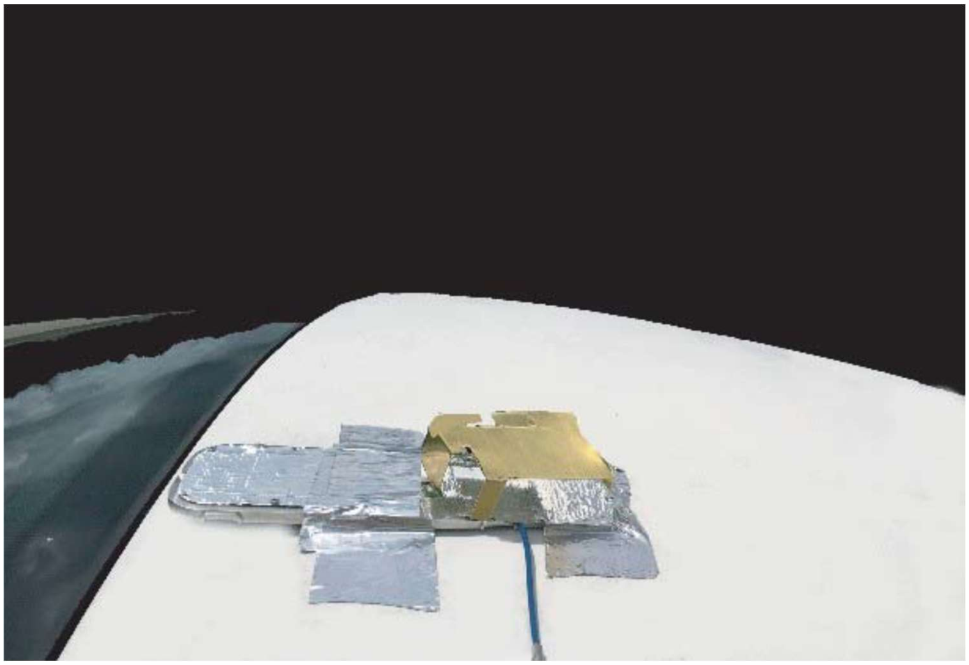

Figure 2.2. Antenna Placement on vehicle roof.

2.3 Low-Profile PIFA Simulation and Measurements Results

2.3.1 VSWR and Vector Surface Current Intensity

The antenna simulated VSWR was captured and compared against the realized antenna measurement as depicted in Figure 2.3. It is noticed that across the operating bands of 5G and V2X, the measured VSWR is better than 3.3:1 (approximately 5.4 dB return loss). The VSWR plot also shows a reasonable rejection for GNSS frequencies.

The vector surface current distribution of the antenna measured in (A/m) is plotted in Figure 2.4. At each frequency, the intensity and direction of the current distribution are presented along the entire structure. It can be noticed that the low frequency bands present the most intense current in the structure especially at the feeding plate and shorting pin where the direction of current is in-phase between them. While going up in the frequency range the surface current starts shifting towards slot 1 structure for frequencies up to 3.8GHz. Figure 2.4 also shows that at the high end of 5G frequencies and DSRC, the current shifts from slot 1 towards slot 2 structure.

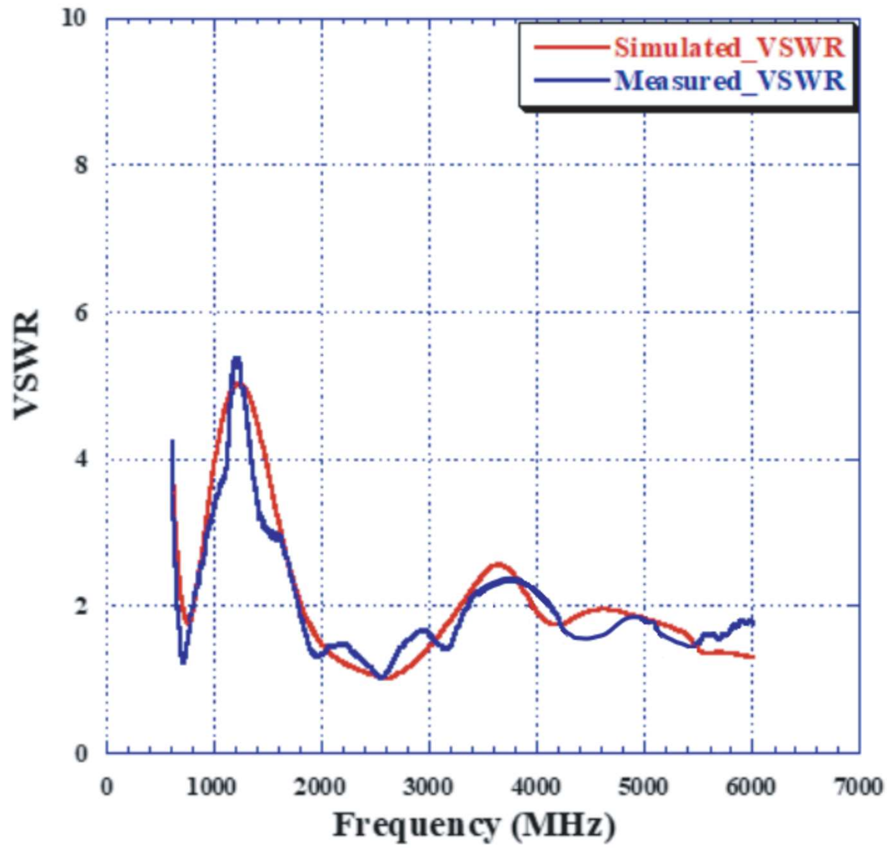

Figure 2.3. On GND simulated and measured VSWR.

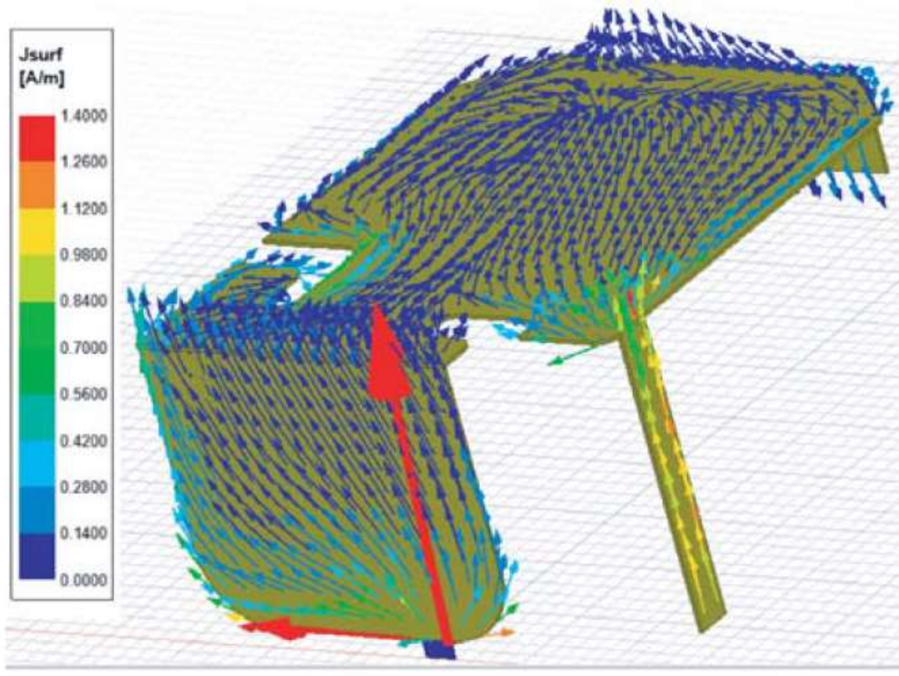

(a)

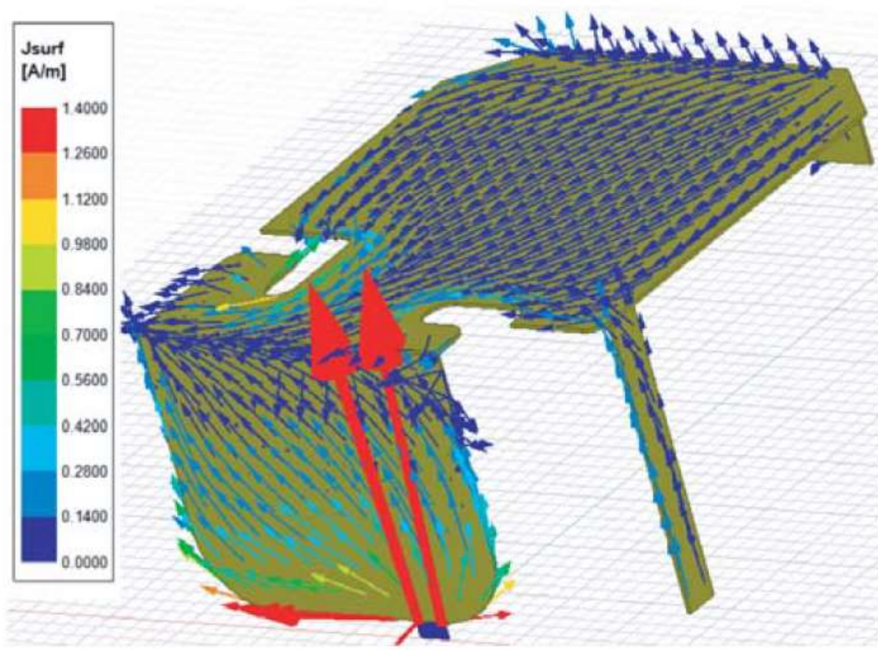

(b)

Figure 2.4. Simulated vector surface current distribution measured in (A/m) at different 5G and DSRC frequencies. (a) 617MHz, (b) 1900MHz, (c) 3600MHz, (d) 5000MHz, and (e) 5900MHz.

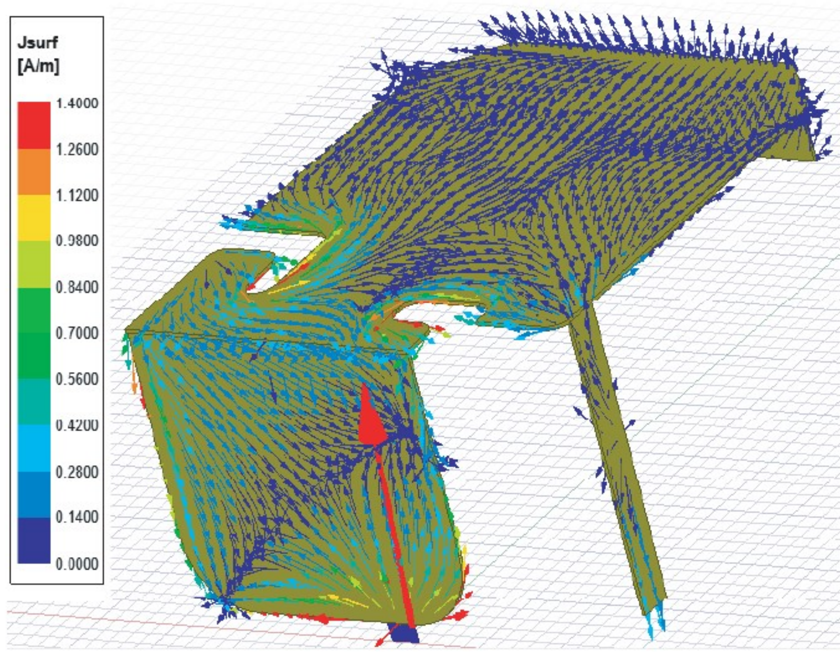

(c)

Figure 2.4. Continued.

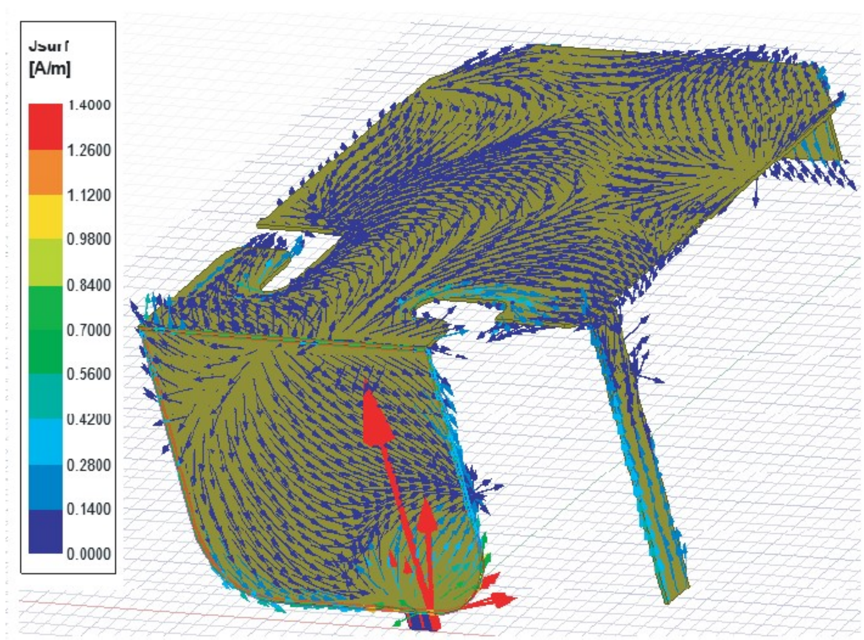

(d)

Figure 2.4. Continued.

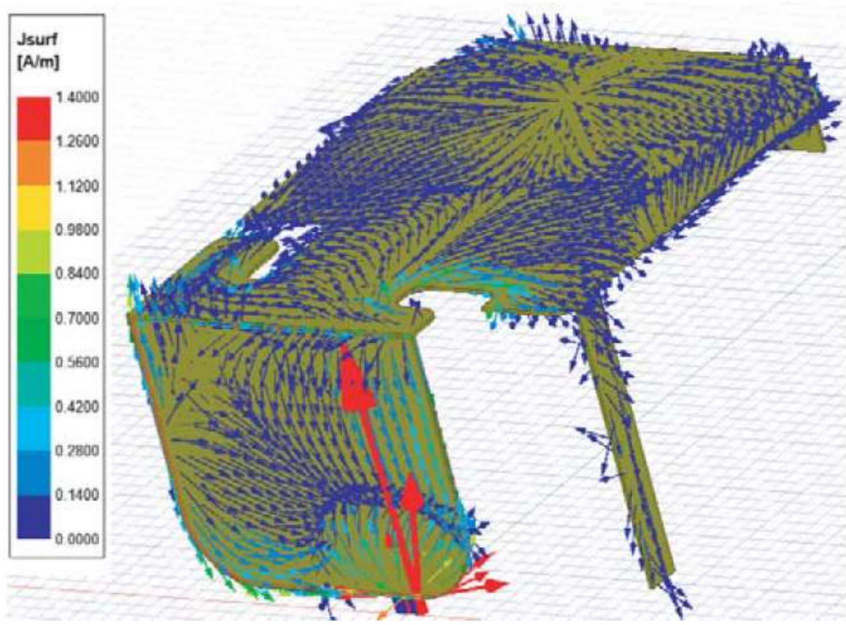

(e)

Figure 2.4. Continued.

2.3.2 Equivalent Circuit Model of Antenna

Figure 2.5. shows the equivalent circuit model for the wideband PIFA antenna which is used to further illustrate how the antenna functions. The method of designing this circuit is presented in [22] derived from the VSWR response. Figure 2.5. shows the response of the circuit model using ADS software compared with the simulated VSWR of the antenna. The circuit consists of multiple RLC resonance circuits which simulate low, mid, and high frequency resonances in addition to GNSS filtering as presented by the vector current distribution on the PIFA.

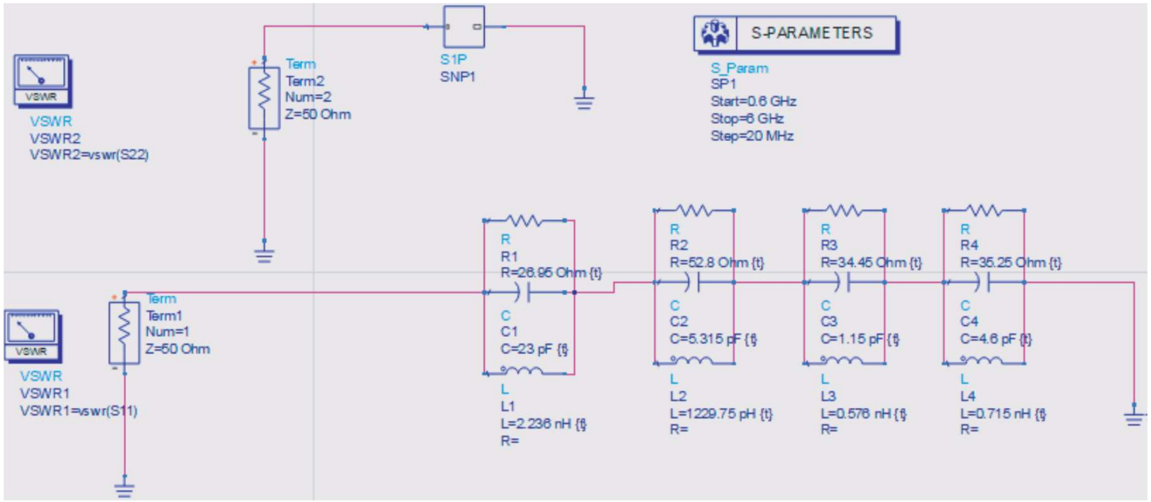

(a)

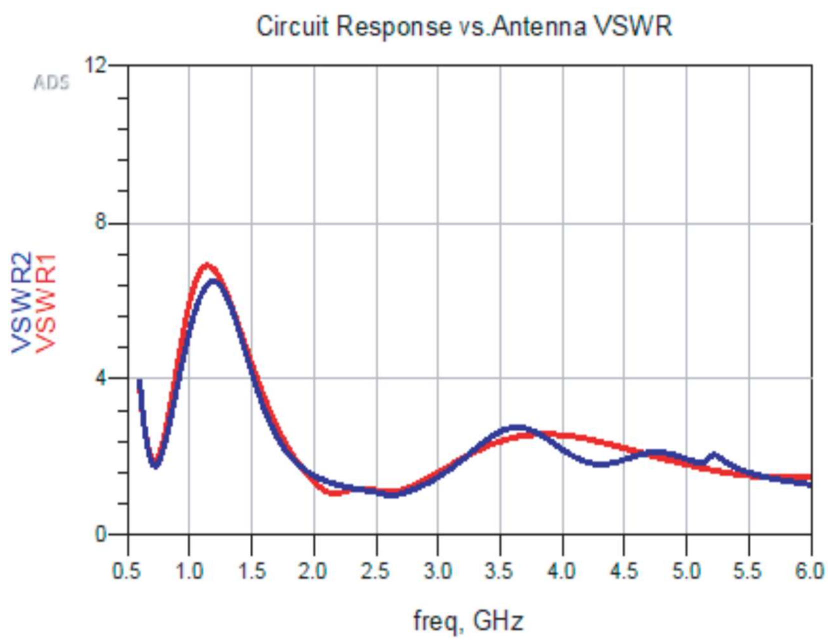

(b)

Figure 2.5. Equivalent lumped elements circuit model using ADS and comparison between the circuit response and antenna's VSWR. (a) Equivalent electrical circuit model of the antenna. (b) Circuit response vs. antenna VSWR.

2.3.3 Radiation Pattern, Efficiency, and Linear Average Gain

In Figure 2.6, radiation patterns of horizontal cuts at elevation 80 degrees are presented for frequencies 617 MHz, 1.9GHz, 3.6 GHz, and 5 GHz. It can be concluded that for low frequencies the patterns tend to have a good omnidirectional behaviour; however, for higher frequencies, radiation patterns appear more directive. At 3.6GHz, it seems directive towards the side of slot 1 while at 5GHz it appears directive at slot 2 angles from the front and back sides of the element. Moreover, the average gain observed from vehicle radiation patterns is found to be −2.1dBi, −1 dBi, 0 dBi, and 0.9 dBi at frequencies 617 MHz, 1.9GHz, 3.6 GHz, and 5 GHz, respectively. It is important for V2X radiation patterns to avoid having extreme minimum values (nulls) as it will influence the coverage range at certain azimuth angles. Figure 2.7. shows the radiation pattern for 5.9GHz frequency measured on GND and on a vehicle at elevation 90 degrees. The vehicle radiation pattern tends to be more directive towards the back side of the car which could result from reflections caused by the roof's curvature with a peak gain of 4.4 dBi at azimuth angle 230 degrees without having a minimum value lower than −12 dBi.

The measured antenna efficiencies on GND and vehicle for 5G bands have been presented in Figures 2.8.(a), (b), and (c). It can be noticed that the 5G GND measurement has an average of 83% efficiency across all frequency bands, whereas the vehicle measurement has a reduced average efficiency of 72% that could result from reflections of EM waves from the roof curvature and paint which worsens the grounding of the antenna, especially at the low frequency bands. The measured antenna efficiency for V2X frequencies is shown in Figure 2.8.(d). The GND and vehicle efficiencies seem to have close values across the band. This could be reasoned by the size of the ground surrounding the antenna since at these high frequencies the area of the ground plane can be reduced without having major losses, unlike the cases at lower frequency bands. The measured GND efficiency has an average of 71% across the band while the measurement on the vehicle has an average of 69%.

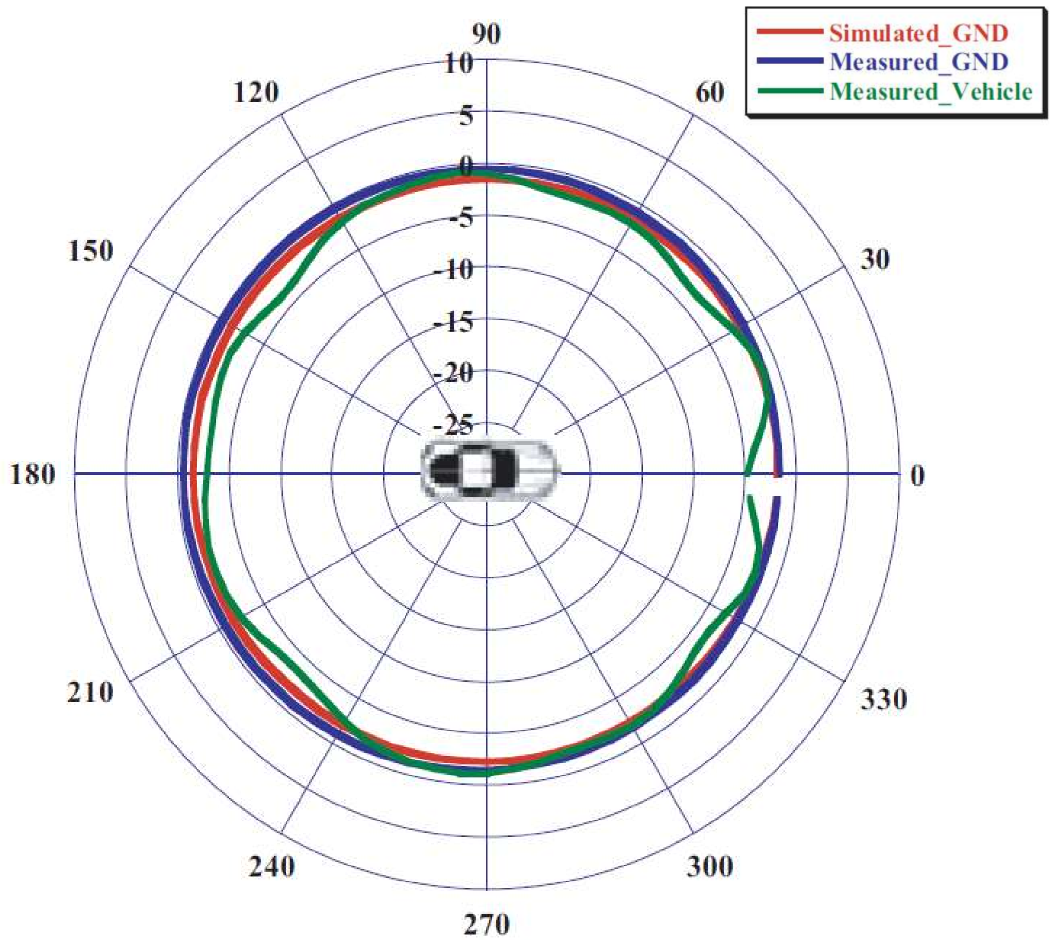

(a)

Figure 2.6. Radiation pattern of simulated, measured on GND, and measured on vehicle gain in (dBi) at 80 deg. of elevation at frequencies: (a) 617 MHz, (b) 1900 MHz, (c) 3600 MHz, and (d) 5000 MHz.

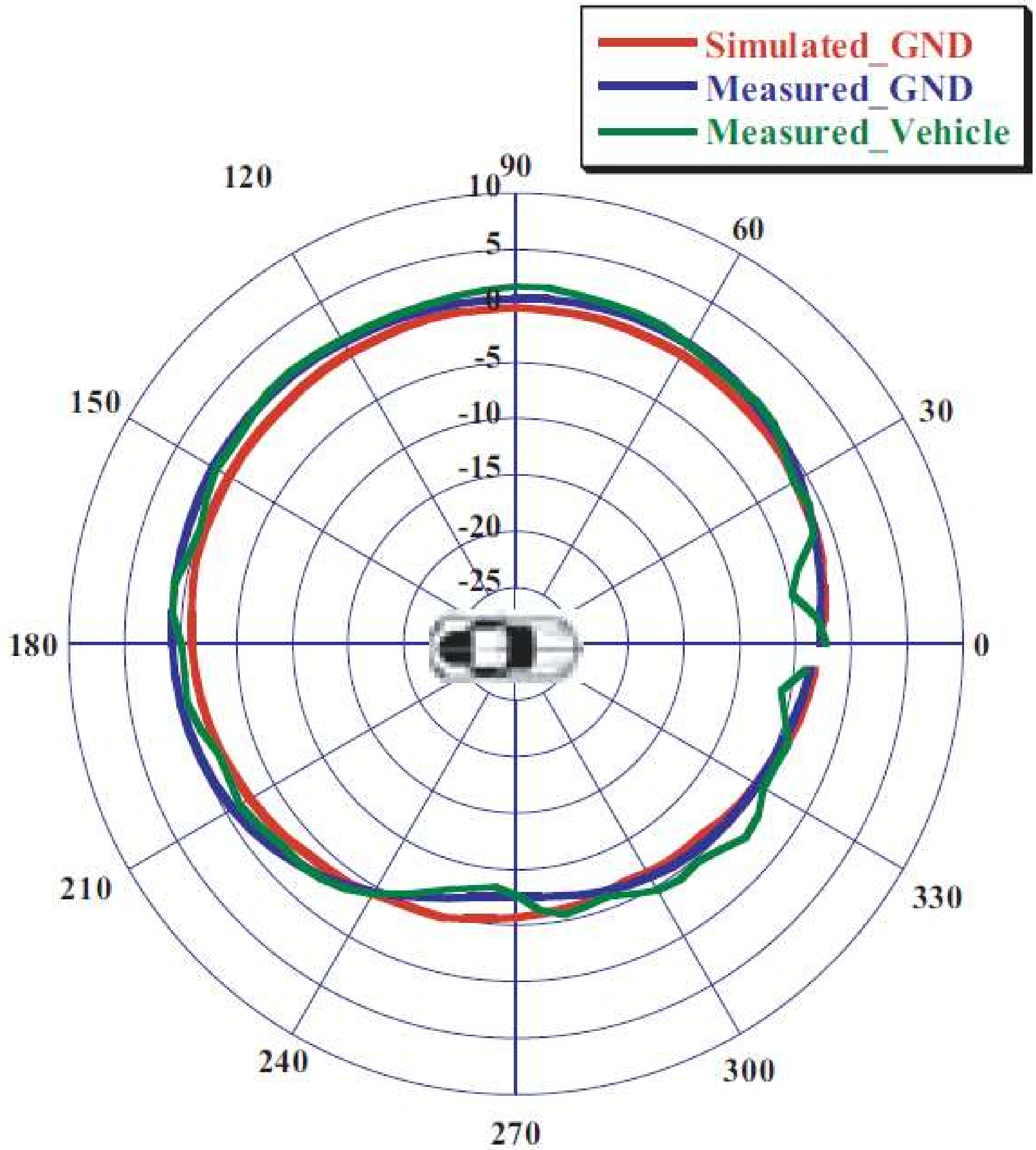

(b)

Figure 2.6. Continued.

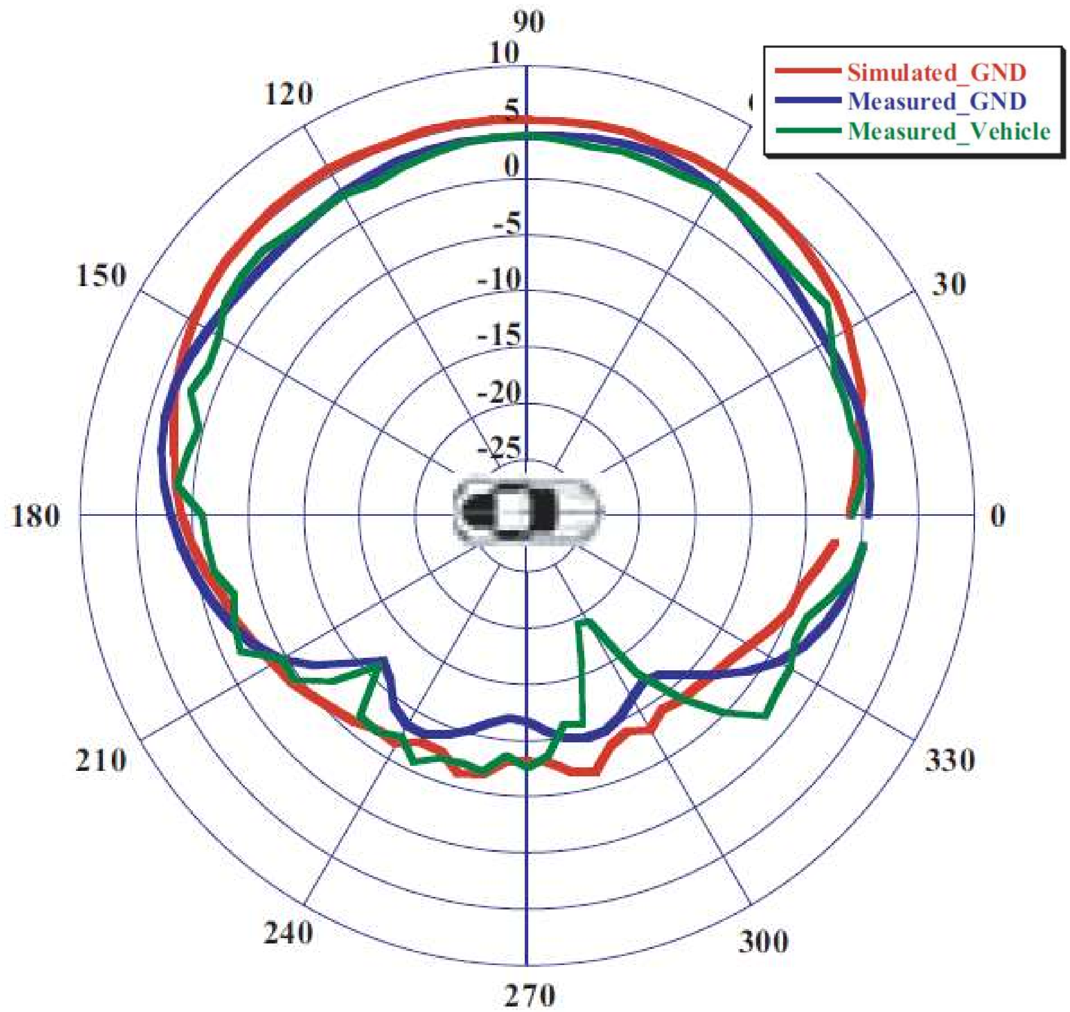

(c)

Figure 2.6. Continued.

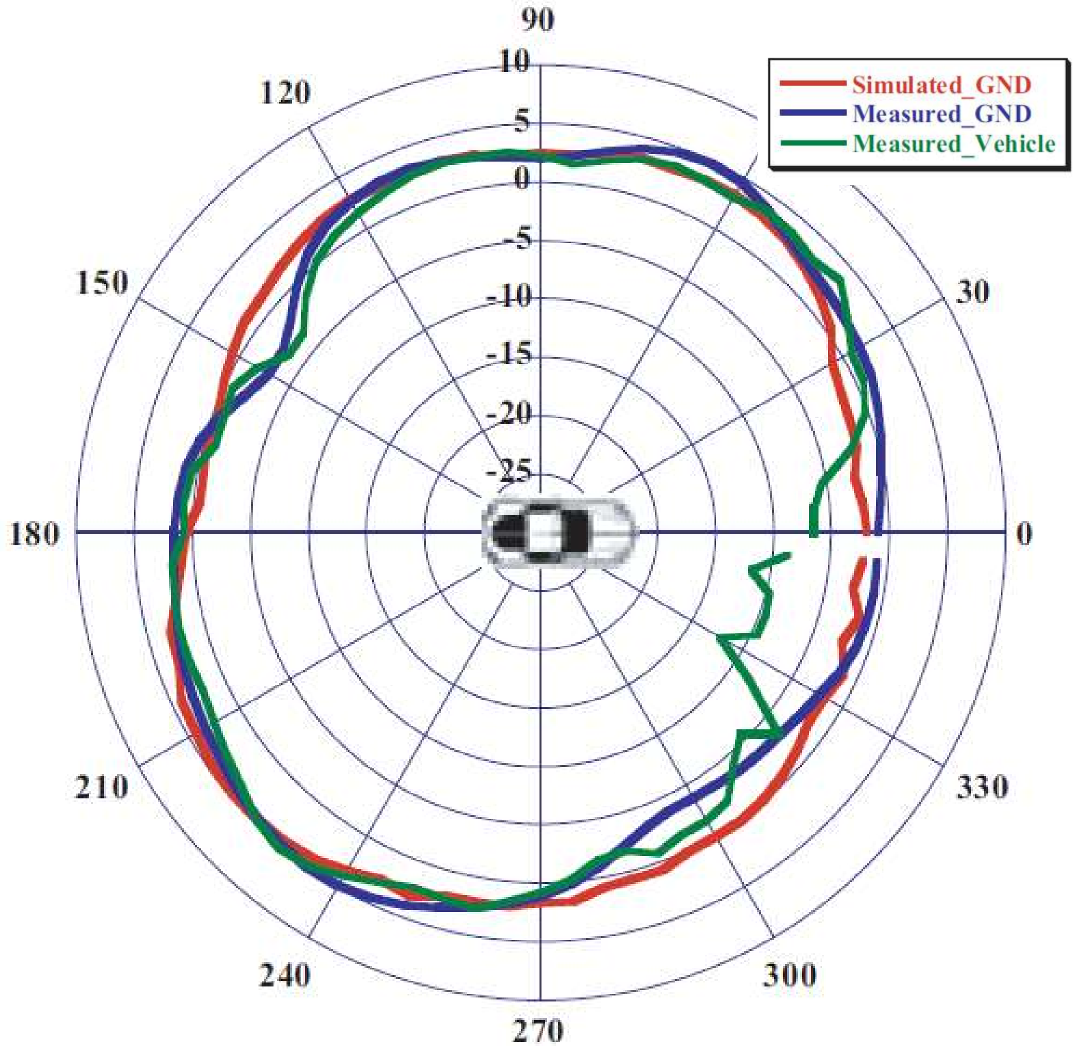

(d)

Figure 2.6. Continued.

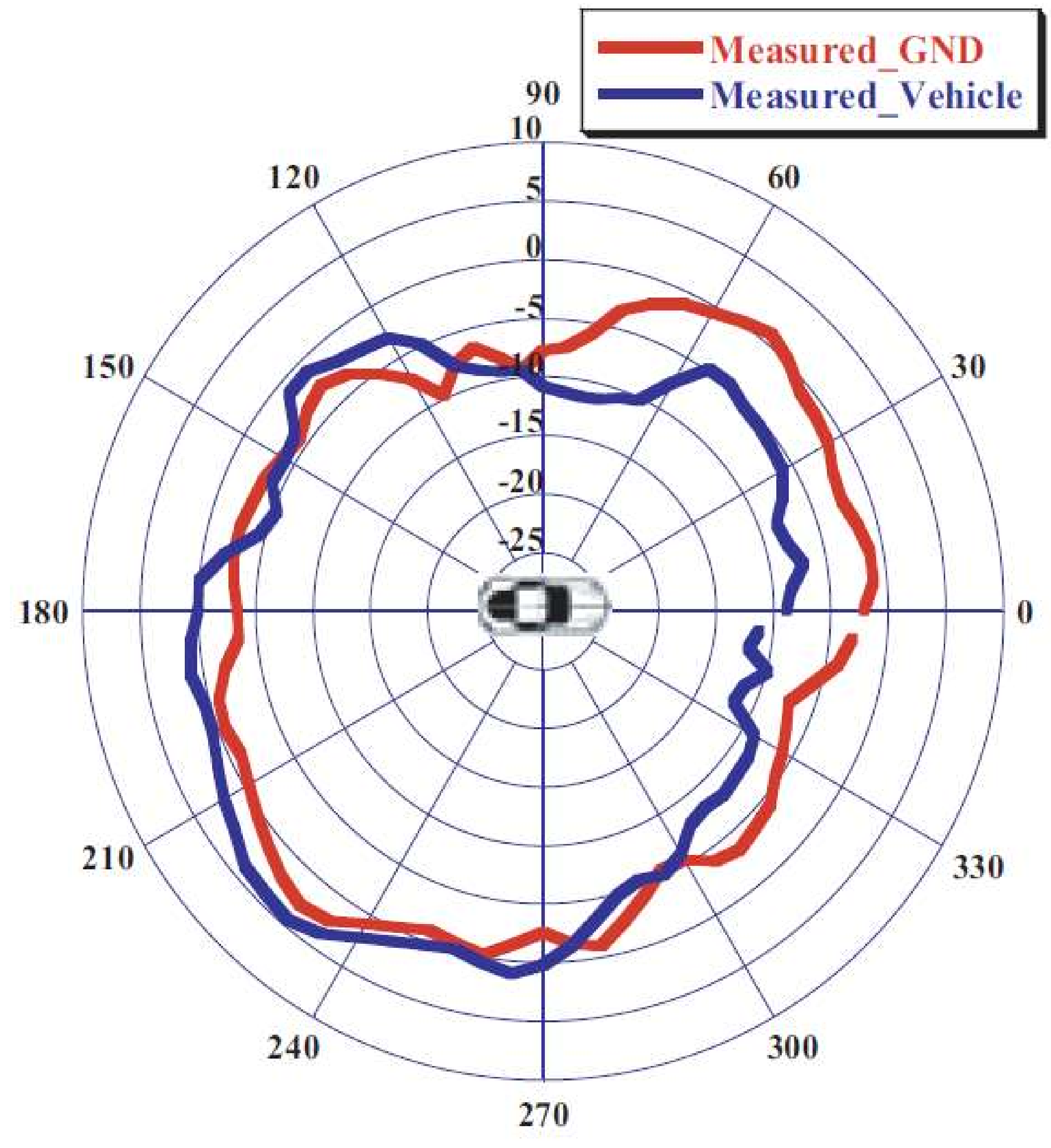

(a)

Figure 2.7. Gain in (dBi) radiation pattern measured on GND and on vehicle at 90 degrees of elevation at 5.9GHz frequency.

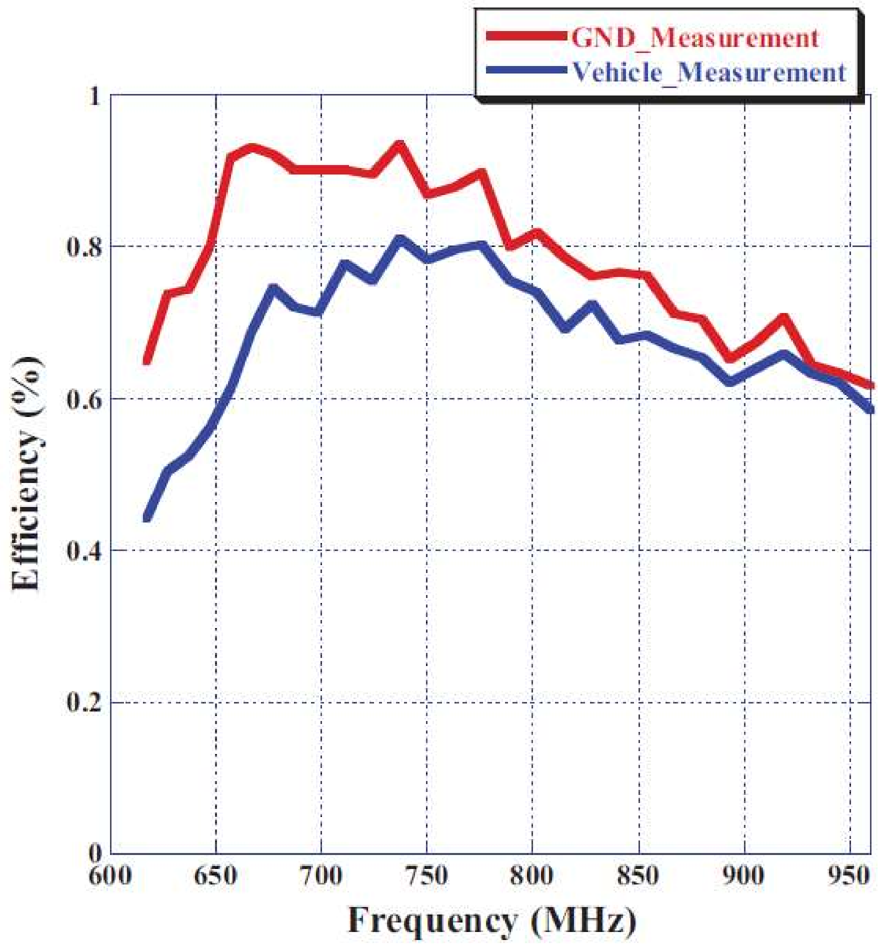

(a)

Figure 2.8. Antenna efficiency measured on ground plane and on vehicle for 5G and V2X frequencies: (a) 617 MHz–960 MHz, (b) 1710 MHz–2690 MHz, (c) 3400 MHz–5000 MHz, (d) 5850 MHz–5925 MHz.

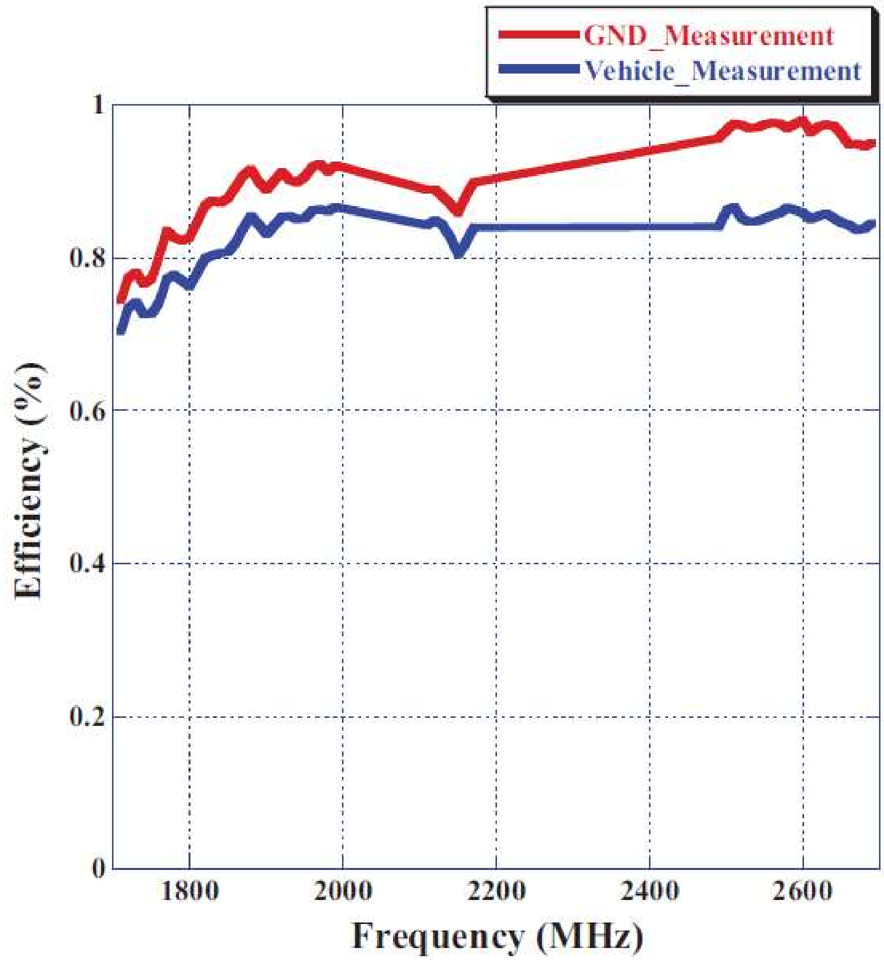

(b)

Figure 2.8. Continued.

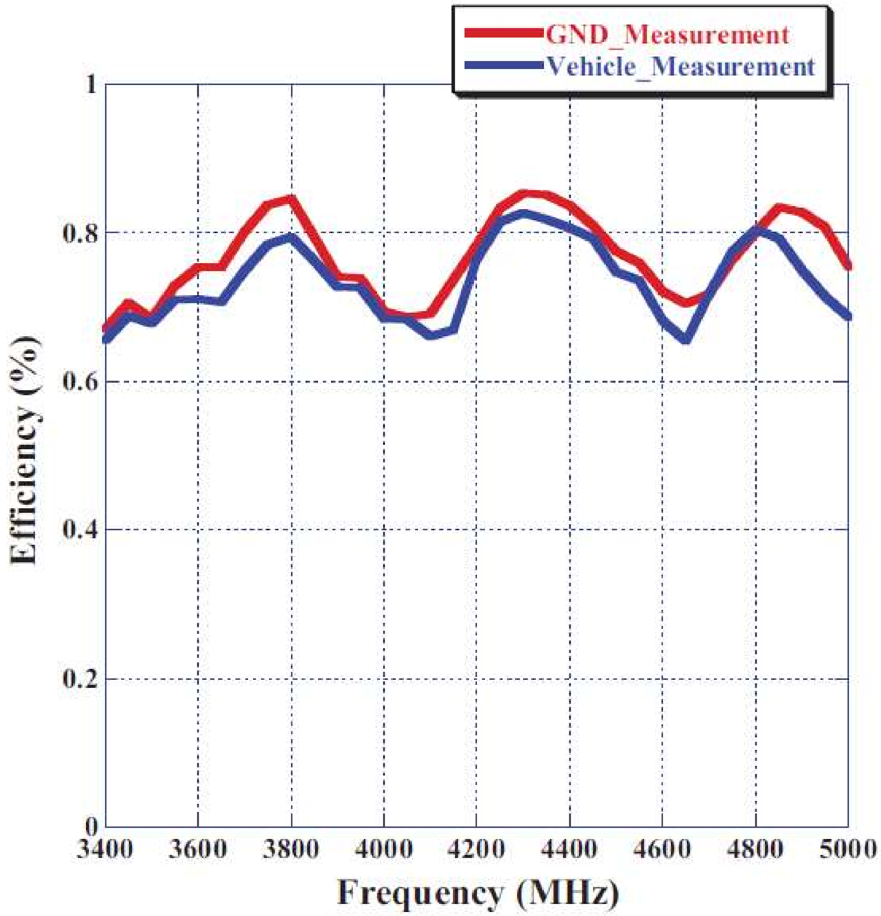

(c)

Figure 2.8. Continued.

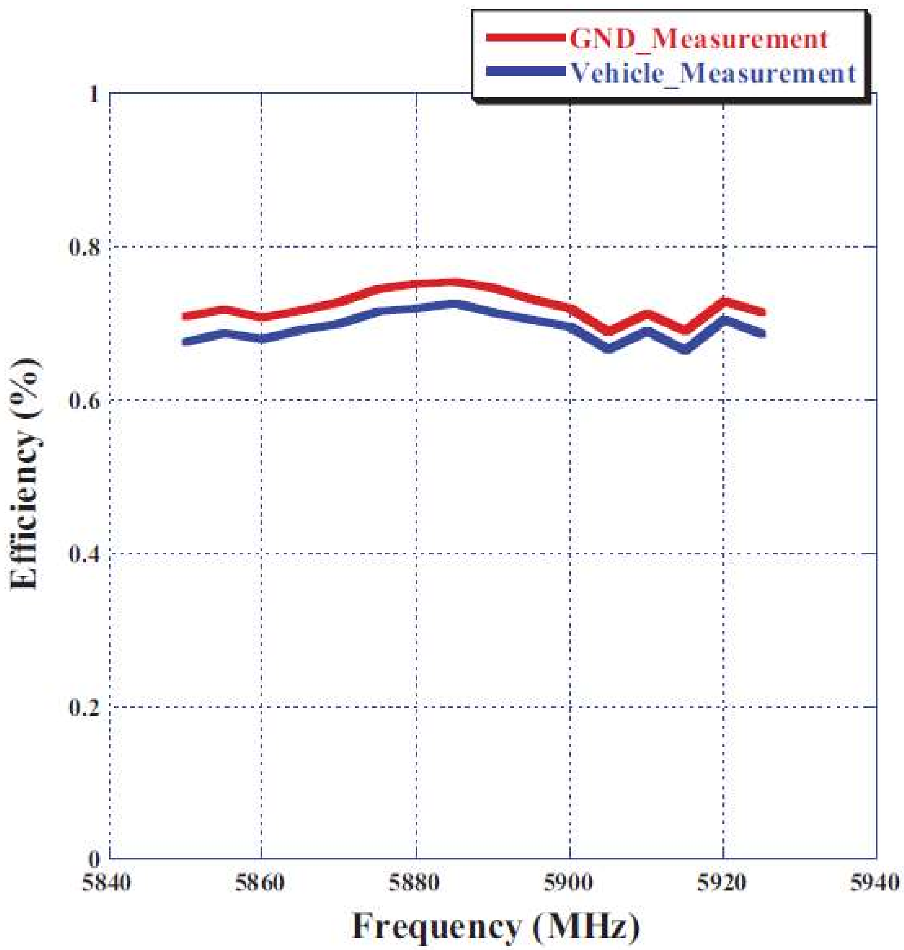

(d)

Figure 2.8.   Continued.

Linear Average Gain (LAG) across different elevations is a significant method to validate the performance of 5G/V2X antennas. LAG is computed by calculating the average summation across the azimuth (phi) of LAG at every theta angle from 75 to 87 degrees across the whole frequency band then converting the results to dBi by using the formula (2.2):

$$\text{LAG (dBi,f)} = 10^{*} \log \text{(average gain across phi)} \tag{2.2}$$

The elevation angles from 75 to 87 degrees presents the incident angles of RF signals from cellular towers that gets received by the antenna. Figures 2.9. (a), (b), and (c) show the LAG measured across all frequency bands from 75 to 87 degrees of theta. In general, vehicle LAG is slightly lower than GND LAG; however, both measurements perform better than −2dBi across the entire band, with most of the frequency range measuring positive values which indicate a good antenna performance. Figure 2.10. shows the LAG measured for V2X frequencies across elevation angles 80 to 96 degrees. The vehicle’s LAG is slightly better in this case than the GND LAG, and this results from below the horizon angles (91–96 degrees). The ground plane at these angles is blocking the signal path to the antenna, while on vehicle this effect is less because of the vehicle’s roof and curvature. However, it can be noted that in both measurements, the LAG values are better than −0.87 dBi across all frequency points.

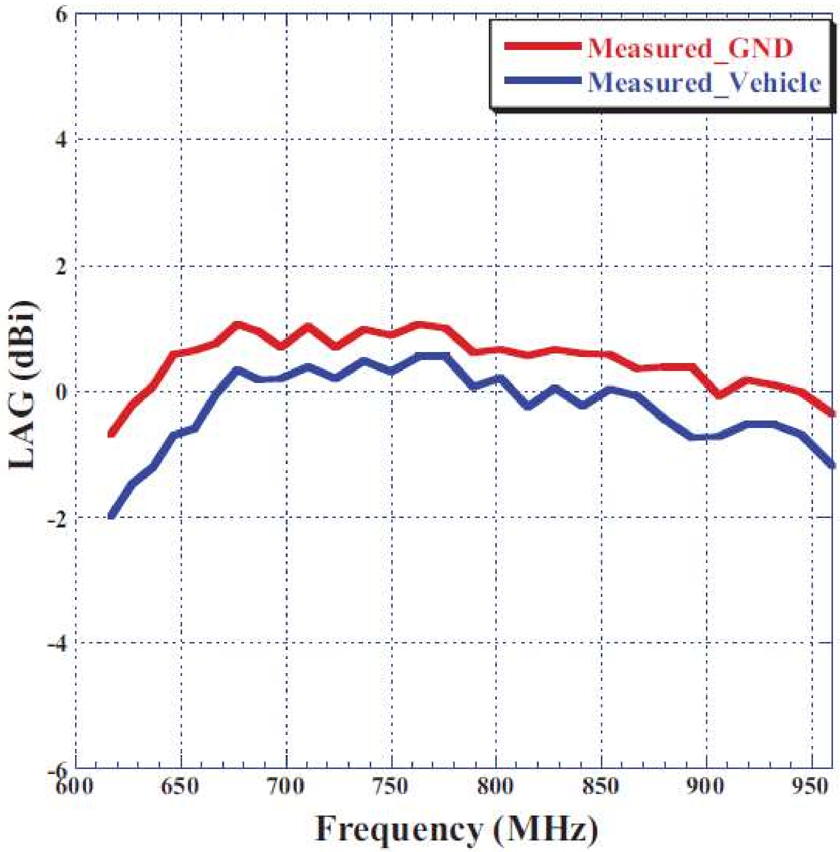

(a)

Figure 2.9. Measured LAG in (dBi) on GND and on vehicle for 5G frequencies from theta equals 75 to 87 degrees: (a) 617 MHz–960 MHz, (b) 1710 MHz–2690 MHz, (c) 3400 MHz–5000 MHz.

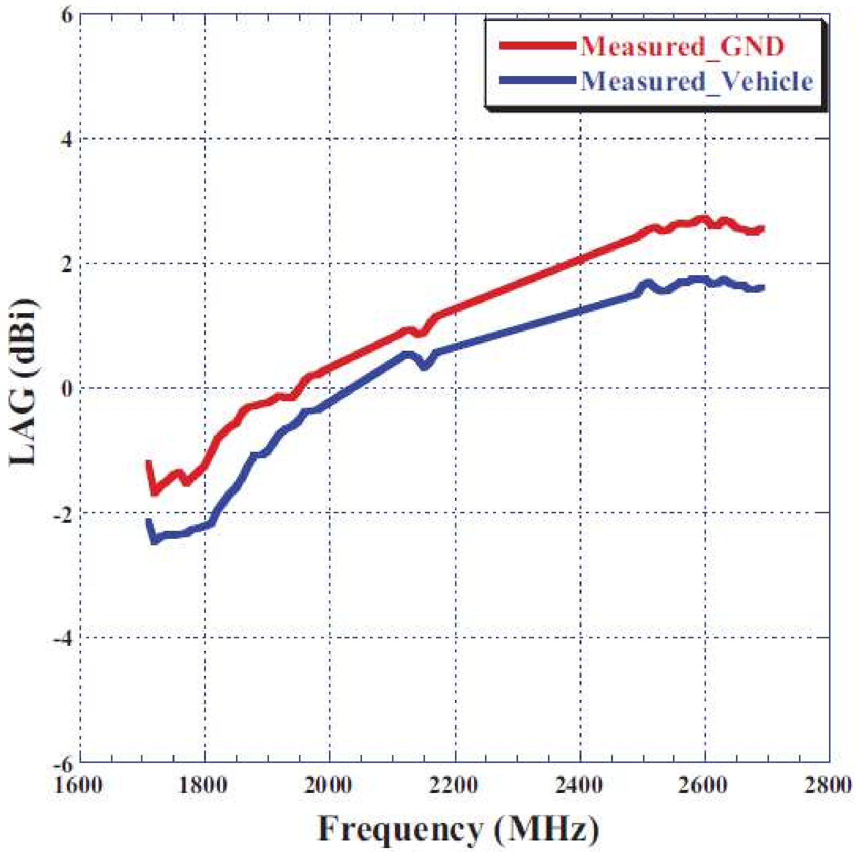

(b)

Figure 2.9. Continued.

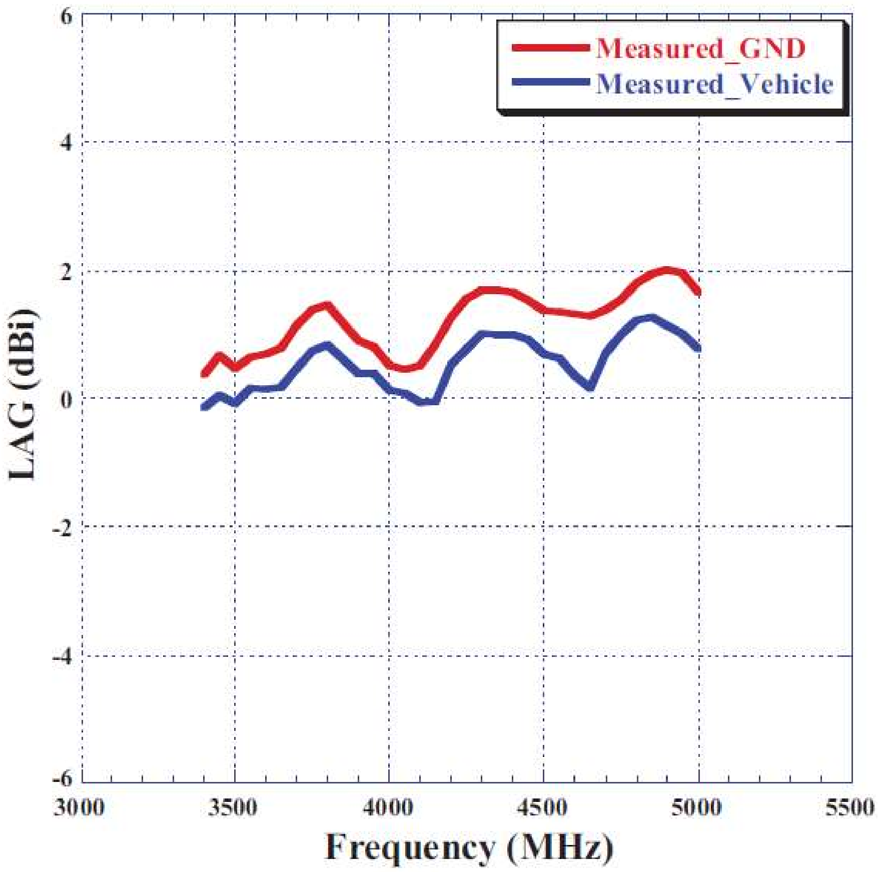

(c)

Figure 2.9. Continued.

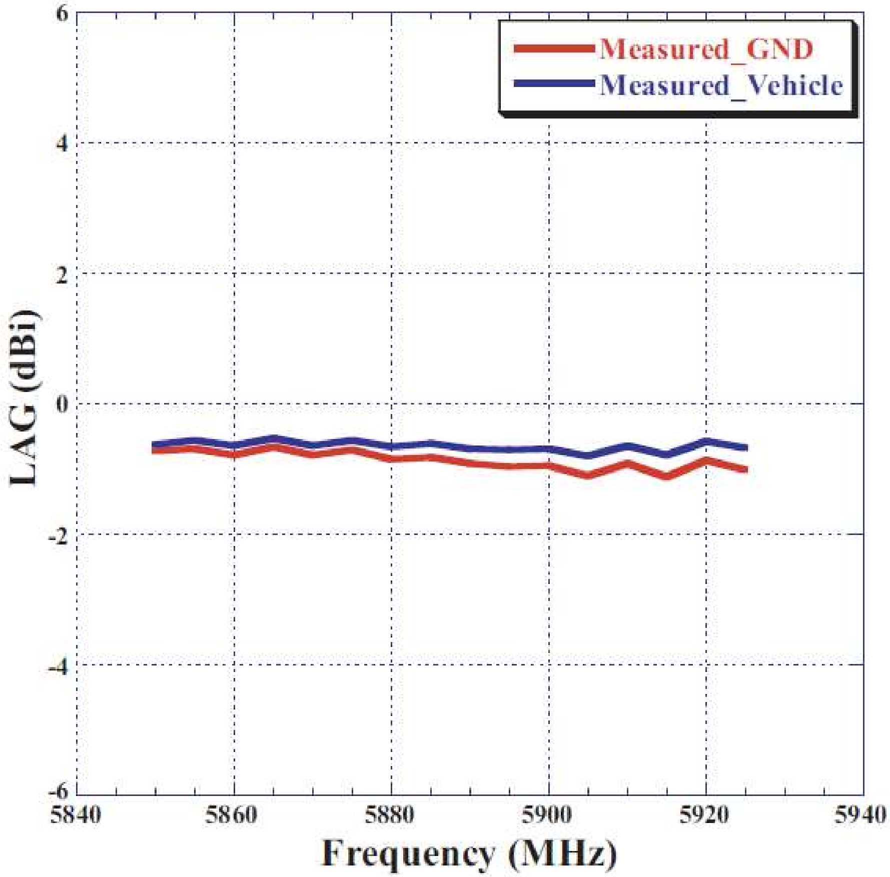

Figure 2.10. Measured LAG in (dBi) on GND and on vehicle for DSRC frequencies from theta equals 80 to 96 degrees.

The findings in this section show that the proposed antenna in this research performs very well in terms of radiation efficiency, vertical linear gain, and matching properties, all of which are in line with the OEM design objectives and requirements indicated in Table 2.2. The results also show a good alignment between simulation measurements which shows a good analysis of the design. The following section presents a parametric investigation of various geometrical parameters of the design.

2.4 Parametric Analysis

In this section, parametric study of significant geometrical parameters and features in the antenna design is presented using simulation. In reference to Figure 2.1. and Figure 2.2, the parameters that are investigated include:

- Height of element H
- Length of the element L
- Width of the element W
- Width of the rectangular feeding plate W_f
- Width of the shorting pin Ws
- Length and width of slot 1 (S_{1L}, S_{1w})
- Length and width of slot 2 (S_{2L}, S_{2w}).

Figure 2.11. shows the variation of VSWR for three different values of H including 23 mm, 28 mm, and 33mm. It can be noticed that parameter H influences low and high frequency bands. This is because decreasing height H will reduce the volume of the antenna, and hence operating bandwidth is less especially in the low band region. Also, reducing the height will tune the antenna towards higher frequencies for both low

and high frequency bands as can be seen in Figure 2.11. Choosing the value 28mm for (*H*) is optimal to meet the size limitation requirement with acceptable RF performance.

Furthermore, changing the value of parameter *L* has a significant role in the low frequency bands. As shown in Figure 2.12, increasing the value of *L* will support a bigger wavelength current in the low frequency band which will improve VSWR at 617MHz at the expense of higher VSWR at 960MHz.

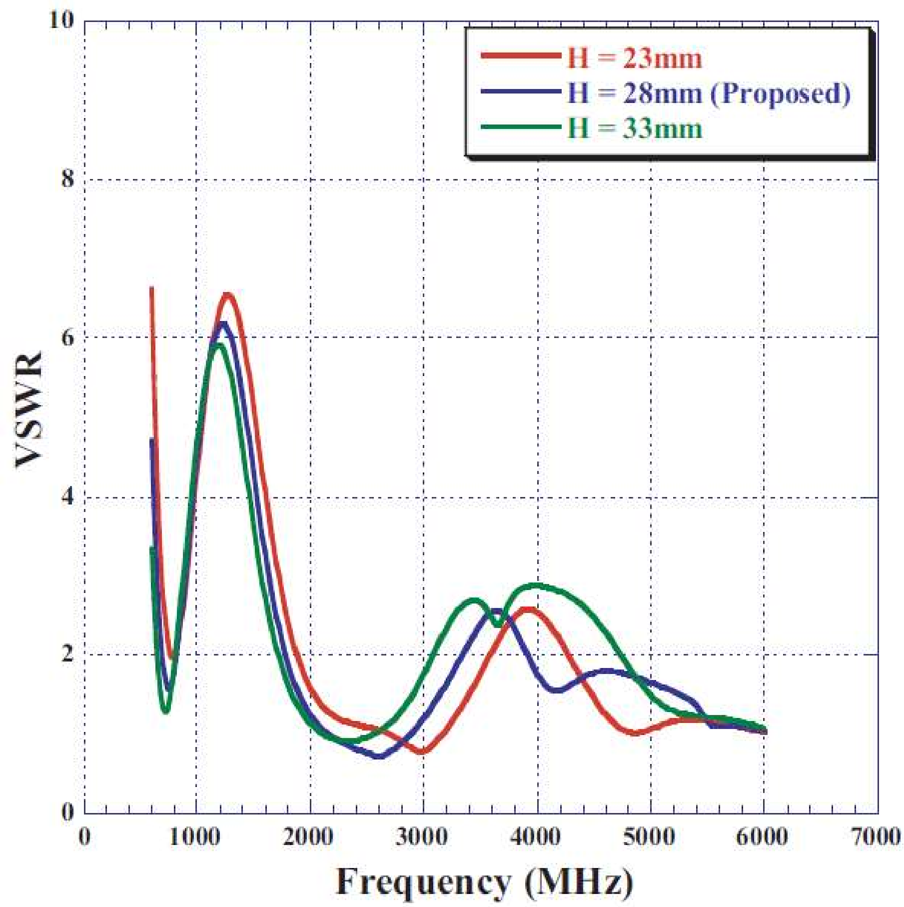

Figure 2.11. VSWR of varying the height of the element *H*.

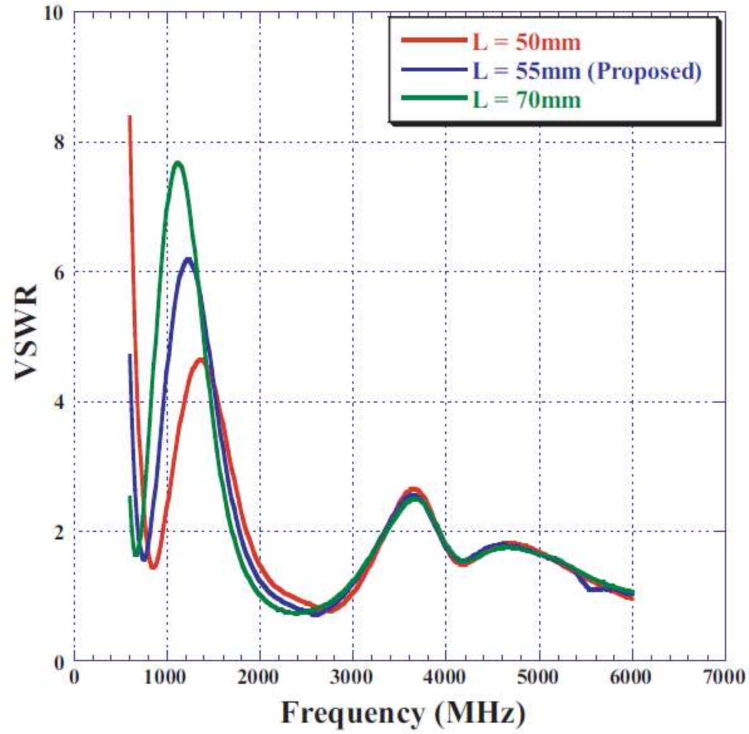

Figure 2.12. VSWR of varying the length of the element *L*.

In Figure 2.13, the width of the element *W* is analysed for three different values: 40mm, 50mm, and 60mm. The parameter *W* has a significant effect across the entire operating bands since the location of the shorting pin changes. It can be concluded that reducing the width of the element will reduce the volume of the antenna structure and hence decreases the bandwidth especially at the low band (617 MHz–960 MHz). Reducing *W* also influences the VSWR at the high band since the shorting pin gets closer to slot 2. It can be found that a value of 50mm as proposed in this antenna is optimal for performance and physical size.

The width of the rectangular feeding plate W_f has a role in slightly changing the resonance frequency in the low band as calculated in Equation (2.1). It also has an important role in specifying the bandwidth of the higher bands as shown in Figure 2.14.

Reducing the width of the feeding plate tunes the antenna lower in frequency and reduces the operating bandwidth across the whole range. Hence, choosing W_f to be 29.5mm is suitable for antenna impedance and physical width of the element.

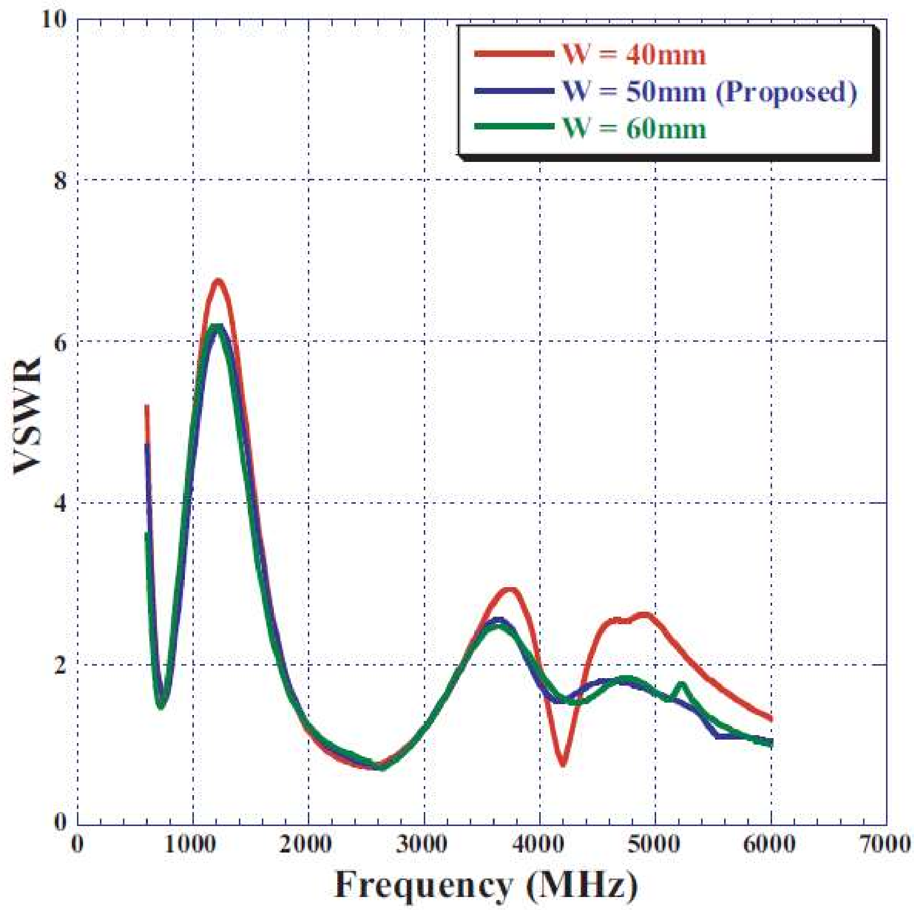

Figure 2.13. VSWR of varying the width of the element *W*.

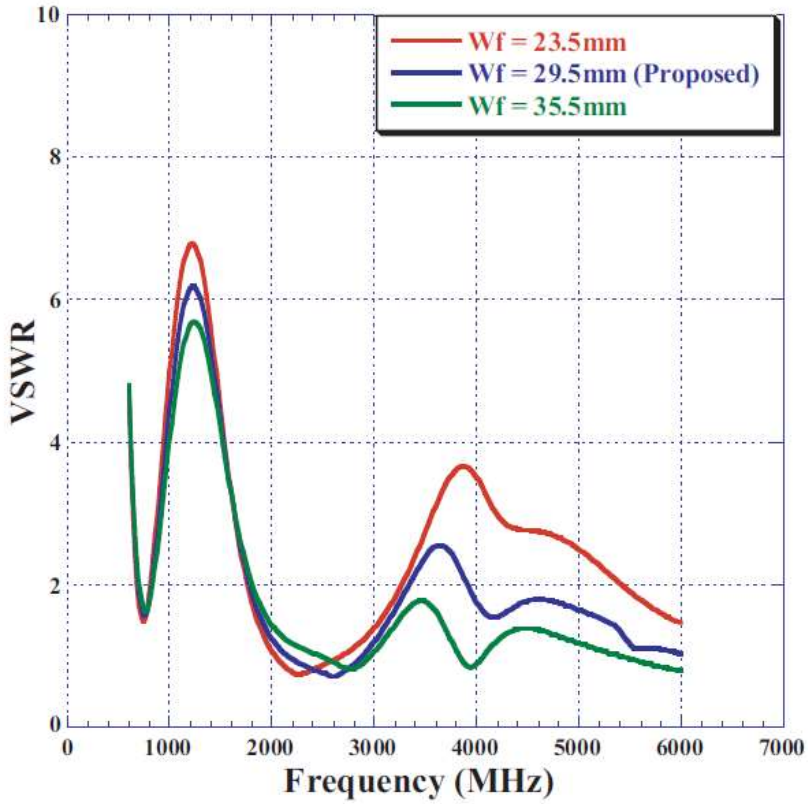

Figure 2.14. VSWR of varying the width of the feeding plate W_f.

Figure 2.15. shows the effect of changing the width of the shorting pin *Ws*. Equation (2.1) shows that *Ws* influences the resonance frequency of the low band. As shown in Figure 2.15, changing the width of the shorting pin among 3 mm, 6 mm, and 9mm does not have a major effect on the high bands, but it shifts the resonance frequency in the low band. In Figure 2.15.(b), it can be noticed that increasing the width of the shorting pin tunes the antenna higher in frequency. Hence, choosing *Ws* to be 6mm is optimal to balance the VSWR across low band frequency range.

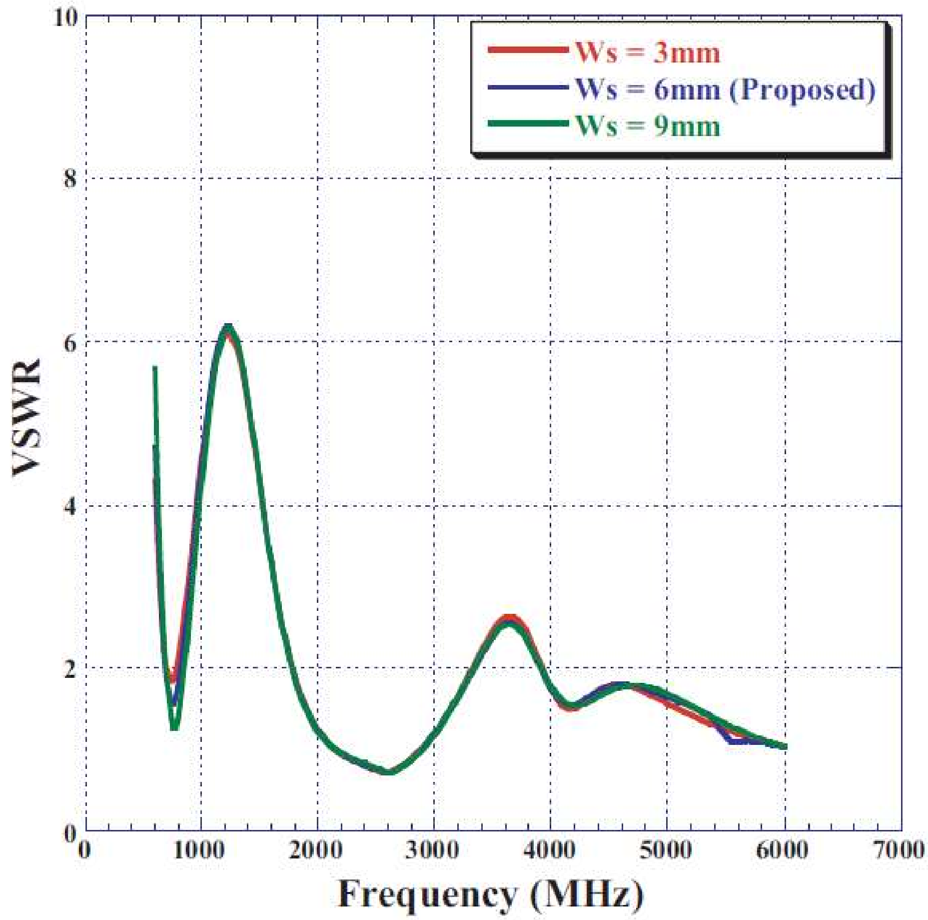

(a)

Figure 2.15. VSWR of varying the width of the feeding plate *Ws*: (a) across low and high band, (b) across low frequency band (617 MHz–960 MHz).

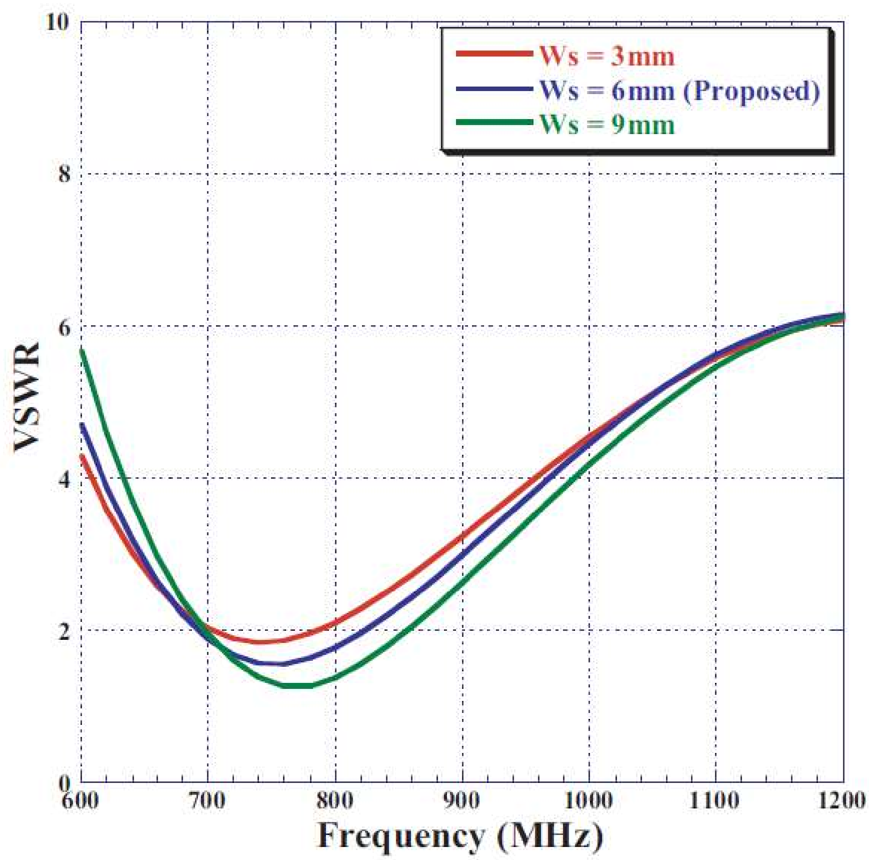

(b)

Figure 2.15. Continued.

To study the effect of changing the length and width of slot 1, S_{1L} and S_{1w}, one parameter is changed at a time while the other one remains at its proposed value. It is observed from Figure 2.16 and Figure 2.17 that varying these parameters will mainly affect the VSWR in the high frequency band. So, choosing S_{1L} and S_{1w} to be 28mm and 11mm respectively will balance the VSWR across the middle frequency bands.

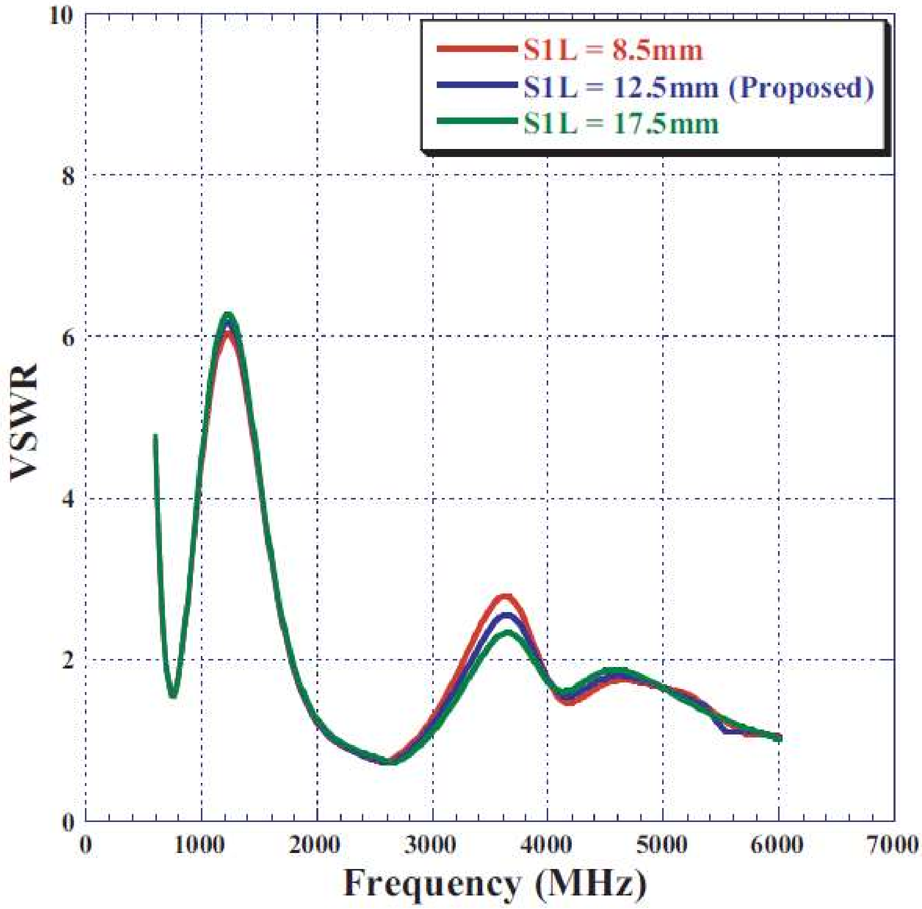

Figure 2.16. VSWR of varying slot 1 length S_{1L}.

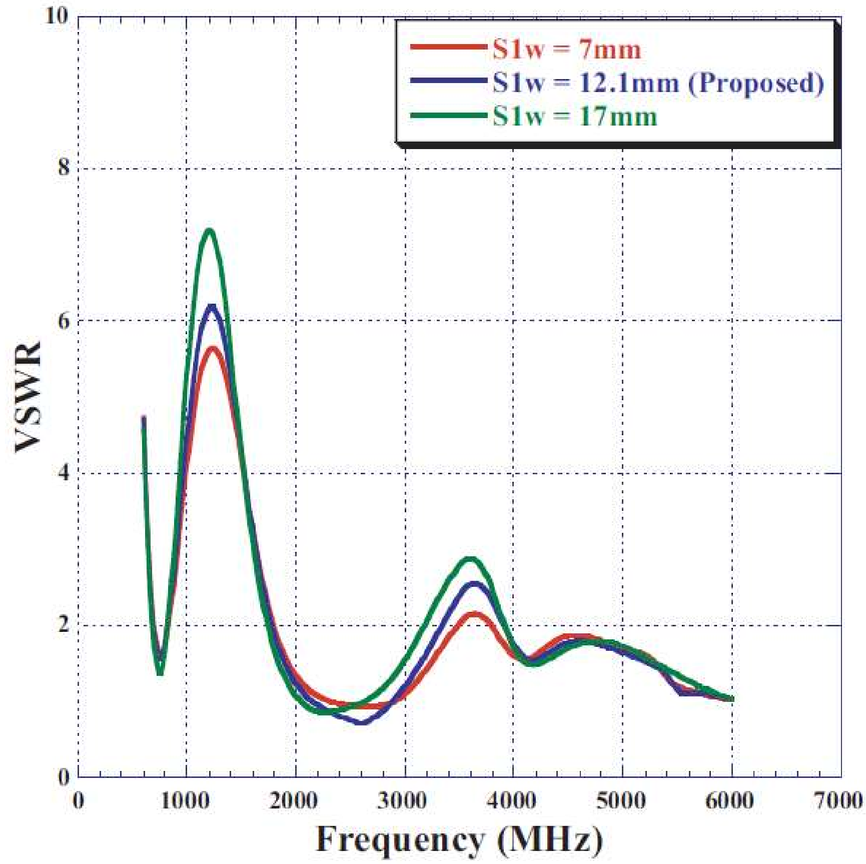

Figure 2.17. VSWR of varying slot 1 width S_{1w}.

Figures 2.18. and 2.19 show the effect of changing the width and length of slot 2 on the VSWR. With reference to Equation (2.1), slot 2 dimensions control the distance between the feeding plate and the shorting pin, so they influence the low band resonance frequency. Figure 2.18. and Figure 2.19 also show the effect on the 5G high frequency and V2X bands as the shorting pin location changes with slot 2 dimensions. Figure 2.20 shows the effect of parameter varying of slot 2 on the V2X gain pattern. It can be concluded that reducing the dimensions of slot 2 will introduce more losses going through the shorting pin since the current will have a faster path to ground. Therefore, choosing slot 2 parameters as proposed will balance the VSWR curve and have a reasonable radiation pattern at V2X frequencies.

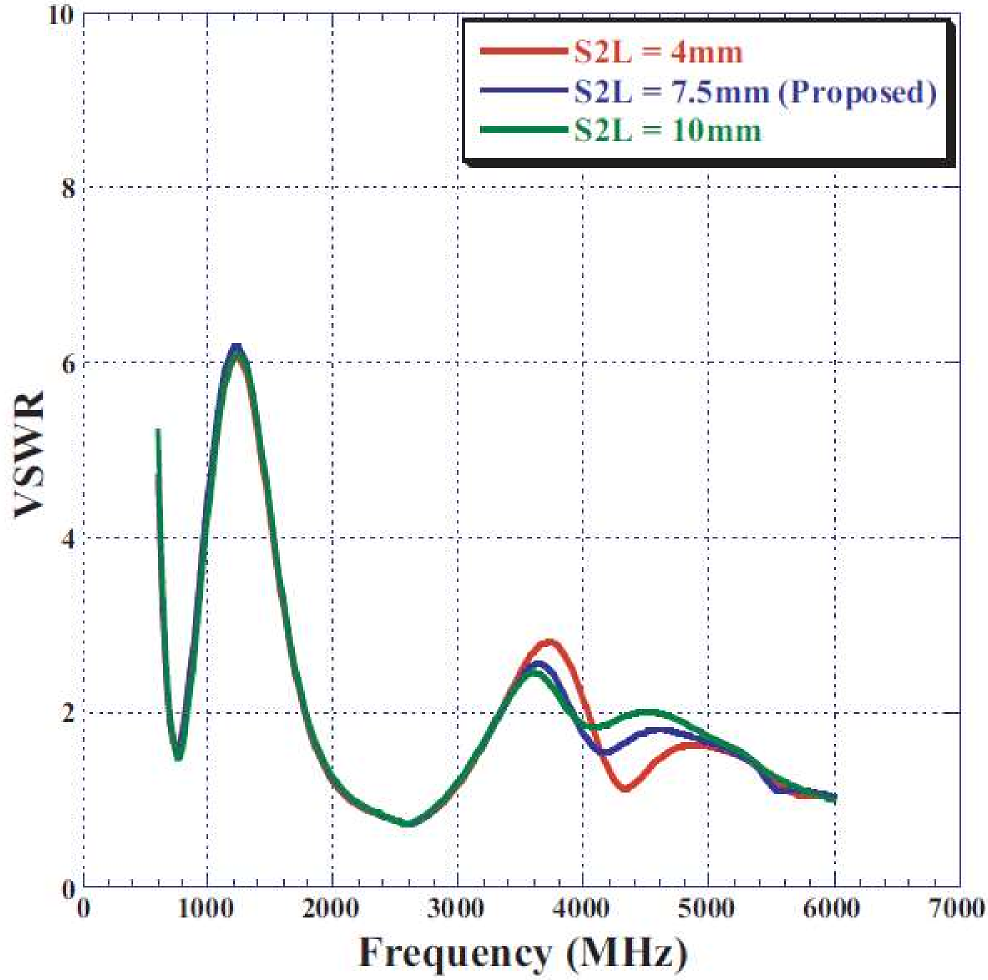

Figure 2.18. VSWR of varying slot 2 length S_{2L}.

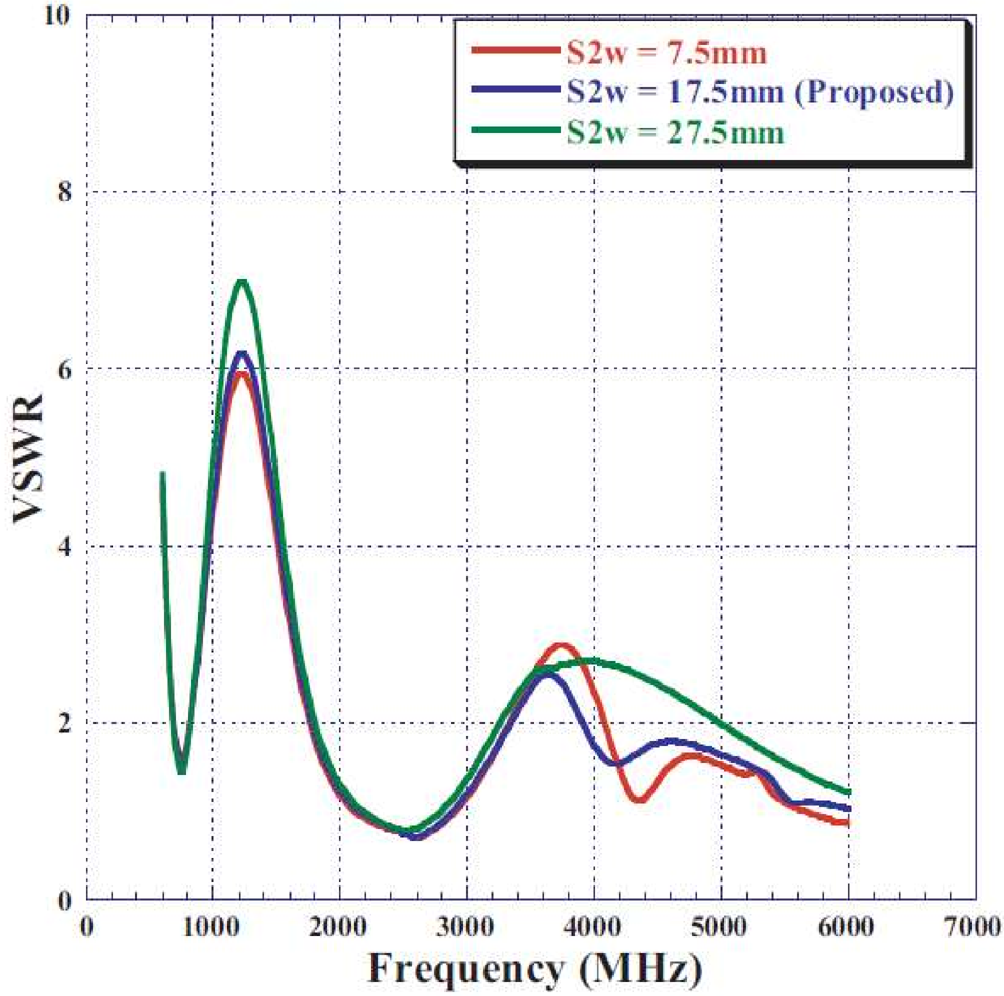

Figure 2.19. VSWR of varying slot 2 length S_{2w}.

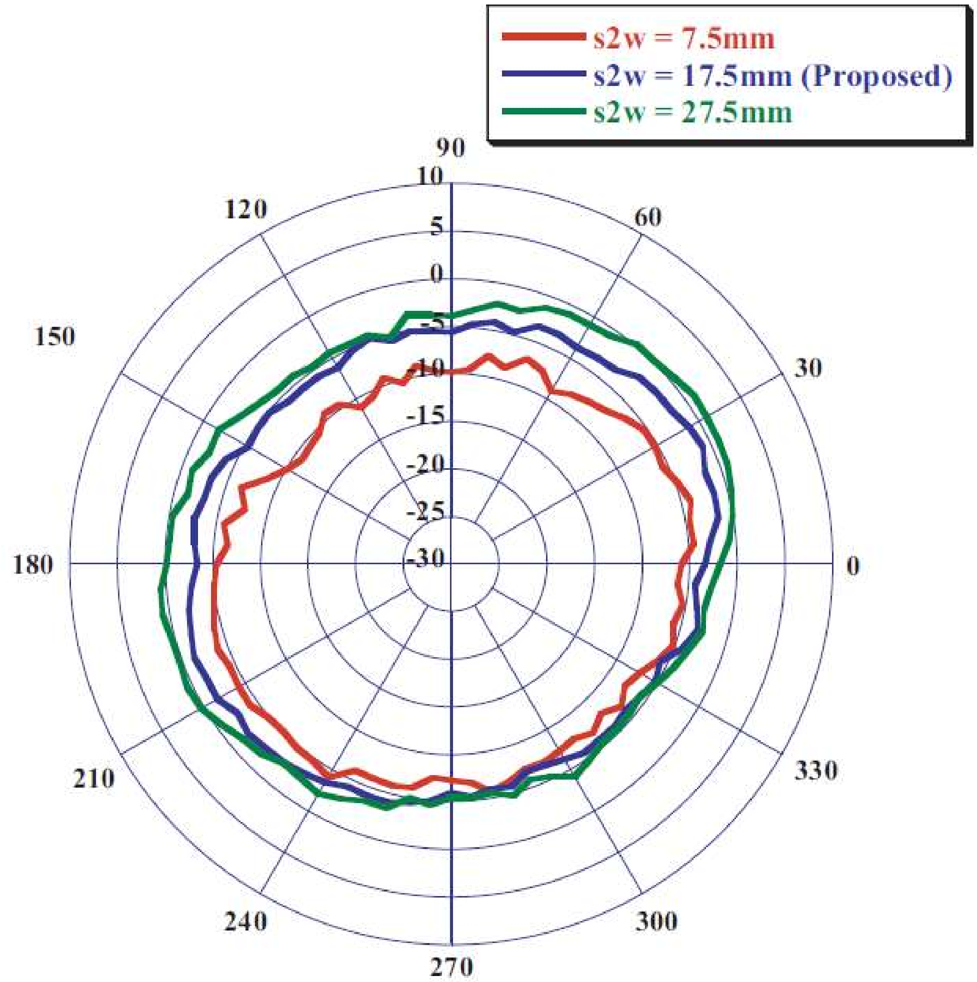

(a)

Figure 2.20. V2X radiation pattern at 5.9GHz varying slot 2 dimensions: (a) varying slot 2 width (S_{2w}), and (b) varying slot 2 length (S_{2L}).

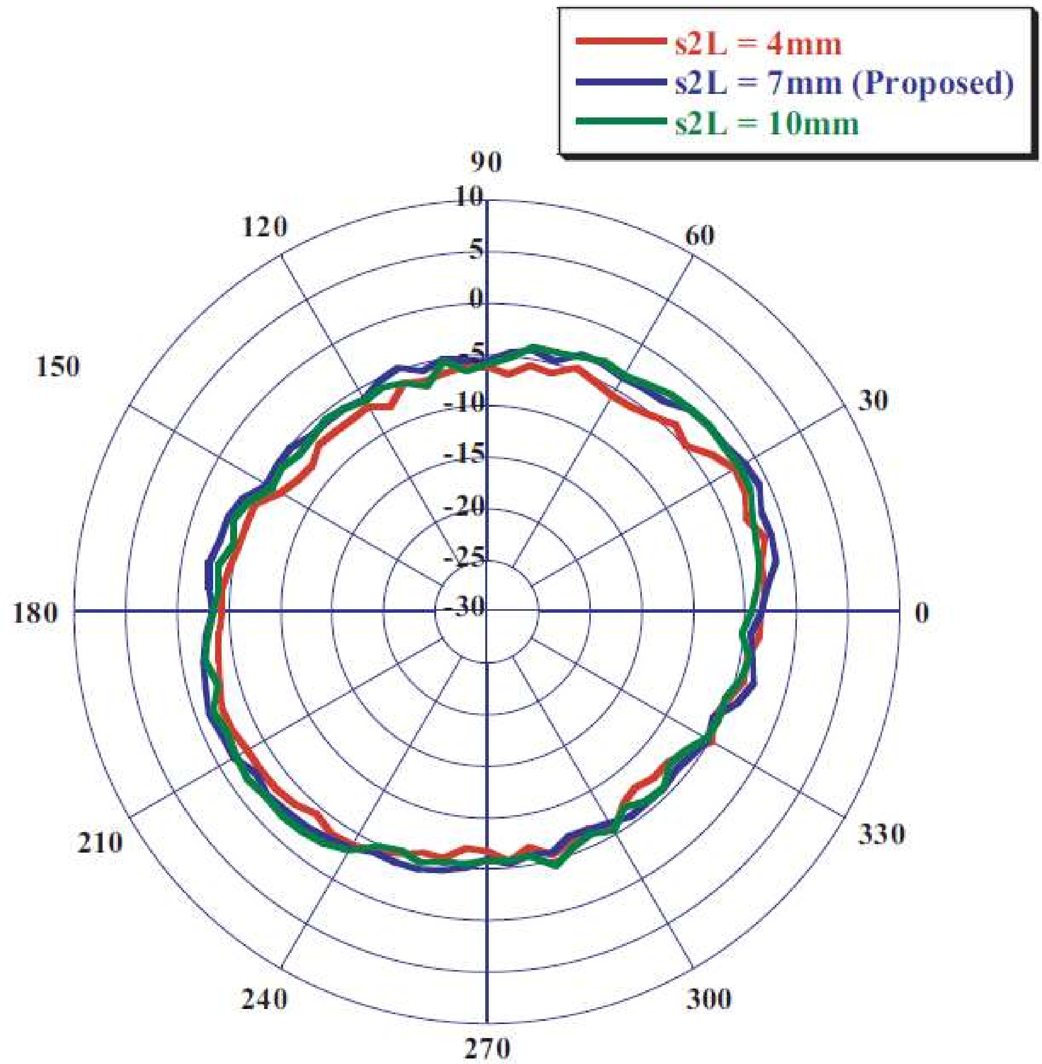

(b)

Figure 2.20. Continued.

In conclusion, the unique geometrical parameters of the PIFA design were thoroughly investigated and related to the antenna's performance. In the APPENDIX section in Table A.1, the designed antenna in this research is contrasted with relevant work in literature in the automotive industry.

2.5 Conclusions

A low-profile wideband antenna has been presented in this work which functions across 5G frequency bands from 617 MHz to 5GHz and across V2X bands from 5850 MHz to 5925 MHz. It consists of a wide rectangular plate at the feeding pin with two cut slots to control high frequency bands and a shorting pin for low frequency bands. The antenna is simulated using the HFSS simulation tool, then measured on a 1-meter rolled-edge GND and on a testing vehicle inside an anechoic chamber. The measurements show a VSWR better than (3.3 : 1) and an average efficiency of 83% on a GND and 72% on the vehicle for 5G frequencies while V2X frequencies have an average efficiency of 71% on GND and 69% on vehicle. LAG of the antenna was measured and has a performance better than -2 dBi across the entire band of 5G/V2X for theta angles from 75-87 degrees. Geometric analysis of different parameters of the design were investigated and the effect of each parameter on antenna performance was shown. It can be concluded that based on the parametric study, the design is resilient and can be manufactured easily with reasonable tolerances. In general, the proposed antenna is a good candidate for low-profile antenna applications on vehicle or shark-fin housing. Future work will be focused on developing a 5G/V2X MIMO system that will provide diversity, increased capacity, and higher throughput.

CHAPTER THREE

5G COMPACT 2x2 AUTOMOTIVE MIMO ANTENNA SYSTEMS

3.1 Introduction

Introducing multiple-input multiple-output (MIMO) systems for cellular 5G and vehicle-to-everything (V2X) applications is essential to meet the requirements of the upcoming autonomous wireless communication systems in the automotive industry. The MIMO system consists of multiple antennas at receiver and transmitter sides which allow it to increase the channel capacity, data rate, and the total throughput of the system without increasing the operating frequency band or the transmit power [39]. The MIMO system also has the benefits of high reliability and low latency in a high electromagnetic scattering environment by using multiple antenna elements that transmit and/or receive independent channels assuming that these elements are highly isolated or uncorrelated [40]. The performance of the MIMO system is highly dependable on the efficient design of the MIMO antennas that should have low correlation between them and a high total antenna efficiency [41] [42].

The following section of this chapter presents performance measures for MIMO antenna systems and multiple low-profile 5G MIMO implementations.

3.2 Key Performance Parameters for MIMO Systems

3.2.1 Envelope Correlation Coefficient (ECC)

The envelope correlation coefficient (ECC) is a key performance metric used to describe the amount of correlation being added to RF channels by the MIMO antenna system. Hence, a low value of ECC (i.e., high isolation between antenna elements) is needed to achieve the requirements of the MIMO antenna diversity. In [43], the authors describe three main ways to calculate the ECC. The first method uses only the S-parameters of the antenna elements and assumes that the antennas are lossless which in practice would not yield accurate results since most antennas are lossy. The second method also uses the S-parameters of the antenna elements, but it adds port efficiencies of each antenna which gives a more practical result. However, this improvement only works when the efficiency of each antenna element is better than 60%. The third method, which is used in this work, analyzes the radiation patterns of the electric field of each antenna element and the spatial power distribution of the signal to calculate the ECC which gives more accurate and effective results than the first two methods [43].

In [41] and [43], the authors present an accurate and effective method to calculate ECC by using the electrical radiation pattern of each antenna element measured at certain azimuth and elevation angles, and can be summarized in equation (3.1) [41] [43]:

$$\rho_{e,ij} = \left| \frac{\int_0^{2\pi}\int_0^{\pi}(XPR\,.\,E_{\theta i}\,.\,E_{\theta j}^{*}\,.\,P_{\theta}\,+\,XPR\,.\,E_{\phi i}\,.\,E_{\phi j}^{*}\,.\,P_{\phi})\sin(\theta)\,d\theta d\phi}{\sqrt{\prod_{k=i,j}\int_0^{2\pi}\int_0^{\pi}\left(XPR\,.\,E_{\theta k}\,.\,E_{\theta k}^{*}\,.\,P_{\theta}\,+\,XPR\,.\,E_{\varphi k}\,.\,E_{\varphi k}^{*}\,.\,P_{\phi}\right)\sin(\theta)d\theta d\phi}} \right|^2 \tag{3.1}$$

Where $E_{\theta i}$ and $E_{\theta j}$ are the electric field components in the elevation angle direction while $E_{\varphi i}$ and $E_{\varphi j}$ are the components in the azimuthal angle direction for antennas i and j. XPR is the cross-polarization discrimination factor that shows the difference between horizontal and vertical polarization of the incident wave. P_{θ} and P_{φ} are the power densities for elevation and azimuth angles. Equation (3.1) can be simplified by assuming XPR equals to 1 and the angular power densities are uniform.

3.2.2 Diversity Gain

Another key parameter for measuring the performance of MIMO systems is the DG which is defined as the quantified enhancement in signal-to-noise ratio (SNR) when the signals are being received by the MIMO antennas and is usually calculated in dB. The DG can be calculated in equation (3.2) as [44]:

$$DG = DG_0 * DF * K \qquad (3.2)$$

Where DG_0 is the diversity gain of the ideal case and is equal to 10dB (which represents the selection combiner diversity gain of two ideal elements with 99% reliability [45]). The degradation factor (DF) shows the effect of the ECC on the diversity gain and is computed as: $\sqrt{(1-\rho)}$. K represents the ratio of the mean effective gain (MEG) between the MIMO antenna elements ($K = MEG_i / MEG_j$). MEG is the effective gain ratio at the antenna element which represents the ratio of the received power over the incident power at that element. For a good channel characteristic, the received signal from the MIMO antenna element should satisfy the condition ($K = MEG_i / MEG_j \sim= 1$).

3.3 Performance Analysis of Multiple Vehicular MIMO Systems

In this section, three different configurations for 2x2 MIMO antenna systems are presented. Each configuration is simulated using HFSS software then fabricated from properly cut metal sheets and measured on both a 1-meter rolled-edge ground plane and a vehicle's roof inside an anechoic chamber. After simulation and chamber measurements, the electric field components are extracted to compute the ECC and DG using a MATLAB script with different parametric analyses presented. Table 3.1 shows the general design goals and performance requirements for the automotive MIMO antenna systems in terms of VSWR, passive isolation, port efficiencies, ECC, and DG.

Table 3.1. 5G MIMO antenna system design Goals and requirements.

Parameter	Value
VSWR	3.3 at 5G bands / 2.5 at V2X bands
Passive Isolation	Minimum 10dB across bands
Port Efficiencies	Minimum 40% across bands
ECC / DG	ECC lower than 0.5 / DG higher than 8.66 dB

3.3.1 2x2 PIFA-Based MIMO with Spatial Diversity

The MIMO in this configuration is based on the low-profile PIFA antenna presented in chapter 2. Two PIFA elements were fabricated and orientated in an opposite way (i.e., mirrored in the y-axis) to have a complementary radiation pattern for each element so that the combined pattern will be omnidirectional. The elements are then measured on 1-meter rolled-edge ground and on a vehicle's roof with 600mm distance between them (1.25 lambda of the lowest frequency of operation "617MHz"). Figure 3.1 shows the simulation and vehicle measurement setup of the MIMO system.

The simulated VSWR for each element was captured and compared against the realized antenna measurement as depicted in Figure 3.2. It is noticed that across the operating bands of 5G and V2X, the VSWR is better than 3.3:1 with a reasonable rejection for navigation system frequencies in the GNSS bands. The passive isolation between the two PIFAs is shown in Figure 3.3. The coupling between the two elements is low since they are separated by a relatively long distance (worst case isolation of 26dB).

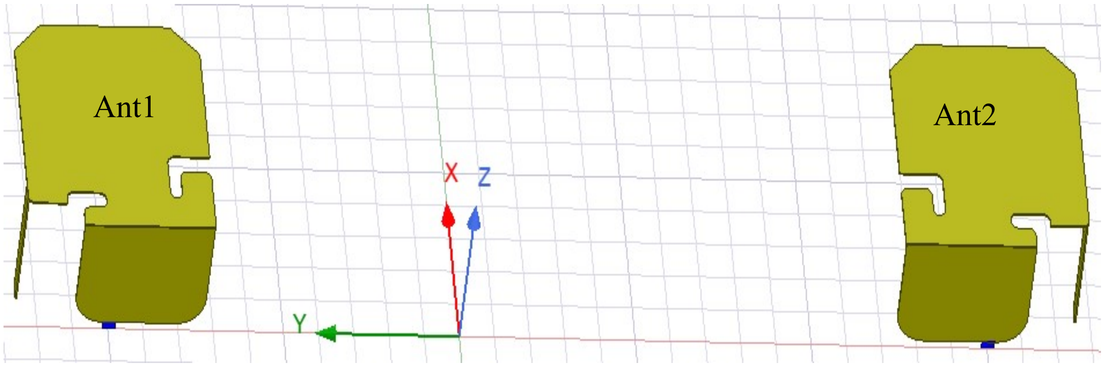

(a)

(b)

Figure 3.1. MIMO Systems Implementation on: (a) Simulation model, and (b) Vehicle's roof.

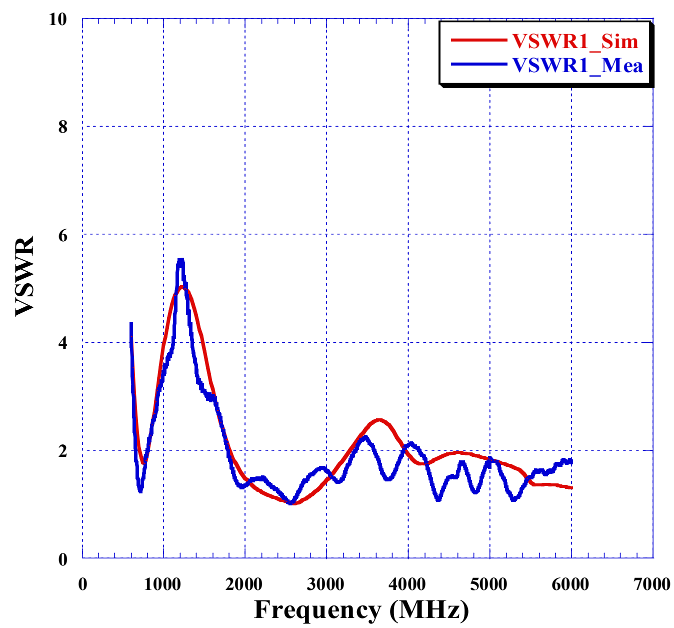

(a)

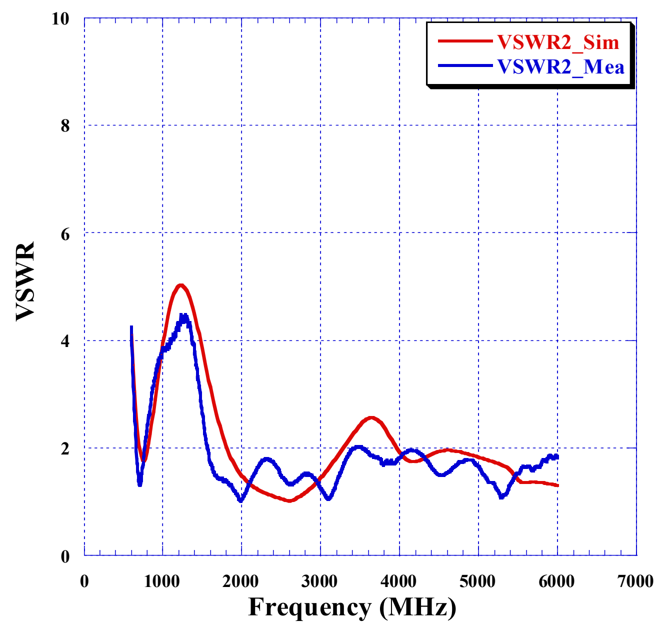

(b)

Figure 3.2. Simulated and measured VSWR for both elements: (a) Ant 1 (left-side PIFA), and (b) Ant 2 (right-side) PIFA.

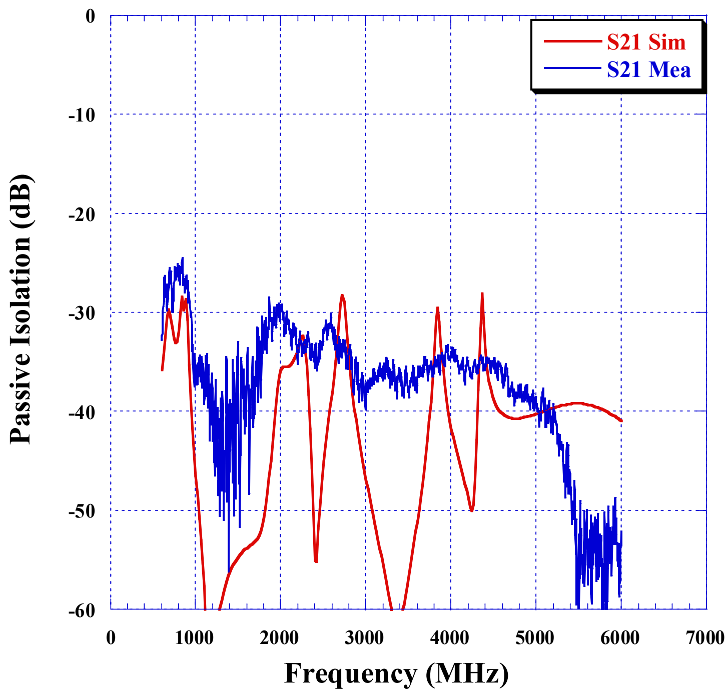

Figure 3.3. Simulated and measured passive isolation between the two elements in dB.

In Figures 3.4(a), (b), (c), and (d), combined radiation patterns of horizontal cuts at theta 80 degrees are presented for frequencies 617MHz, 1.9GHz, 3.6GHz and 5GHz while in Figure 3.4(e), radiation pattern for 5.9GHz is presented at theta 90 degrees. The patterns are measured by terminating one element by 50ohms while measuring the other element, then the two patterns are combined to get an omnidirectional pattern around the entire vehicle. The orientation of each PIFA compared to the other is critical to get the omnidirectional behavior across the entire operating band. Moreover, the average gain observed from the combined vehicle radiation patterns is found to be -0.7dBi, 2.1dBi, 1.8dBi, and 1.1dBi at frequencies 617MHz, 1.9GHz, 3.6GHz, and 5GHz, respectively.

For V2X frequencies, the combined vehicle radiation pattern at 5.9GHz tends to be more directive towards the back side of the car which could result from reflections caused by the roof's curvature and has a peak gain of 6.9dBi at azimuth angle 130 degrees without having a minimum value lower than -11dBi.

The measured radiation antenna efficiencies for the two elements on both GND and vehicle for the 5G and V2X bands are presented in Figure 3.5 (a), (b), (c), and (d). The radiation efficiency of each port is obtained by dividing the realized measured gain from the chamber by directivity across the whole sphere. It can be noticed that the 5G GND measurement has an average efficiency higher than 75% for both elements across all frequency bands whereas the vehicle measurement has a reduced average efficiency of 68%. For V2X frequencies, the measured antenna efficiencies on GND and on the vehicle seem to have close values across the band that is higher than 70%.

The ECC and DG values for this MIMO antenna system at 5G and V2X frequencies have been calculated using a MATLAB script for equation 3.1 and equation 3.2 for simulation and chamber measurements. Figure 3.6 shows these calculations, and it can be noticed that the worst-case value of ECC is around 0.1 at the low frequency band since lower frequency signals support longer wavelengths which require more spacing.

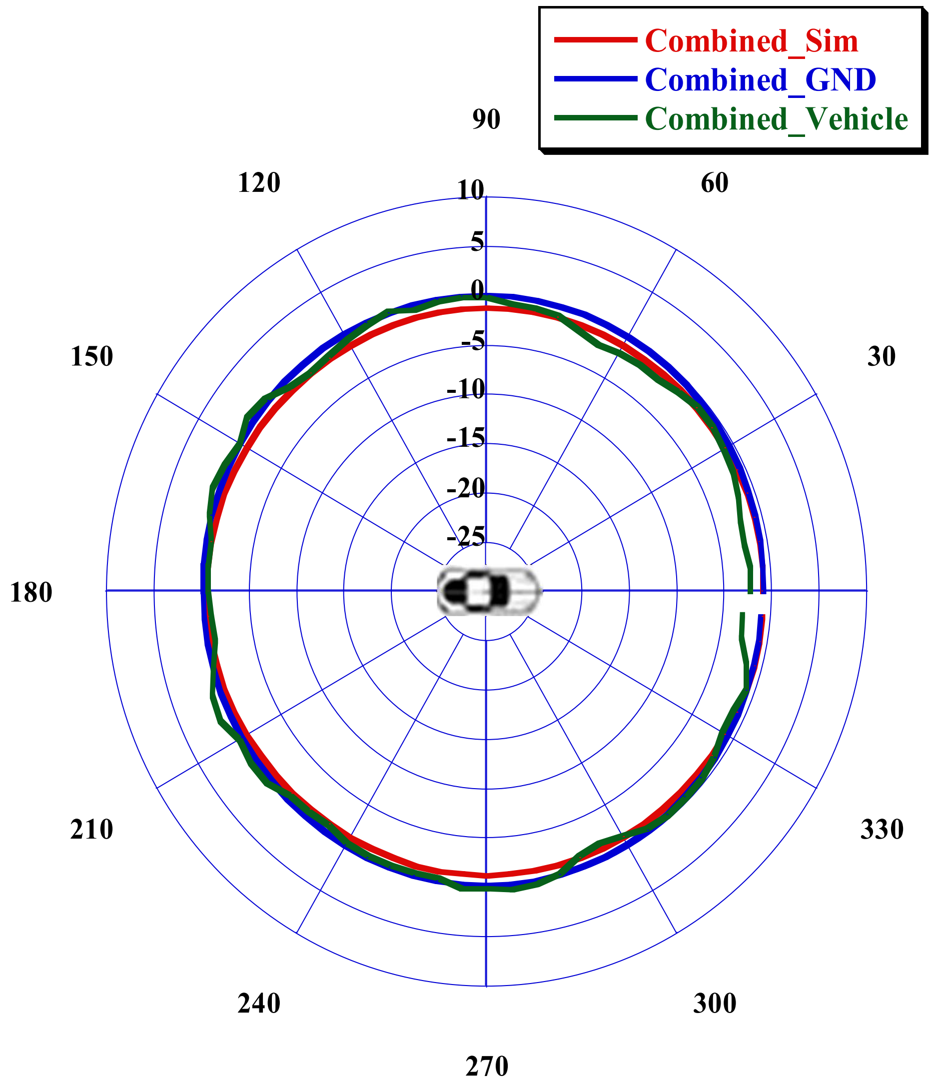

(a) 617MHz

Figure 3.4. Combined Radiation pattern of simulation, GND measurement, and vehicle measurement in (dBi) at theta 80 deg. for frequencies: (a) 617 MHz, (b) 1900 MHz, (c) 3600 MHz, (d) 5000 MHz, and theta 90 deg. for (e) 5.9GHz.

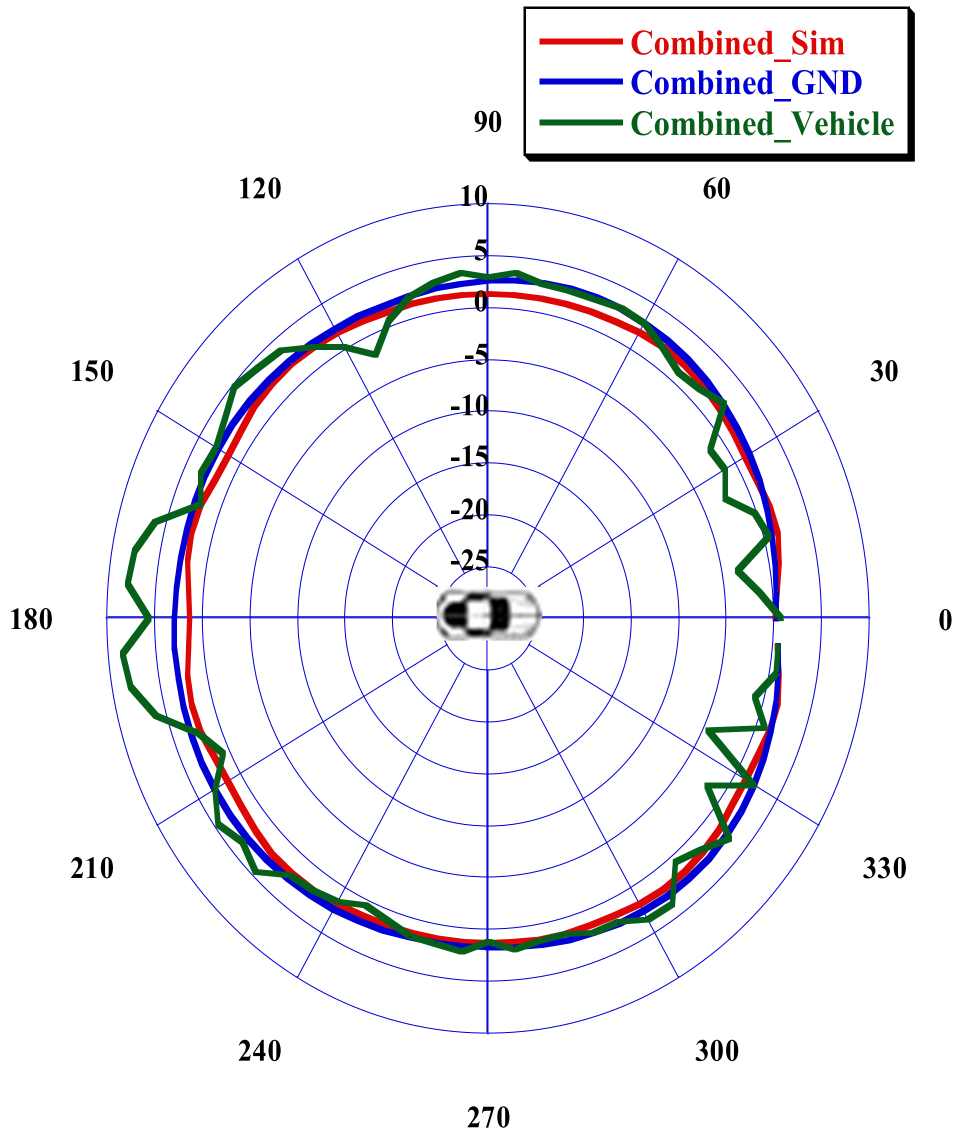

(b) 1900MHz

Figure 3.4. Continued.

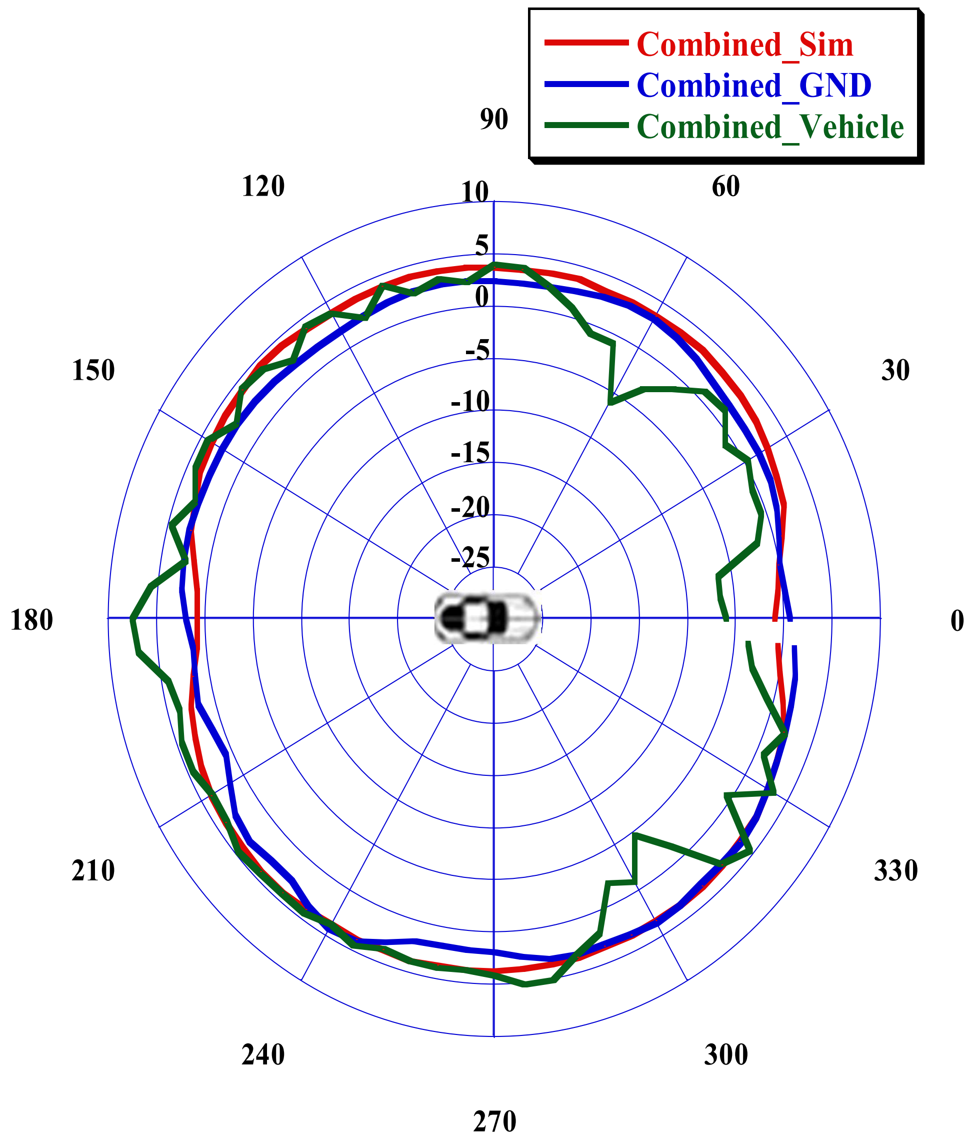

(c) 3600MHz

Figure 3.4. Continued.

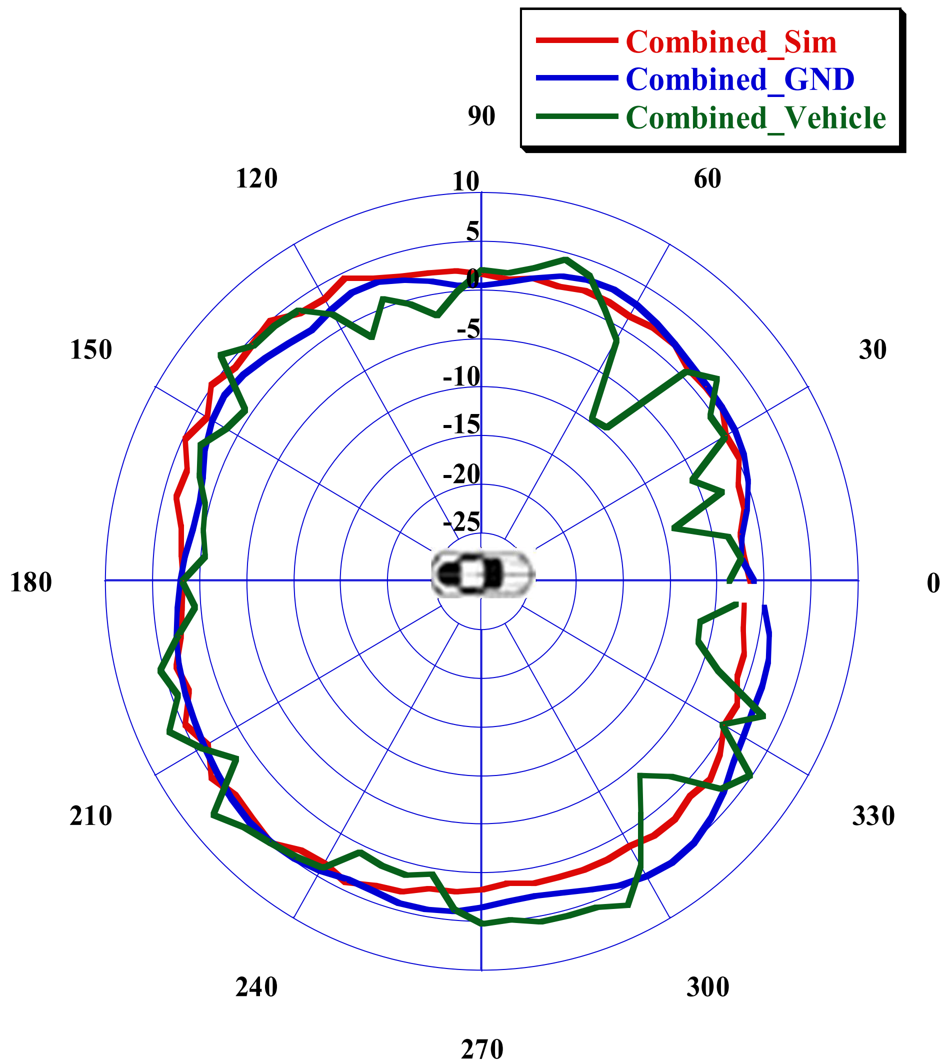

(d) 5000MHz

Figure 3.4. Continued.

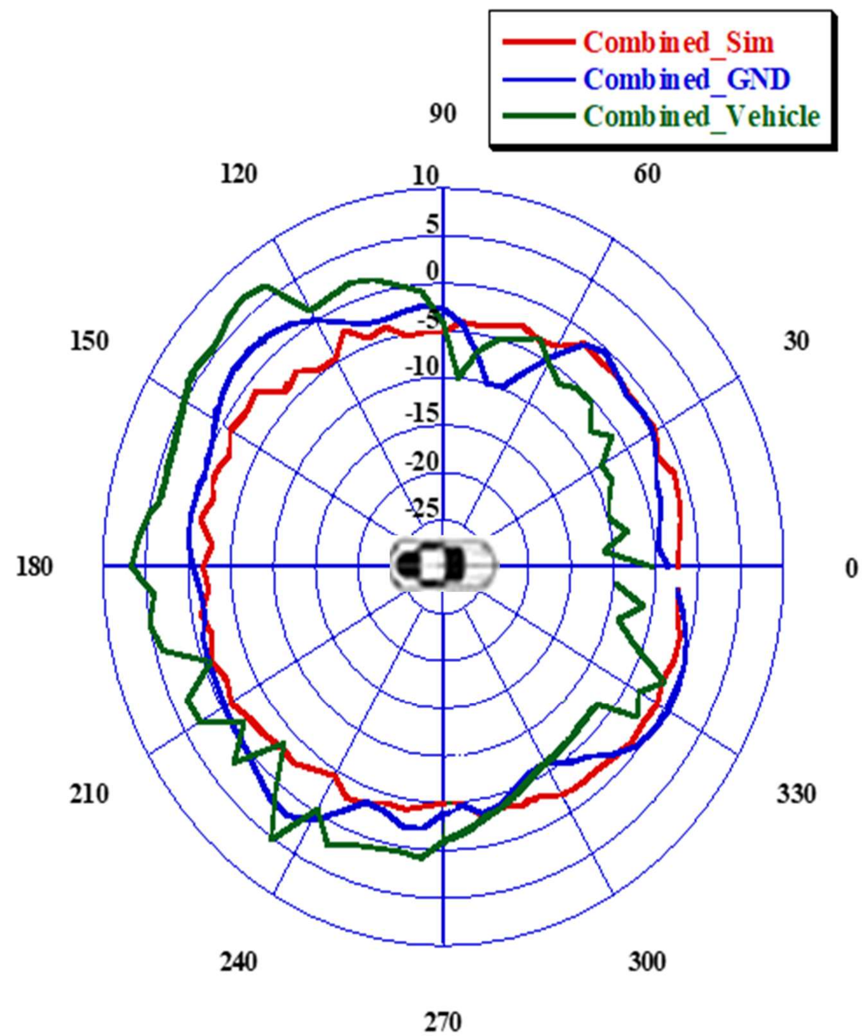

(e) 5900MHz

Figure 3.4. Continued.

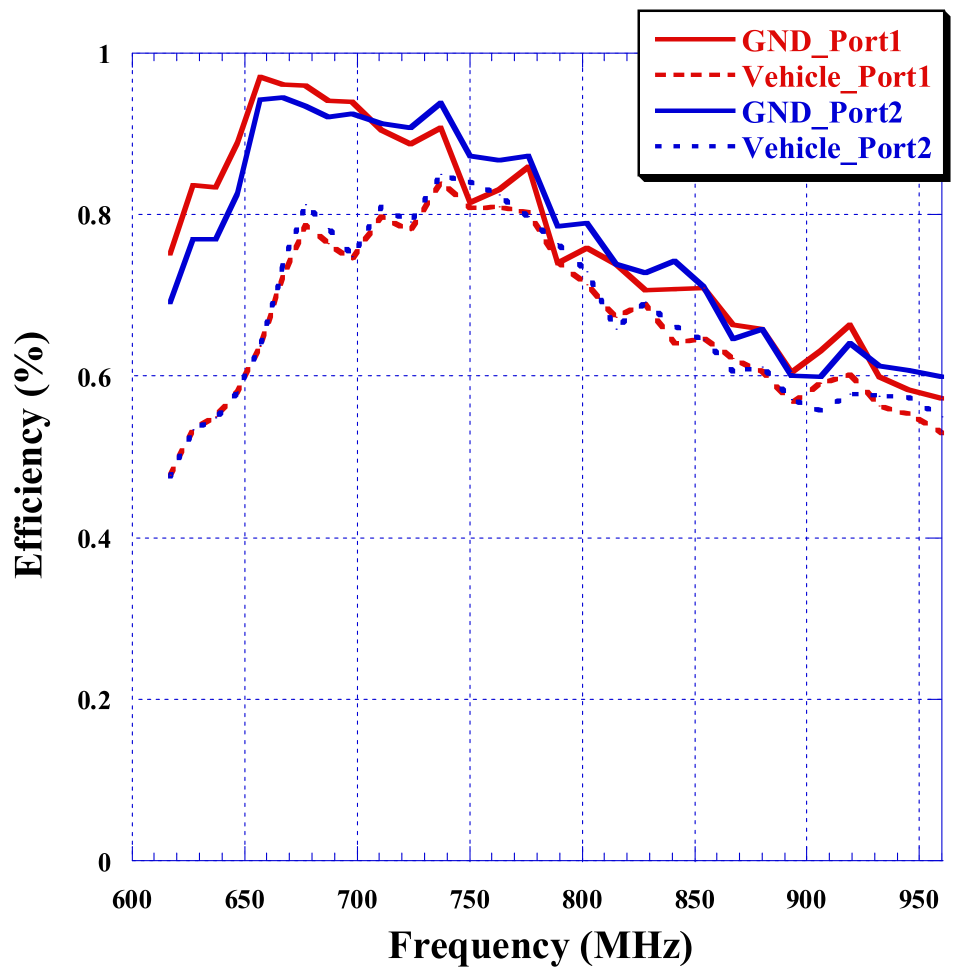

(a) 617MHz-960MHz

Figure 3.5. Antenna radiation efficiency for the two PIFAs measured on ground plane and on vehicle for 5G and V2X frequencies: (a) 617MHz-960MHz, (b) 1710MHz-2690MHz, (c) 3400MHz-5000MHz, (d) 5850MHz-5925MHz.

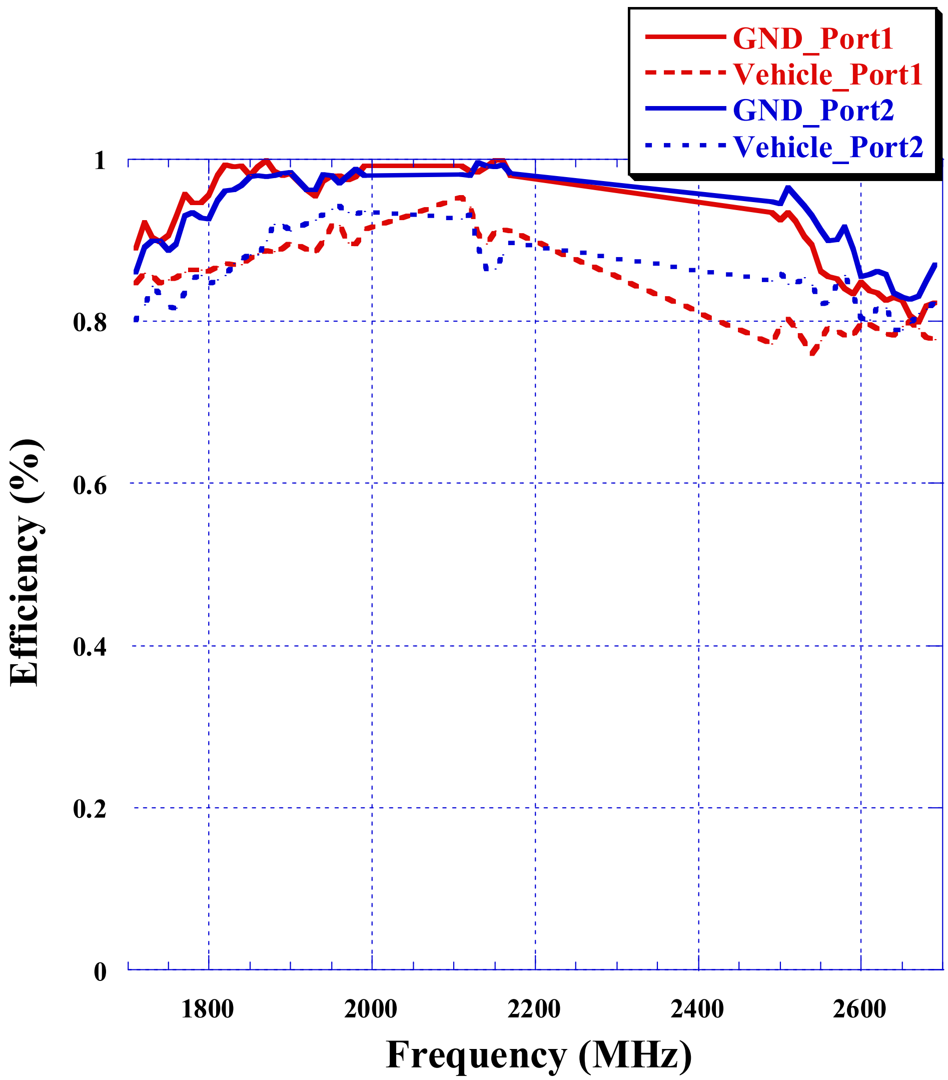

(b) 1710MHz-2690MHz

Figure 3.5. Continued.

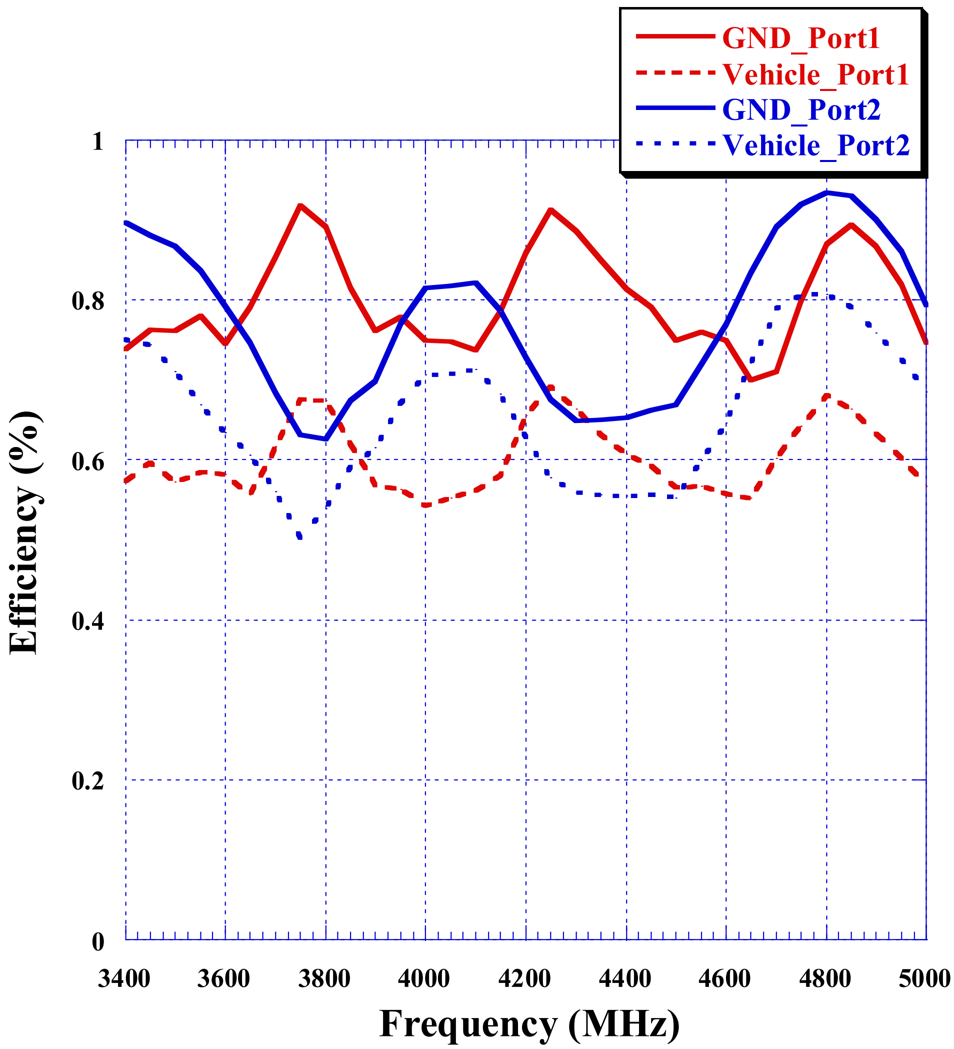

(c) 3400MHz-5000MHz

Figure 3.5. Continued.

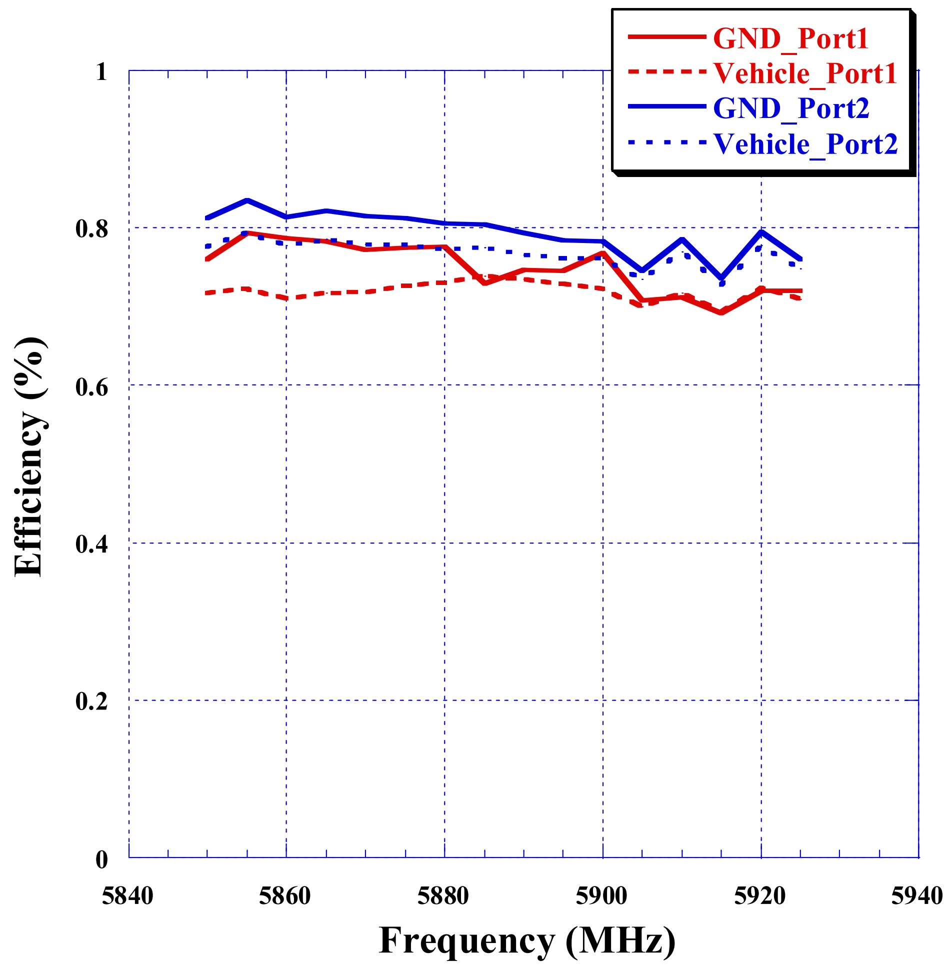

(d) 5850MHz-5925MHz

Figure 3.5. Continued.

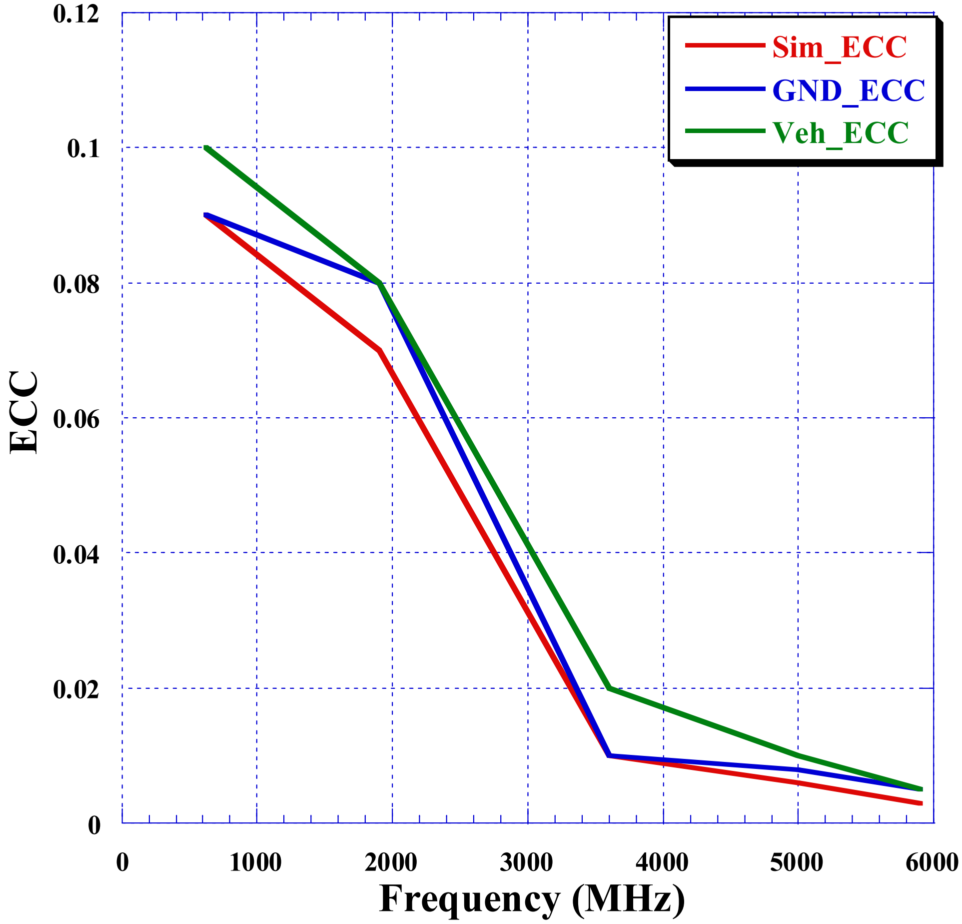

(a) ECC.

Figure 3.6. ECC and DG values for spaced MIMO system: (a) ECC, and (b) DG.

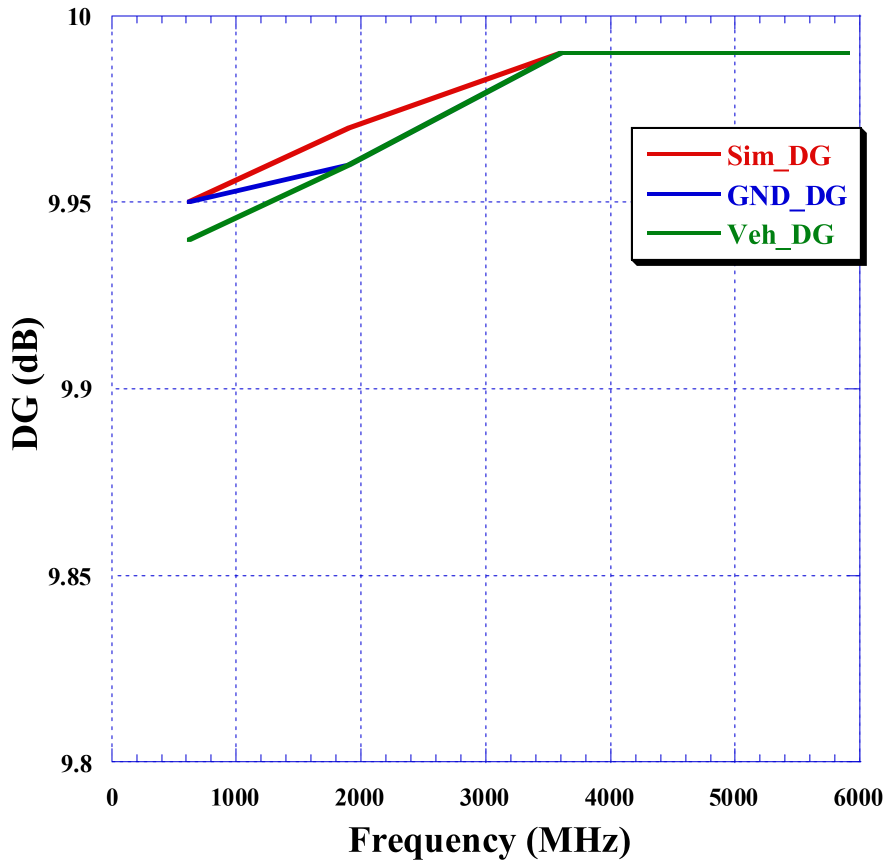

(b) DG

Figure 3.6. Continued.

Next, a parametric study as function of distance between the two elements is presented using HFSS simulation. The distance is changed from 600mm to 120mm, 240mm, and 480mm. The electric field components are exported from each configuration and then processed in MATLAB to see the effect on ECC and DG. Figure 3.7 shows these calculations, and it can be noticed that increasing the distance in this configuration improves the ECC and DG which gives better MIMO performance; however, the size of the vehicle's roof might be a limitation and the antennas should be placed a bit further away from the edges to avoid scattering effects and exhibit reliable grounding.

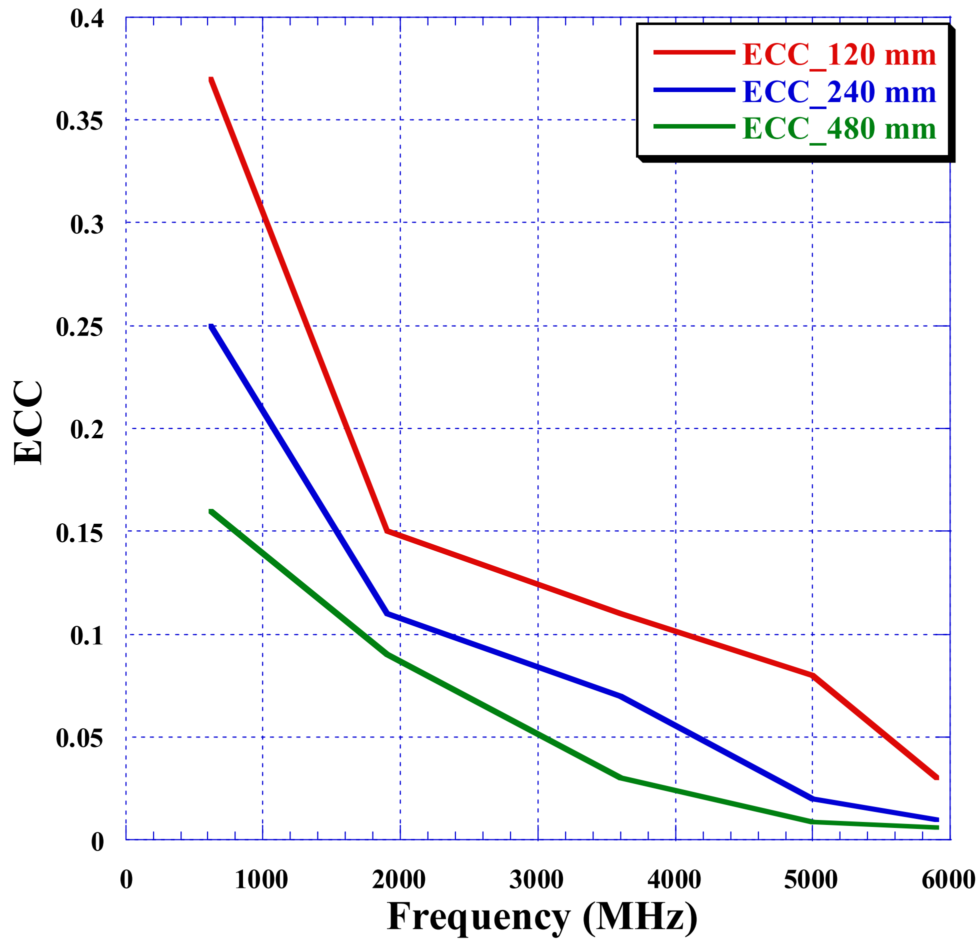

(a) ECC

Figure 3.7. ECC and DG values for different distances: (a) ECC, and (b) DG.

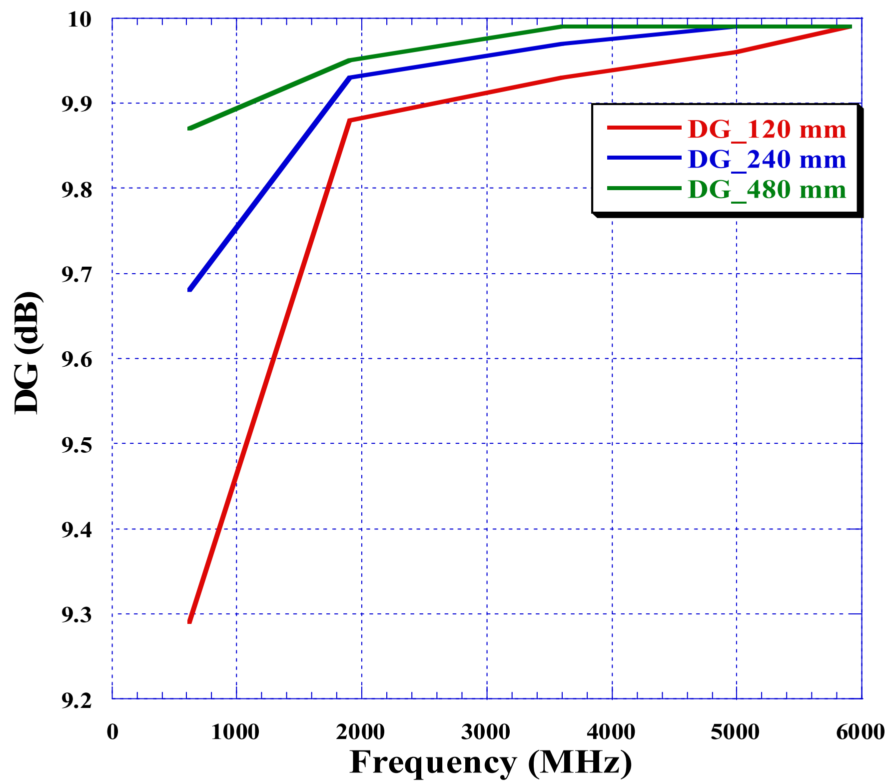

(b) DG

Figure 3.7. Continued.

3.3.2 2x2 PIFA-Based MIMO with Rotational Diversity

In this section, the two PIFA elements were placed on the same PCB with a physical separation of 120mm between them (0.25 lambda of the smallest operating frequency “617MHz”). The elements are oriented in an opposite way to have a complimentary radiation pattern that results in a combined omnidirectional pattern. The simulation and vehicle measurement setup for this configuration is shown in Figure 3.8. The elements are placed in the back center of the roof as in low-profile housing module.

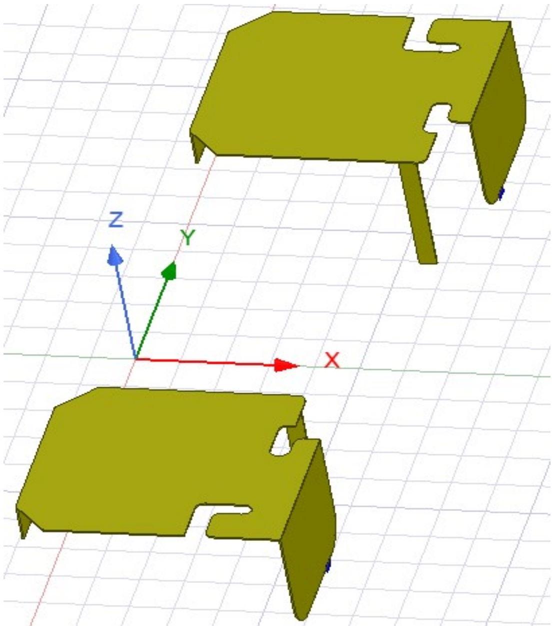

(a) Simulation model

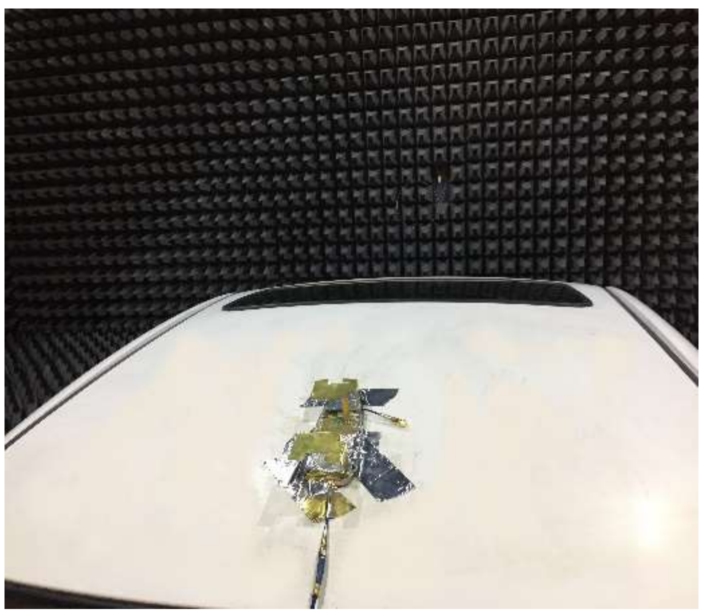

(b) Vehicle's roof.

Figure 3.8. Simulation and vehicle measurement setup of the rotational PIFAs: (a) simulation model, and (b) Vehicle's roof.

The simulated VSWR for each element in this configuration is shown in Figure 3.9. The VSWR is better than 3.3:1 across 5G and V2X bands, while also having acceptable filtering for GNSS bands. The passive isolation between the two PIFAs is shown in Figure 3.10. The worst coupling between the two elements has an isolation of around 11dB at the low frequency bands since they have the longest wavelength in the operating frequency range.

In Figure 3.11(a), (b), (c), and (d), combined radiation patterns of horizontal cuts at theta 80 degrees are presented for frequencies 617MHz, 1.9GHz, 3.6GHz and 5GHz while in Figure 3.11(e), radiation pattern for 5.9GHz is presented at theta 90 degrees. In reference to Figure 3.8, the orientation of each element is in the opposite side to get an omni directional pattern across the operating frequency range. Moreover, the average gain observed from the combined vehicle radiation patterns is found to be -1.3dBi, 0.6dBi, 1.4dBi, and 1.3dBi at frequencies 617MHz, 1.9GHz, 3.6GHz, and 5GHz, respectively. For V2X frequencies, the roof curvature of the vehicle influences the radiation pattern by making it more directive towards the backside of the car. At 5.9GHz, the radiation pattern has a peak gain of 4.9dBi at azimuth angle 240 degrees without having a minimum value lower than -12dBi.

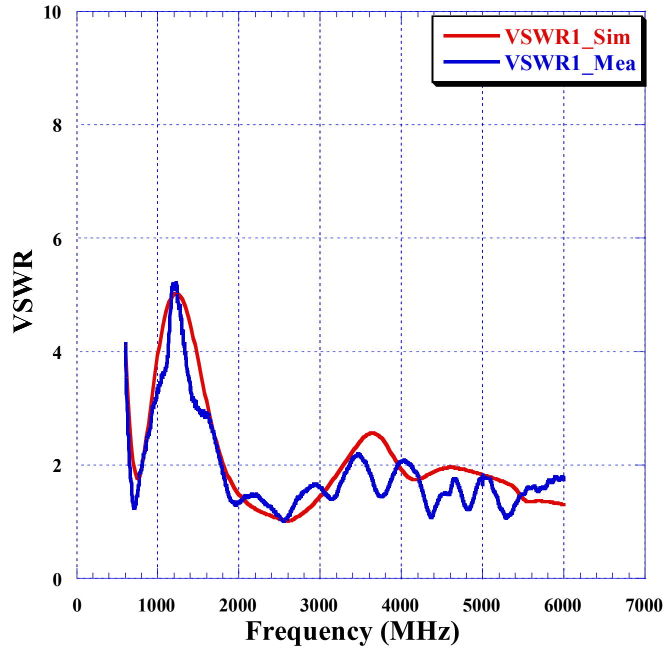

(a) Front PIFA

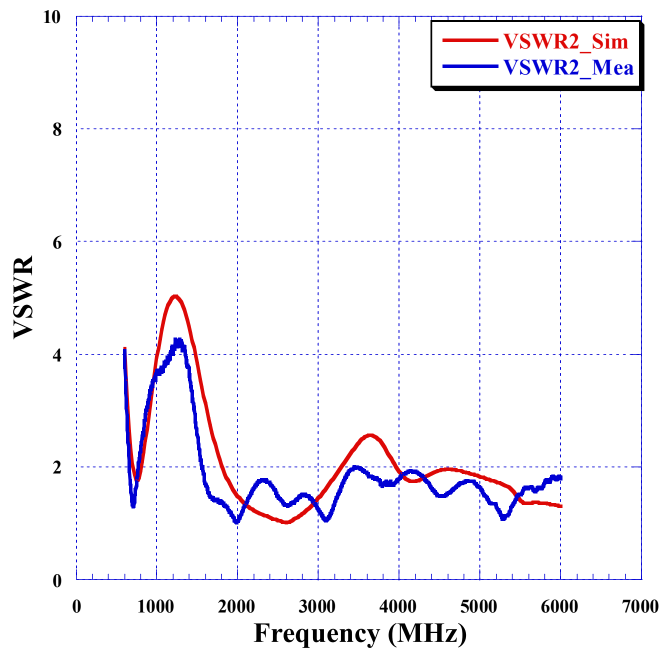

(b) Back PIFA

Figure 3.9. Simulated and measured VSWR of both elements: (a) Ant 1 (front PIFA), and (b) Ant 2(back PIFA).

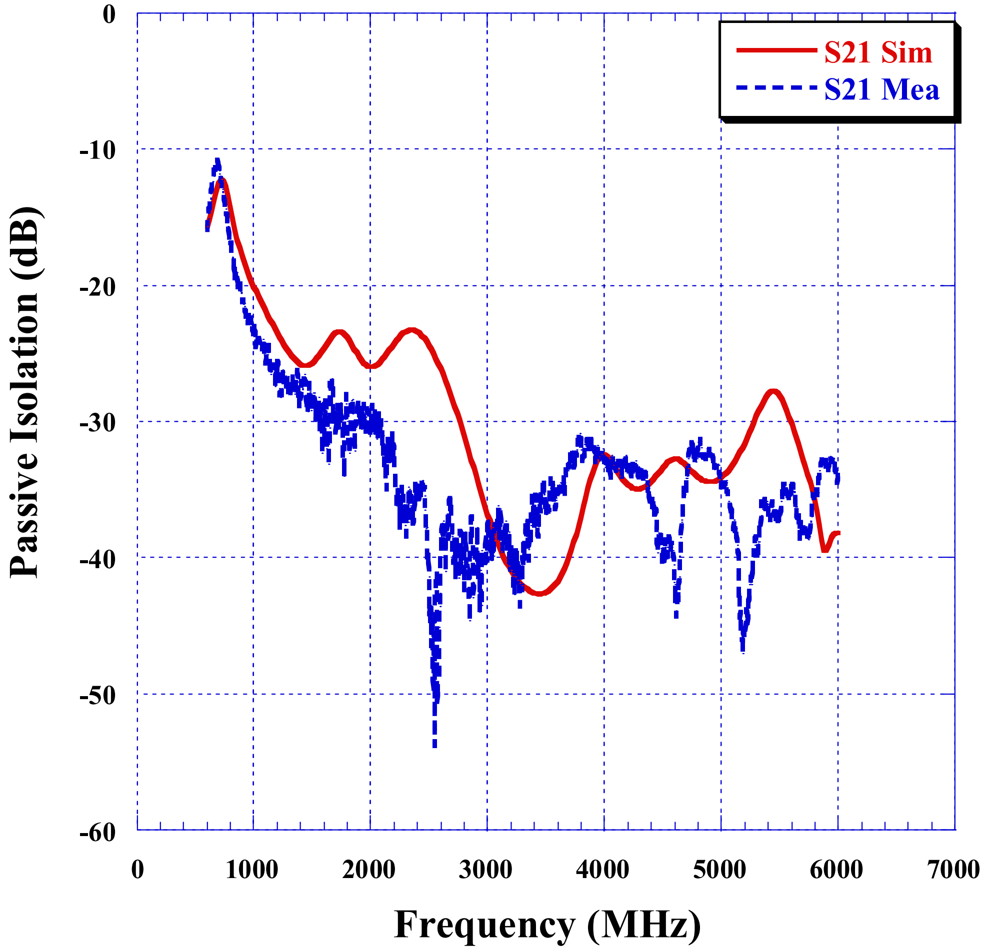

Figure 3.10. Simulated and measured passive isolation between the two elements in dB.

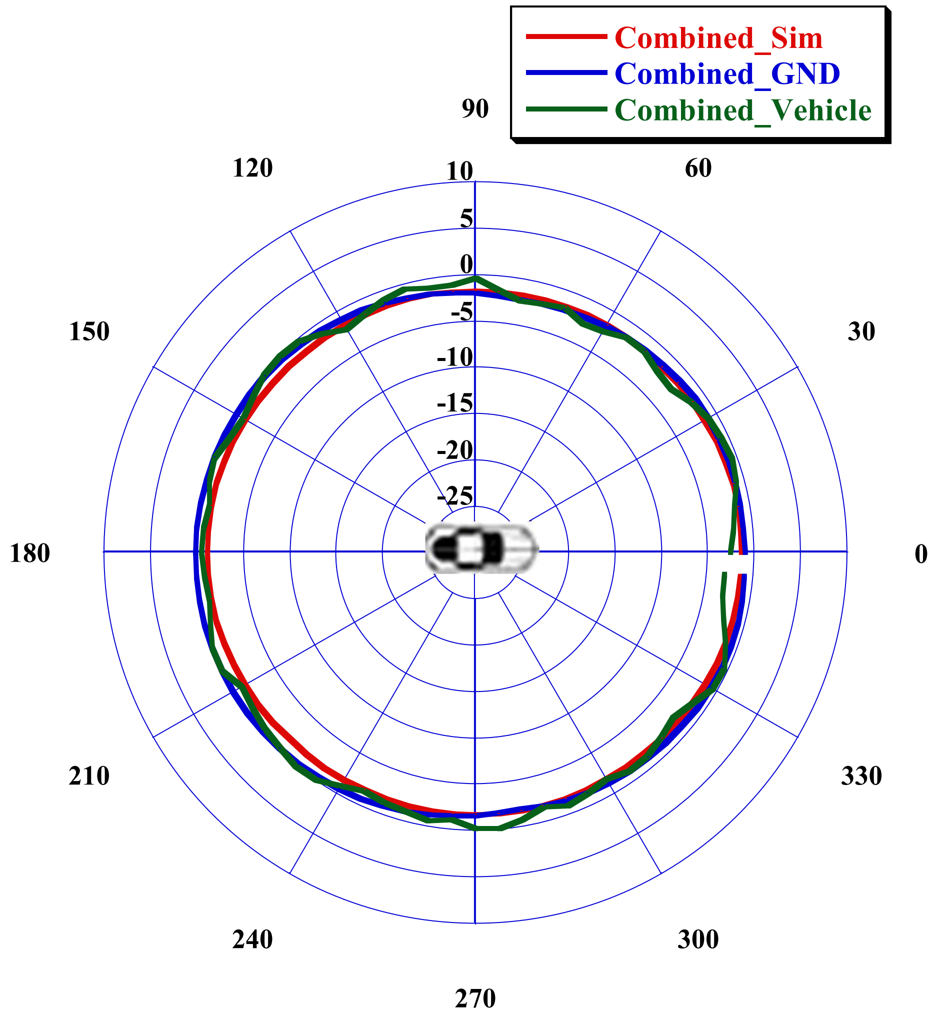

(a) 617 MHz

Figure 3.11. Combined Radiation pattern of simulation, GND, and vehicle measurement in (dBi) at theta 80 deg. for frequencies: (a) 617 MHz, (b) 1900 MHz, (c) 3600 MHz, (d) 5000 MHz, and theta 90 deg. for (e) 5.9GHz.

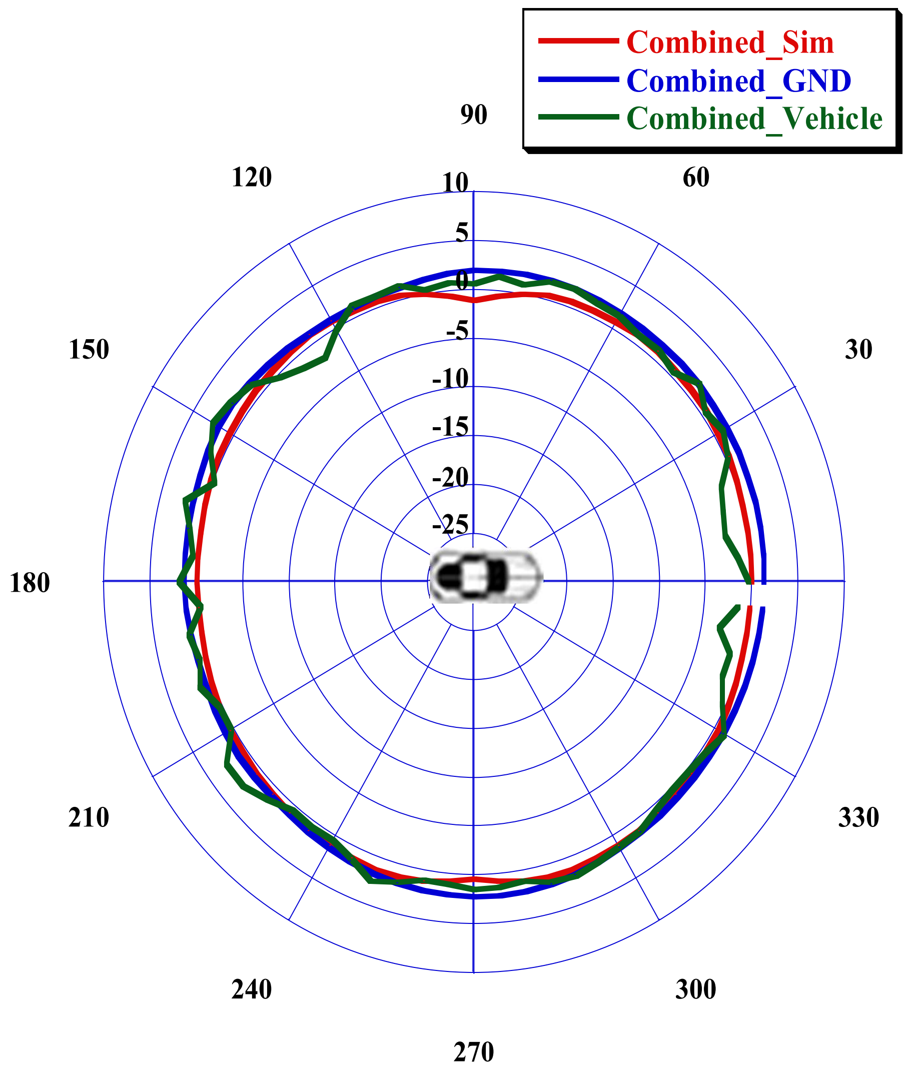

(b) 1900 MHz

Figure 3.11. Continued.

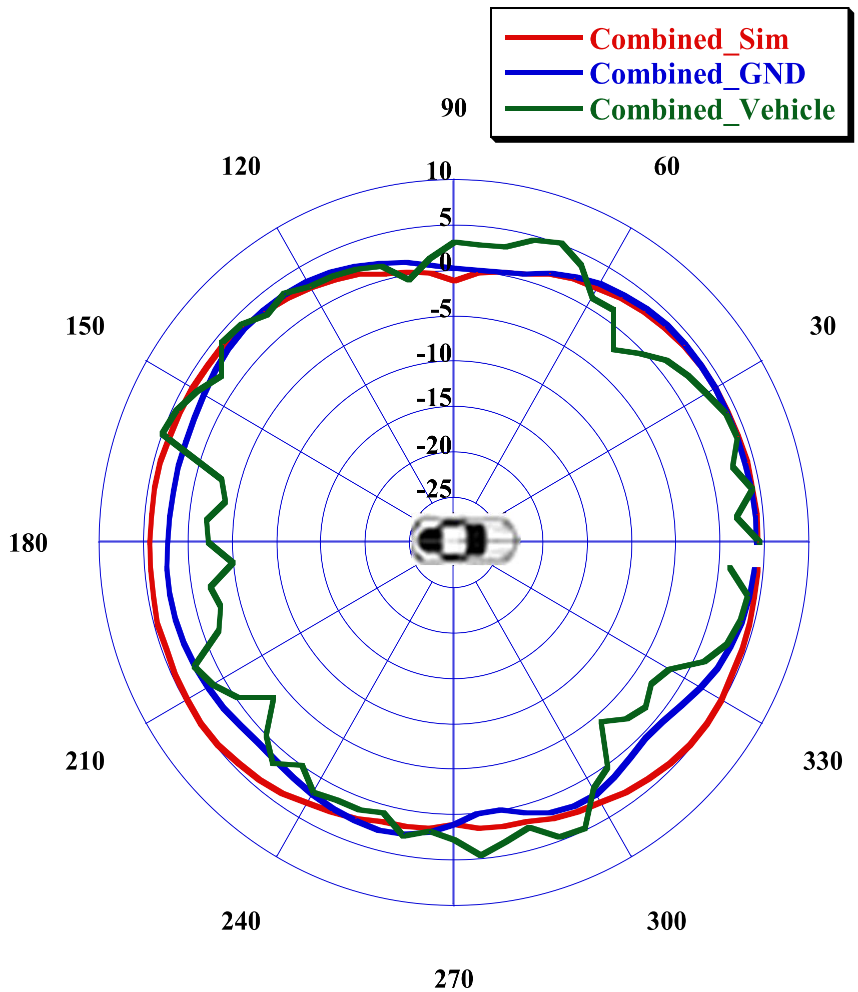

(c) 3600 MHz

Figure 3.11. Continued.

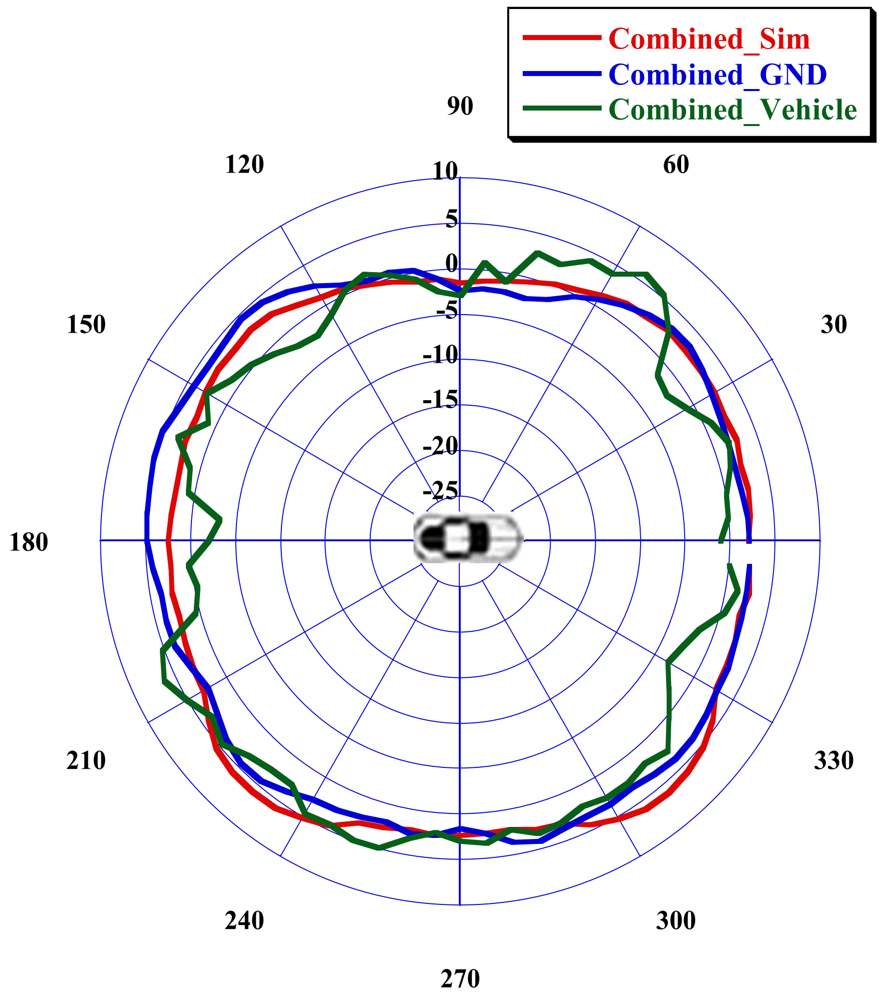

(d) 5000 MHz

Figure 3.11. Continued.

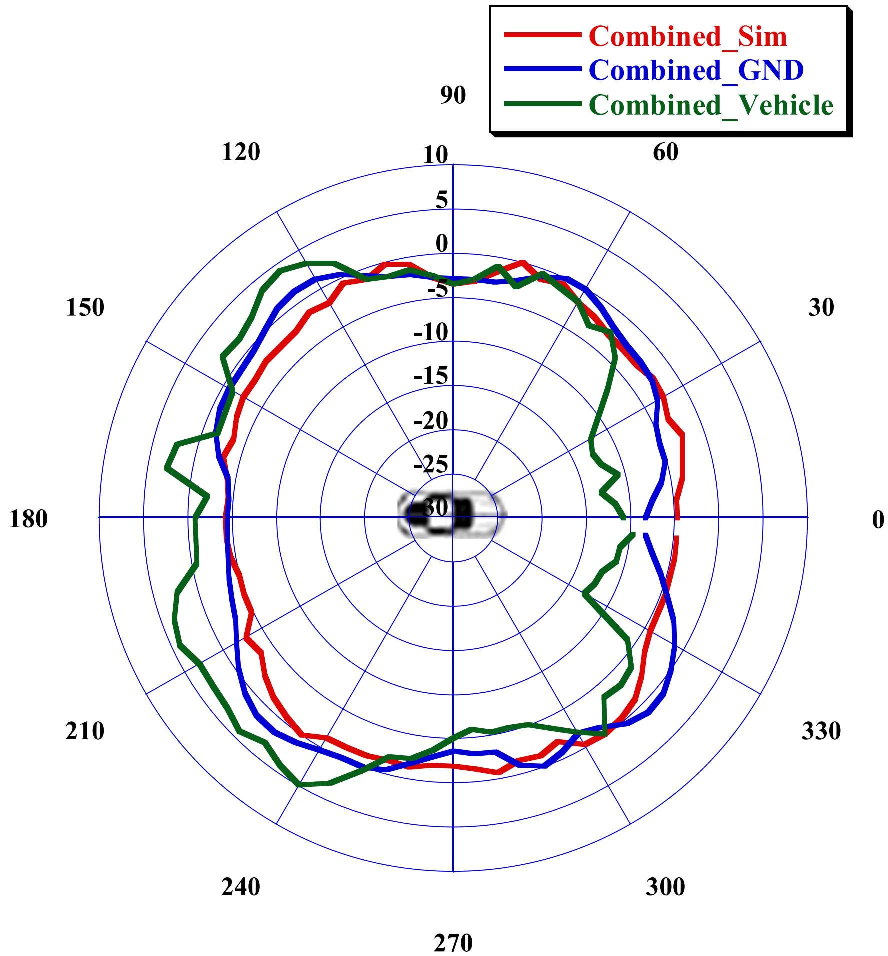

(e) 5900 MHz

Figure 3.11. Continued.

The measured radiation antenna efficiencies for the two elements are shown in Figure 3.12 (a), (b), (c), and (d). It can be noticed that the 5G GND measurement has an average efficiency higher than 67% for both elements while the vehicle measurement has a reduced average efficiency of 60% and higher. For V2X frequencies, the measured antenna efficiencies on the GND and on the vehicle look similar across the band with values higher than 63%.

The ECC and DG were calculated from the electric field components using equation 3.1 and 3.2 in a MATLAB script. Figure 3.13 shows these calculations with a worst-case value around 0.38 in the low frequency bands.

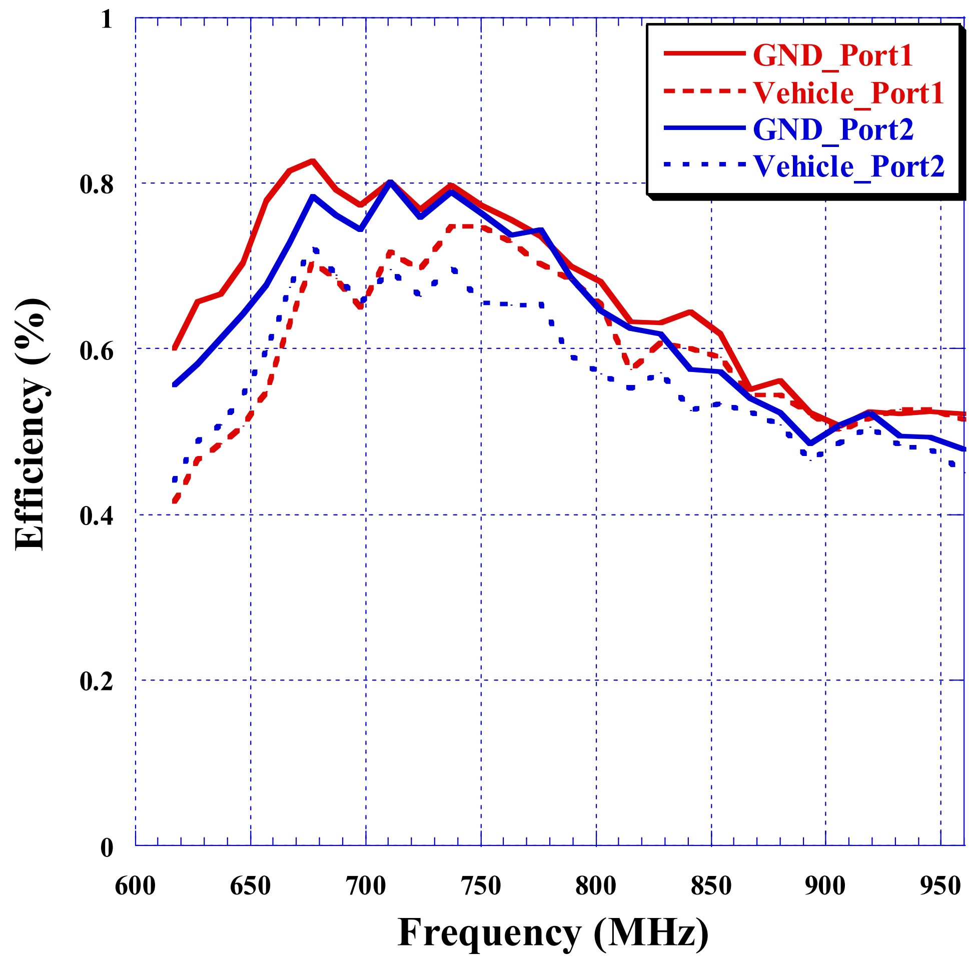

(a) 617MHz-960MHz

Figure 3.12. Antenna radiation efficiency for the two PIFAs :(a) 617MHz-960MHz, (b) 1710MHz-2690MHz, (c) 3400MHz-5000MHz, (d) 5850MHz-5925MHz.

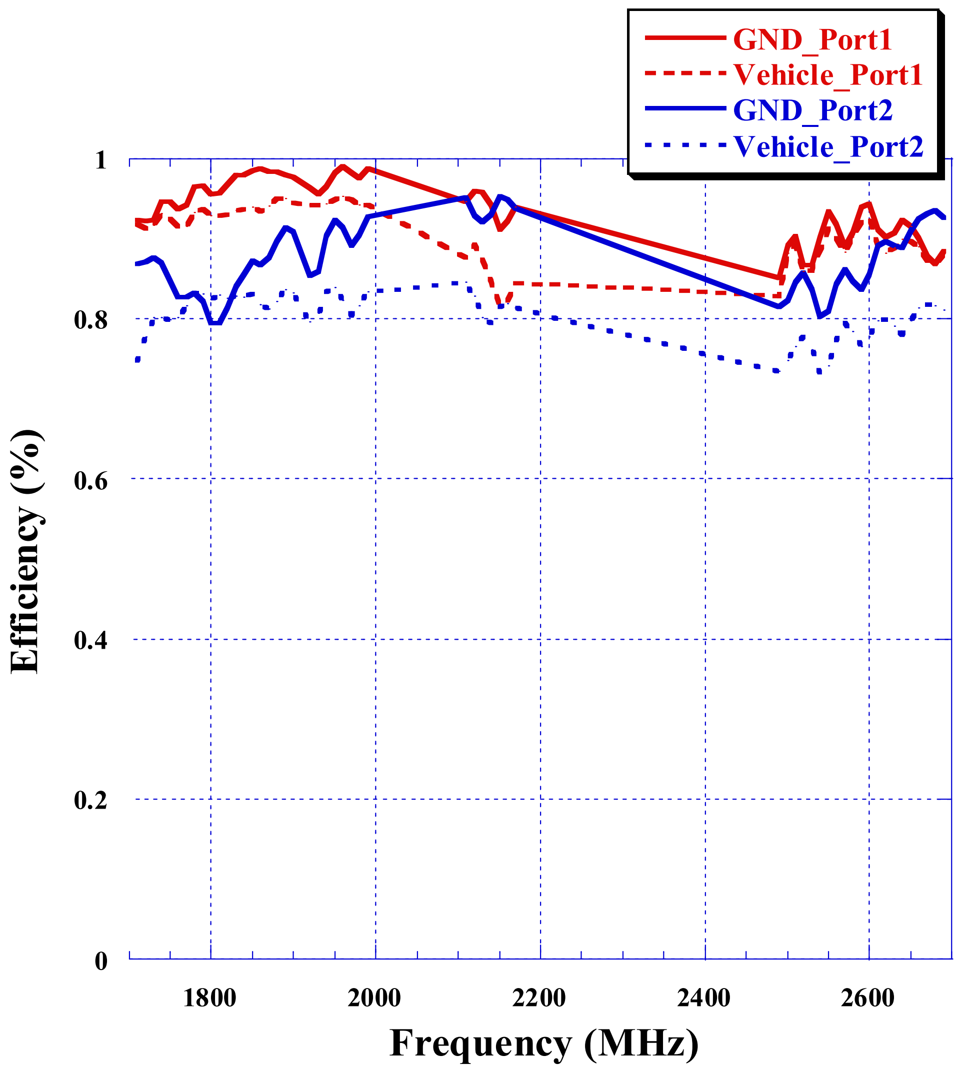

(b) 1710MHz-2690MHz

Figure 3.12. Continued.

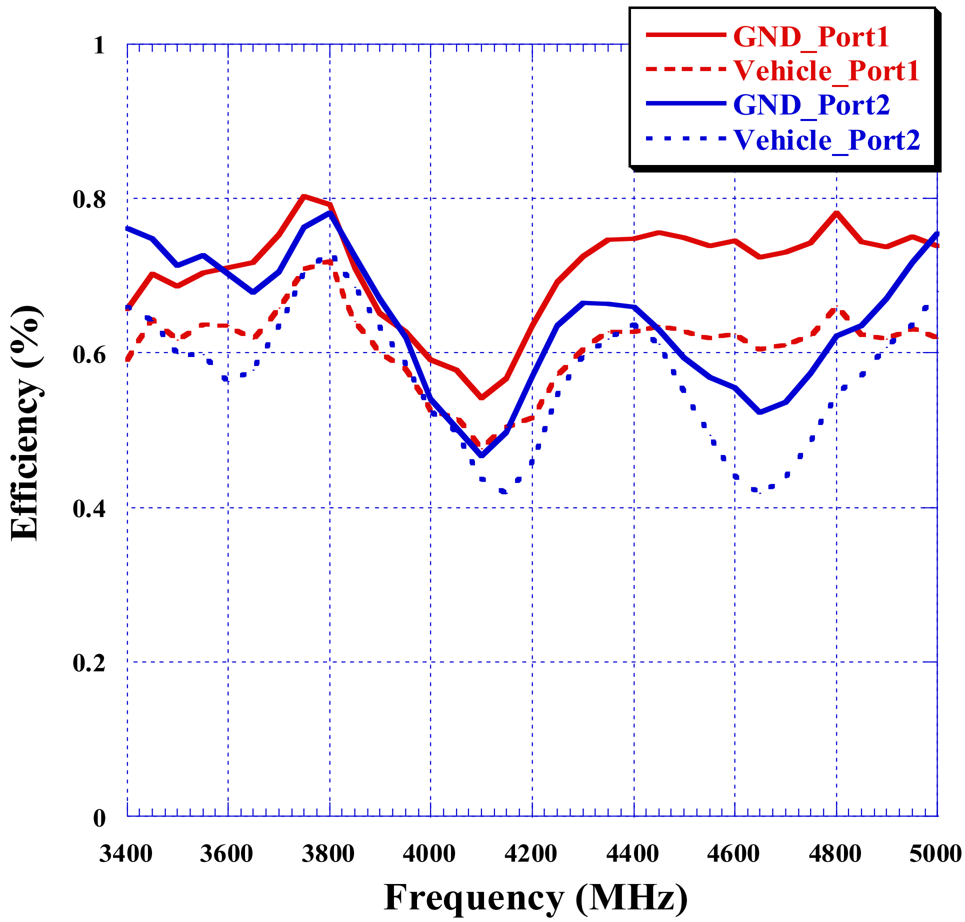

(c) 3400MHz-5000MHz

Figure 3.12. Continued.

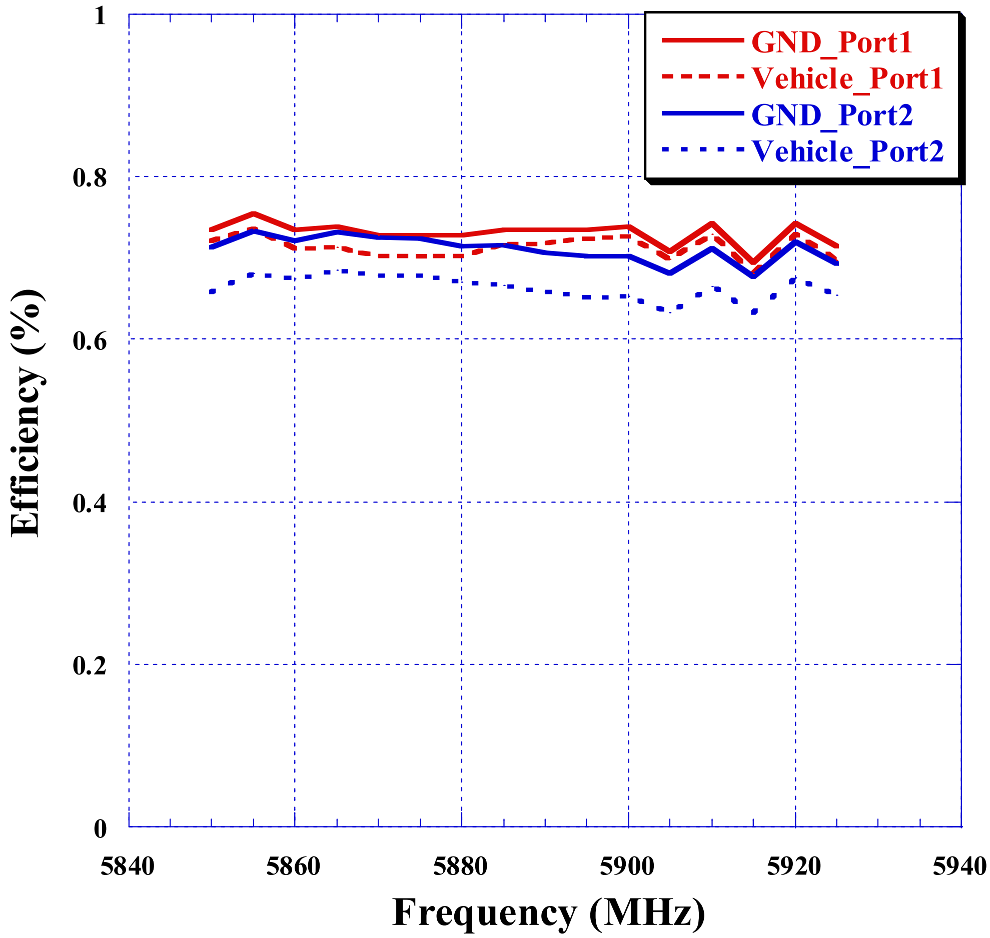

(d) 5850MHz-5925MHz

Figure 3.12. Continued.

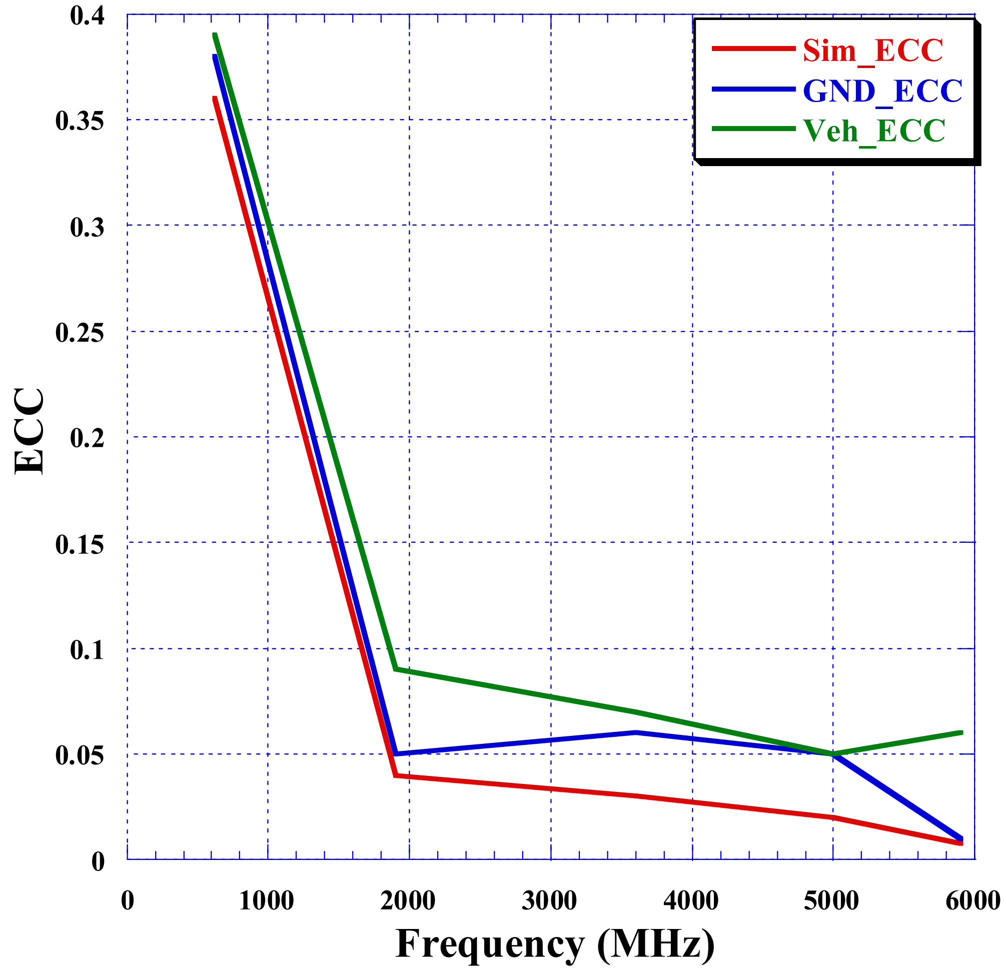

(a) ECC

Figure 3.13. ECC and DG values for rotational MIMO System: (a) ECC, and (b) DG.

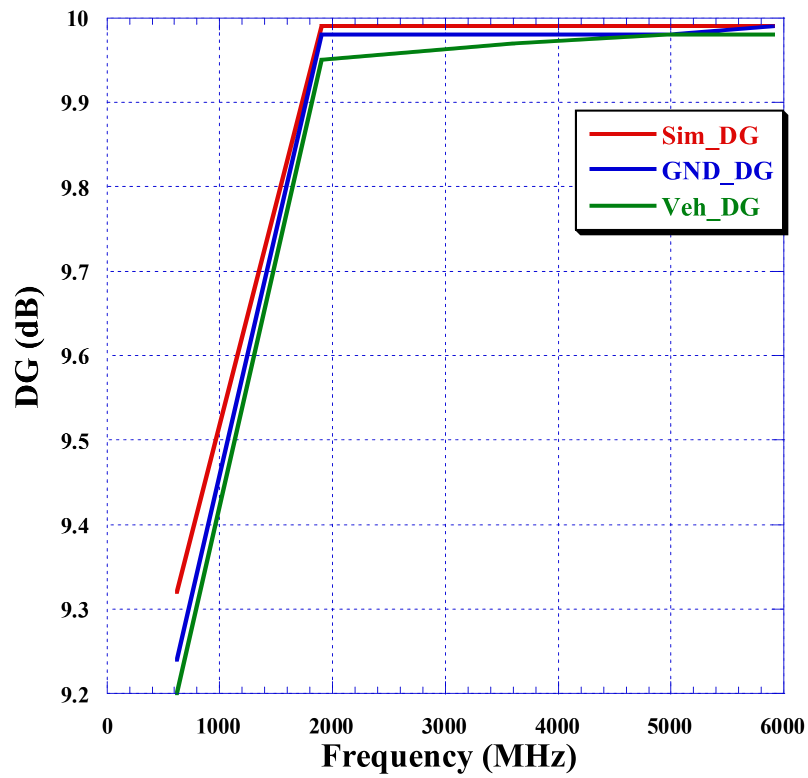

(b) DG

Figure 3.13. Continued.

Simulation via HFSS was used to study the effect of element rotation on the ECC and DG. This was achieved by rotating the front PIFA in the clockwise direction by 90, 180, and 270 degrees on the z-axis while keeping the distance between them fixed (120mm). The results shown in Figure 3.14. Figure 3.15 shows the calculations for ECC and DG at each rotation from the simulation data. By rotating the front PIFA, the distance between the feeding pin, shorting pin, and slots between the two elements is changed. Moreover, the intersection of the radiation pattern between the elements is modified which could help decrease the correlation between the antennas in the MIMO system depending on how the main beam is directed.

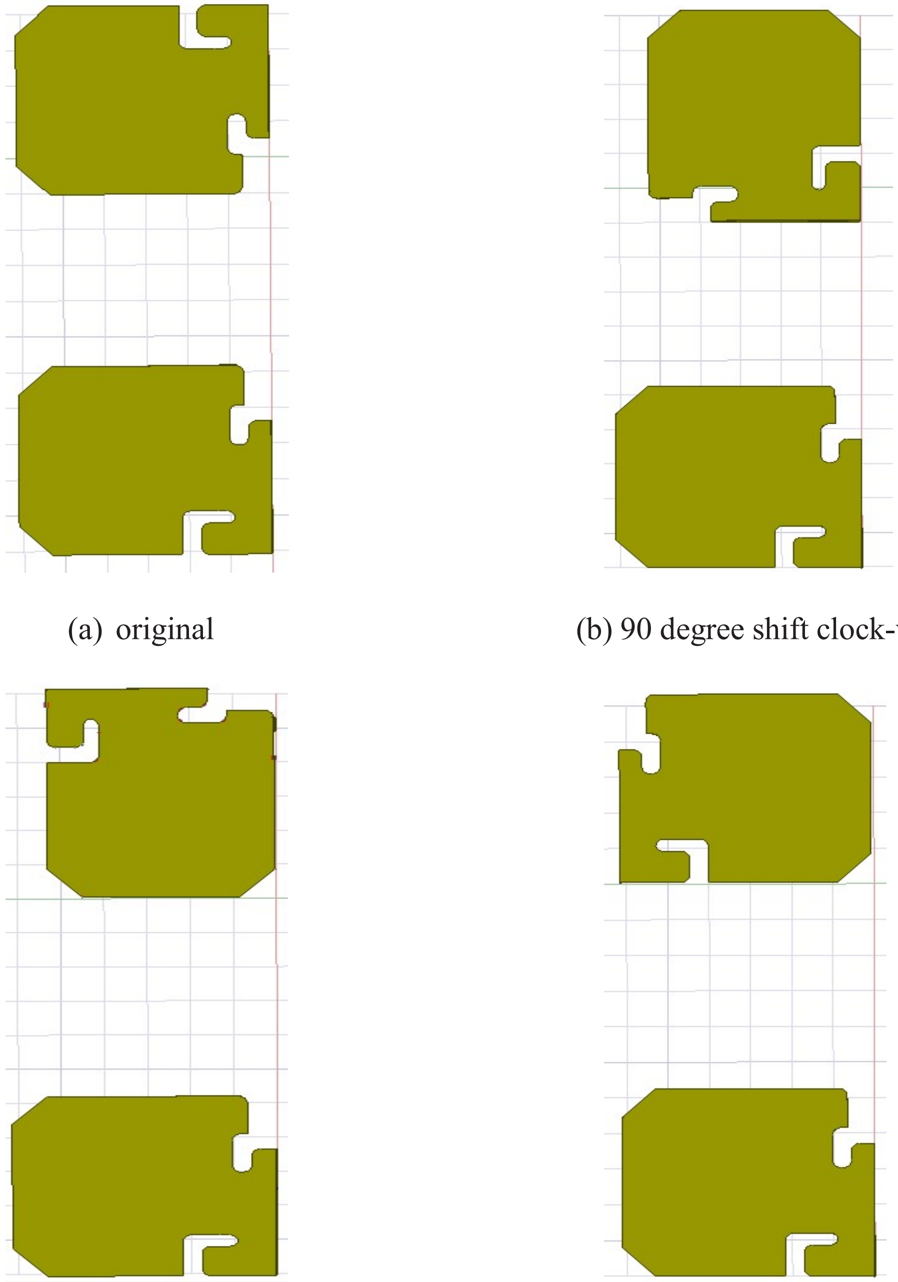

(a) original (b) 90 degree shift clock-wise

(c) 180 degree shift clock-wise (d) 270 degree shift clock-wise

Figure 3.14. Top view of the MIMO antenna system with different rotational positions: (a) original position, (b) 90 degree shift clockwise, (c) 180 degree shift clockwise, and (d) 270 degree shift clockwise.

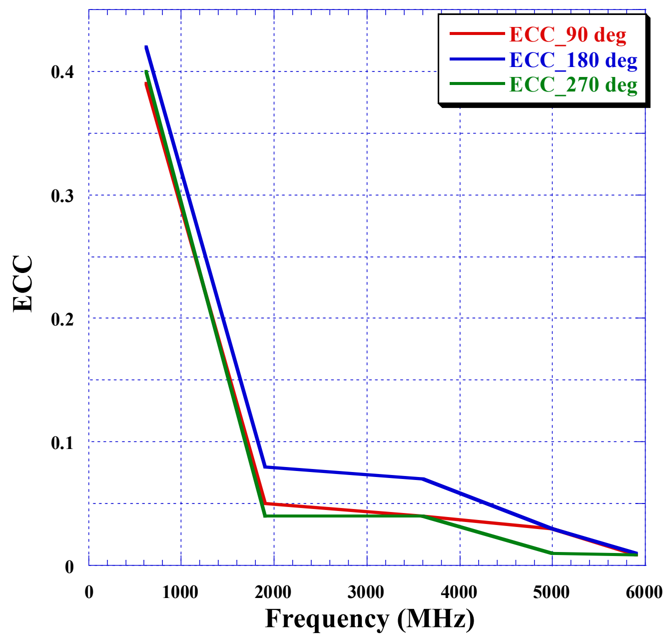

(a) ECC

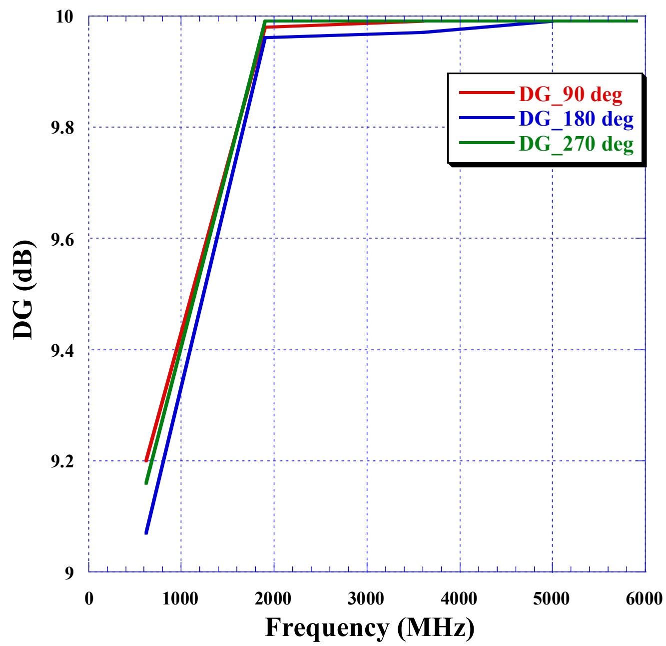

(b) DG

Figure 3.15. ECC and DG Values for different rotations: (a) ECC, and (b) DG.

3.3.3 2x2 Monopole-PIFA MIMO with Orthogonal Diversity

In this section, two antenna elements (monopole and PIFA) are placed on the same PCB with distance between them of 120mm (0.25 lambda of 617MHz). The proposed wide-band monopole covers the same 5G and V2X bands from 617MHz-6GHz with reasonable physical dimensions to be used in a shark fin housing. Figure 3.16 shows the front and side views of the wide-band monopole design in addition to its distinct features and parameters with optimized values in Table 3.2. The monopole design consists of two unique branches: arm 1 and arm 2. The 5G low frequency band (617MHz-960MHz) is covered by arm 1 that operates as a folded monopole structure that has a total radiating length of 96mm which is $\lambda/4$ of the center frequency (780MHz). The middle and high frequency bands for 5G and V2X (1.71GHz-6GHz) are attributed to arm 2 which is another wide monopole branch that has a radiating length of 35.9mm which is $\lambda/4$ of 2.08GHz. The top loaded branch of arm 1 of width 14.9mm increases the radiating length of the antenna to allow it to cover the lower frequencies. An L-shape slot structure exists between arm 1 and arm 2 to separate the low and middle frequency bands in order to reject the GNSS frequencies that resides between the two bands.

In this MIMO system, the monopole introduces a vertical surface current while the PIFA has some portion of the surface current on the horizontal plane especially at the low and middle frequency bands. The simulation and measurement setup on vehicle for this MIMO configuration is shown in Figure 3.17. The elements are placed in the back center of the roof as in a shark fin module style.

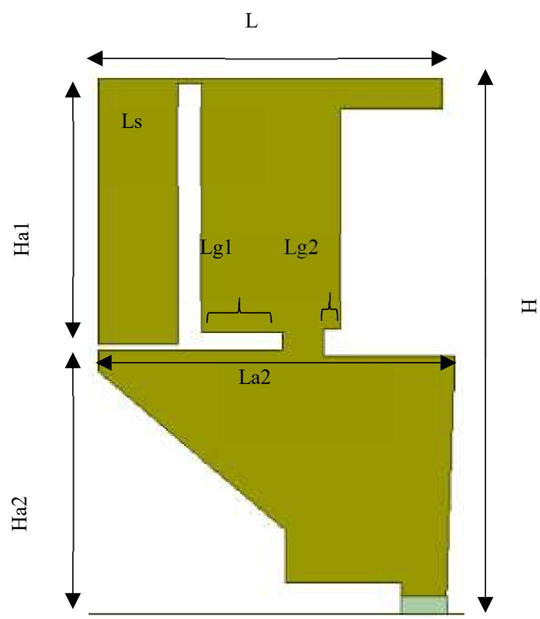

(a) Side-view

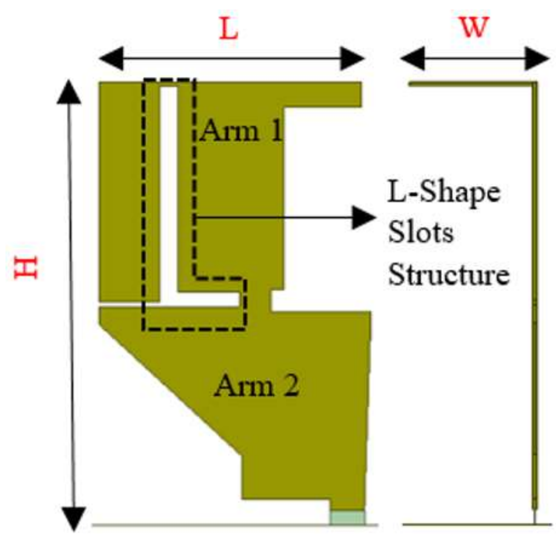

(b) L-shape and front view

Figure 3.16. Compact monopole antenna with side and front dimensions: (a) side view, and (b) L-shape and front view.

Table 3.2. Geometrical parameters Values of the designed antenna.

Parameter	Value (mm)
H	60
L	38.5
W	14.9
H_{a1}	30
H_{a2}	29.3
L_{g1}	9
L_{g2}	2
L_s	2.6
L_{a2}	39.8

The simulated VSWR for each element in this configuration is shown in Figure 3.18. Port 1 and 2 represent the monopole, and PIFA, respectively. Both elements show a VSWR better than 3.3:1 across the 5G and V2X bands while also filtering out the GNSS bands. The passive isolation between the two elements is shown in Figure 3.19. The worst-case isolation between the two elements has a value of 10dB at the low frequency bands.

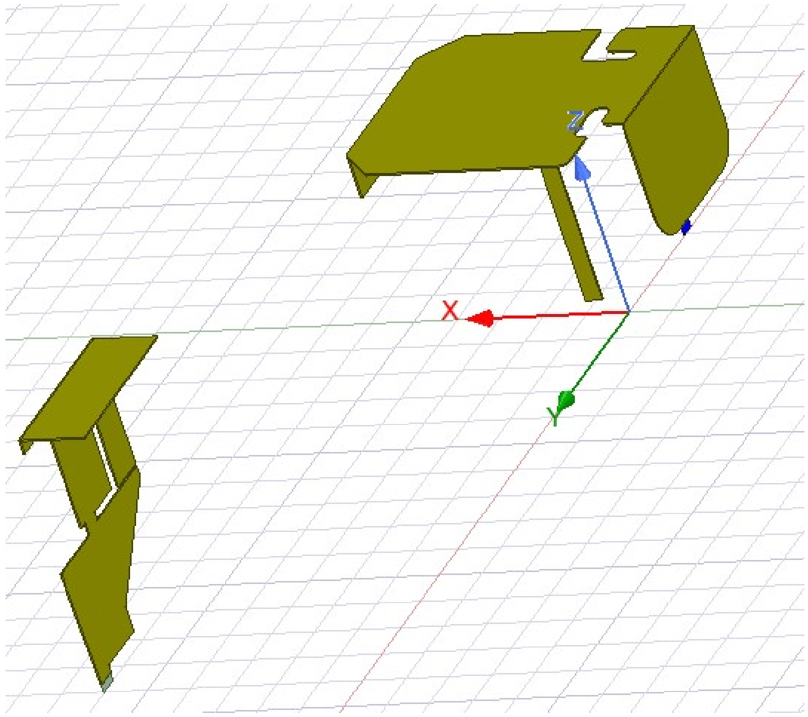

(a) Simulation model

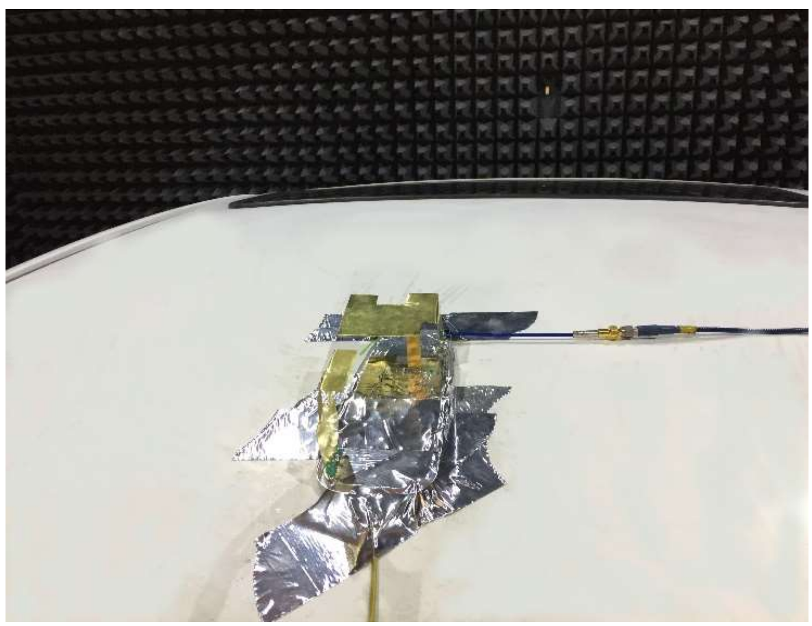

(b) Vehicle's roof

Figure 3.17. Simulation and measurement setup of the monopole-PIFA MIMO system on the vehicle: (a) simulation model, and (b) vehicle's roof.

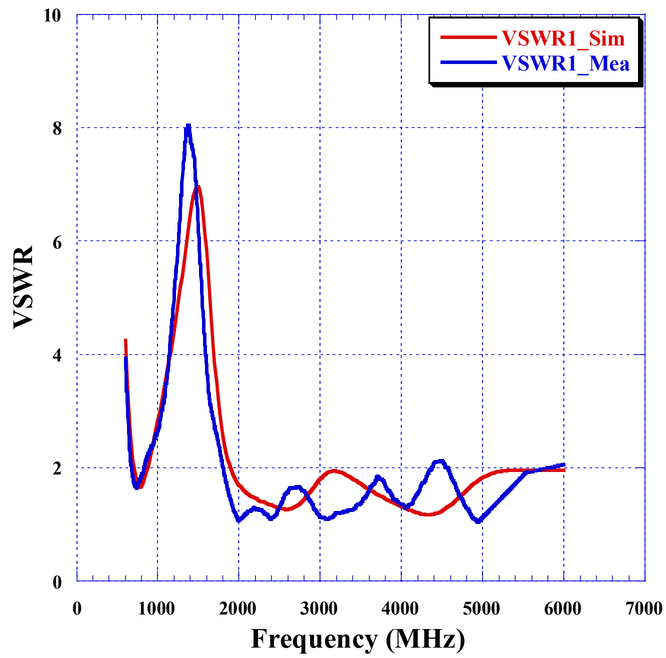

(a) Ant 1 (monopole)

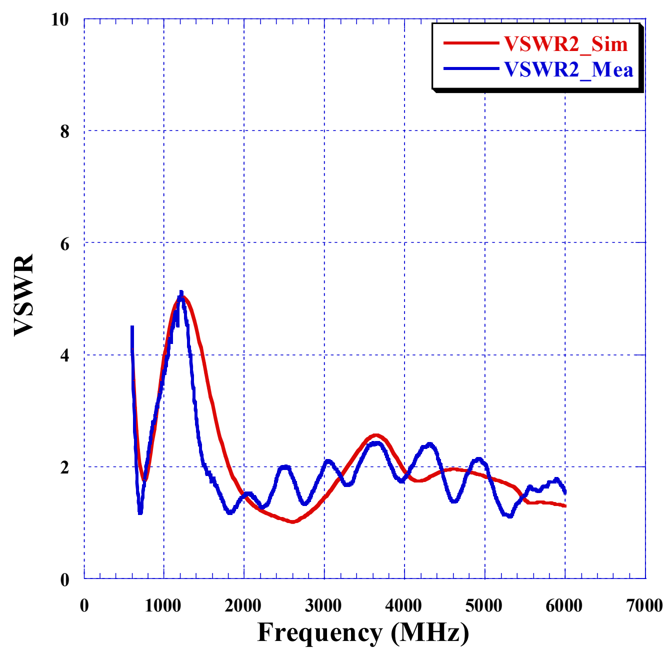

(b) Ant 2 (PIFA)

Figure 3.18. Simulated and measured VSWR for both elements: (a) Ant 1 (monopole), and (b) Ant 2 (PIFA).

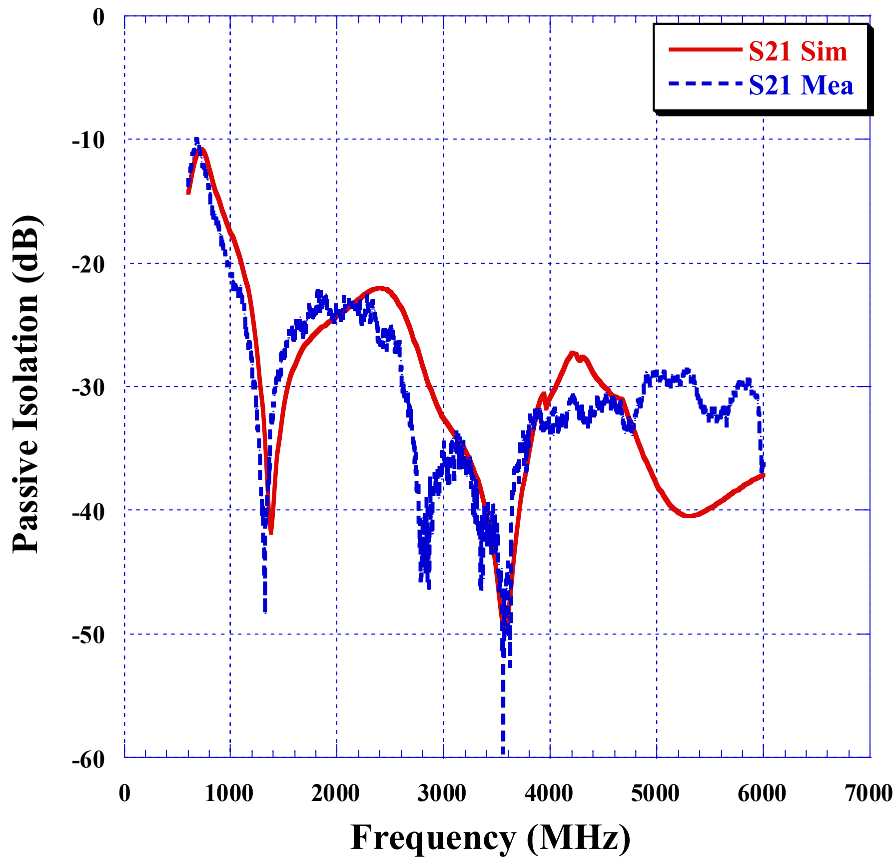

Figure 3.19. Simulated and measured passive isolation between the two elements in dB.

The combined radiation patterns for the two elements are shown is Figure 3.20. The average gain observed from the combined vehicle radiation pattern is found to be -1.1dBi, 2.3dBi, 0.38dBi, and 0.97dBi at frequencies 617MHz, 1.9GHz, 3.6GHz, and 5GHz, respectively. For V2X frequencies, at 5.9GHz, the radiation pattern has a peak gain of 6dBi at azimuth angle 225 degrees without having a minimum value lower than -11.2dBi.

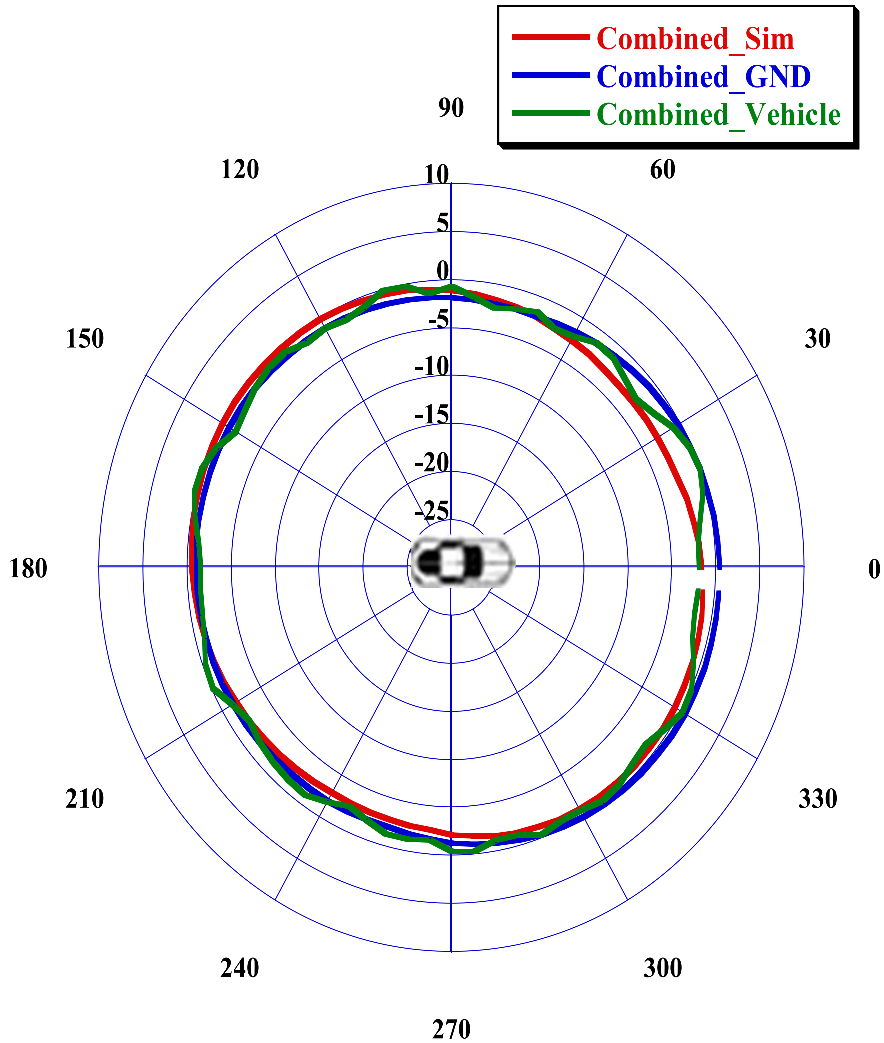

(a) 617 MHz

Figure 3.20. Combined Radiation pattern of simulation, GND measurement, and vehicle measurement in (dBi) at theta 80 deg. for frequencies: (a) 617 MHz, (b) 1900 MHz, (c) 3600 MHz, (d) 5000 MHz, and theta 90 deg. for (e) 5.9GHz.

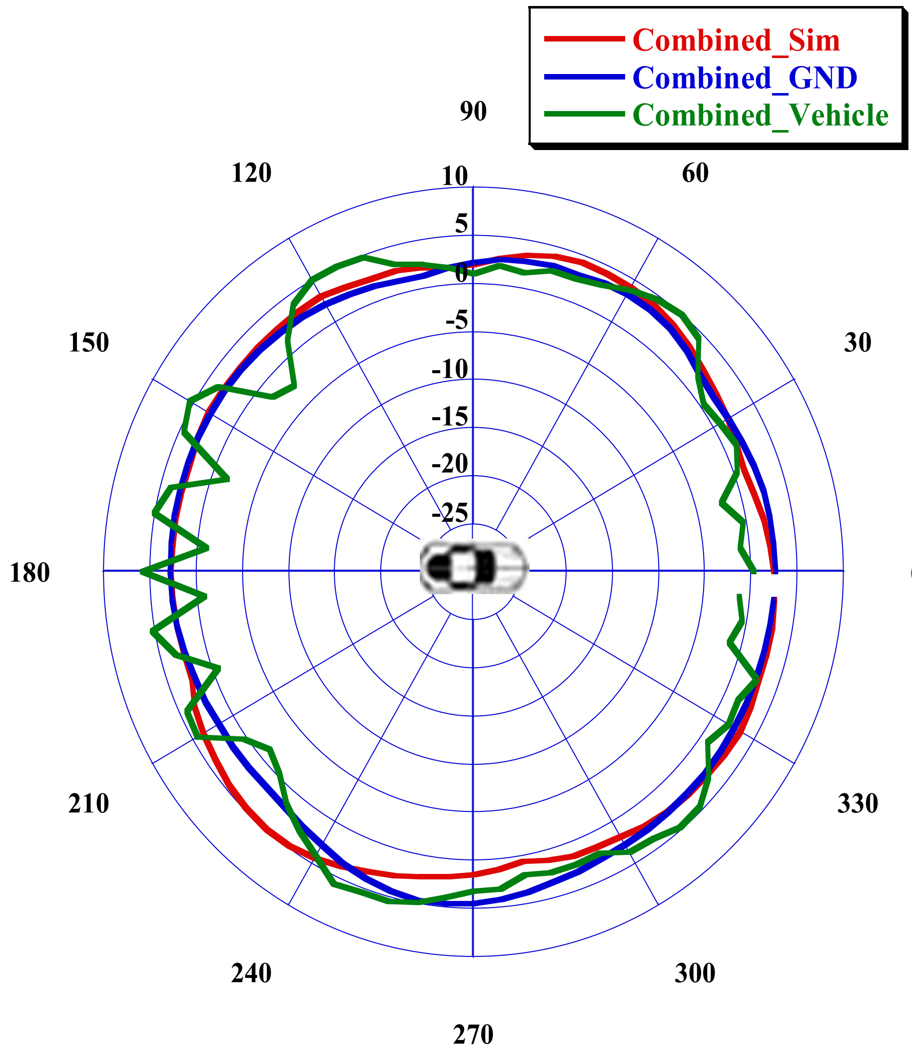

(b) 1900 MHz

Figure 3.20. Continued.

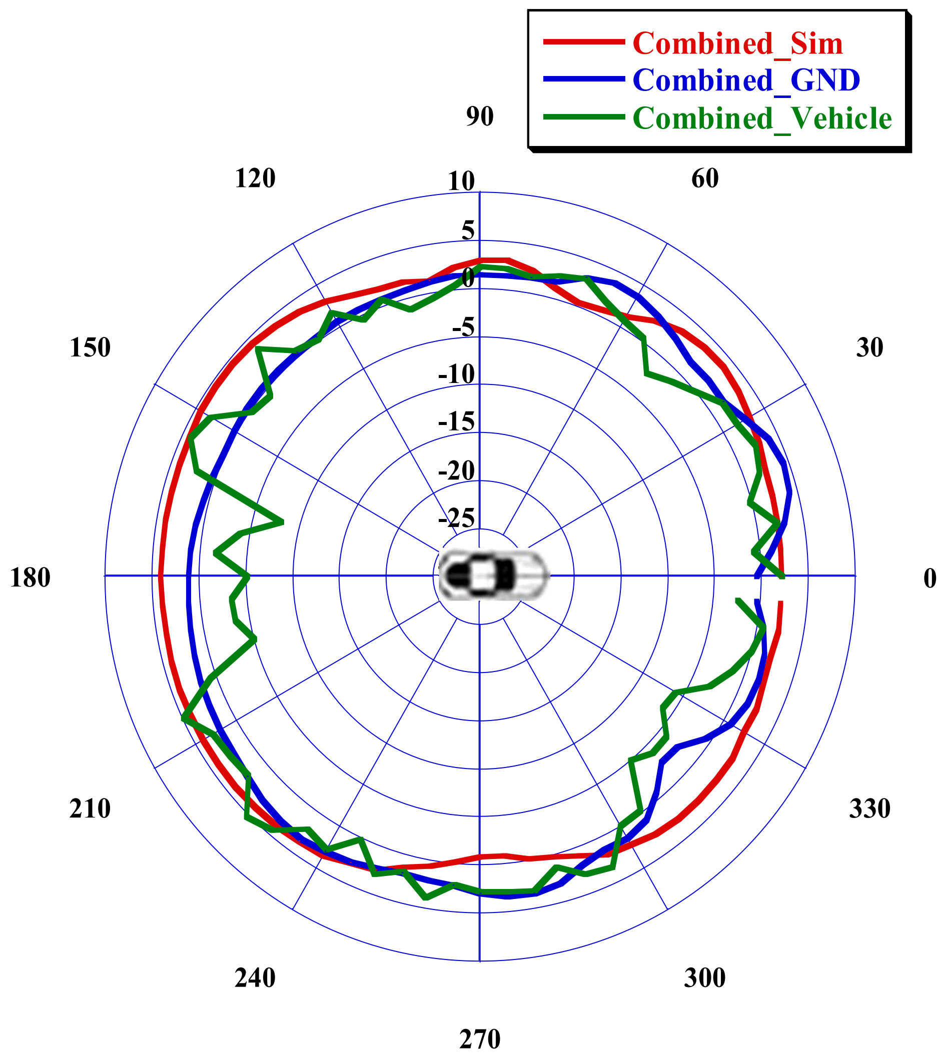

(c) 3600 MHz

Figure 3.20. Continued.

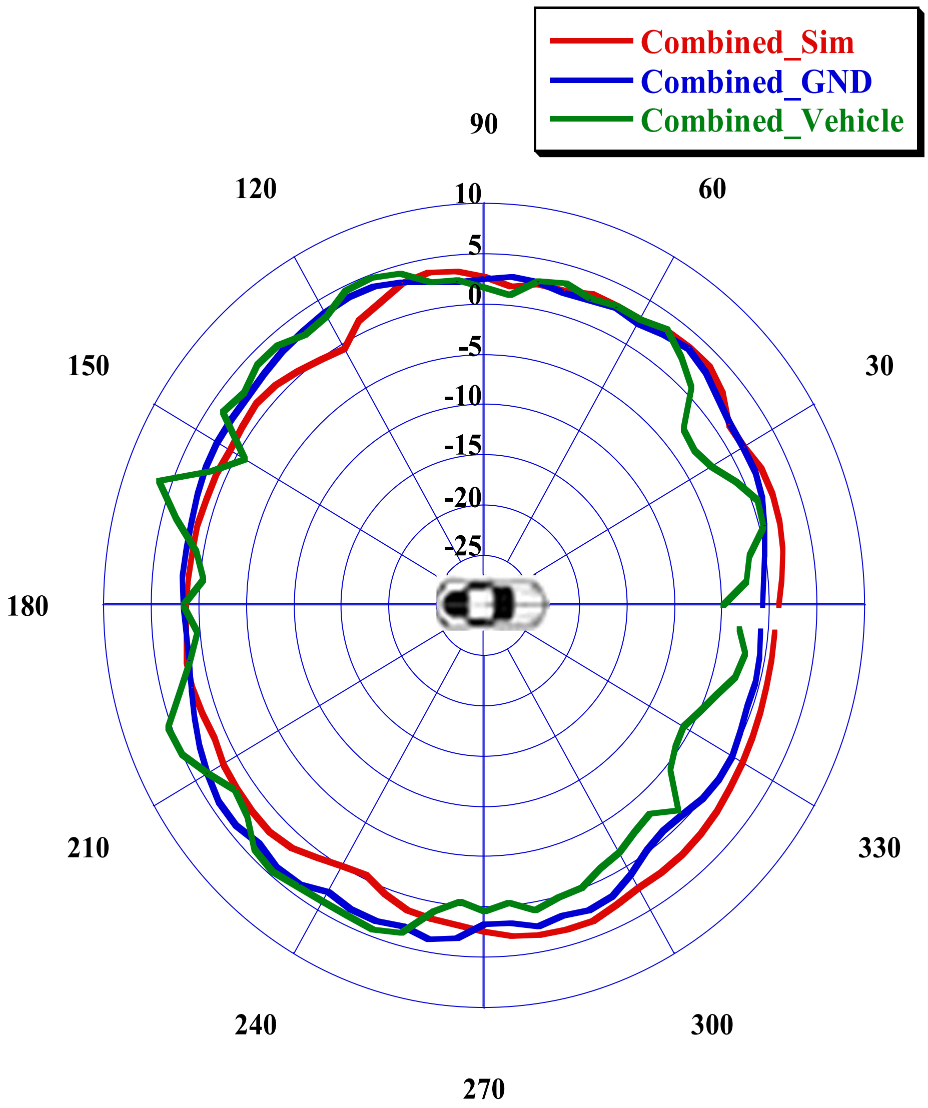

(d) 5000 MHz

Figure 3.20. Continued.

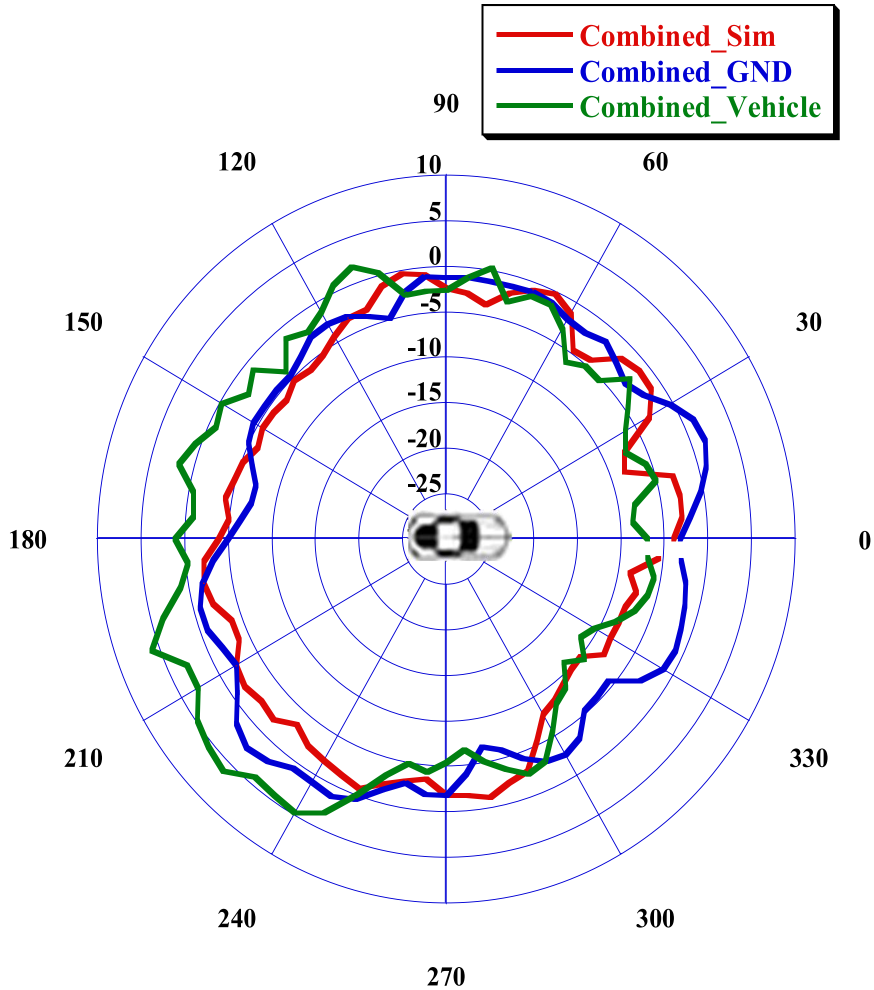

(e) 5900 MHz

Figure 3.20. Continued.

The measured radiation antenna efficiencies for the two elements are shown in Figure 3.21. It can be noticed that the 5G GND measurement has an average efficiency higher than 72% for both elements across all frequency bands whereas the vehicle measurement has a reduced average efficiency of 64%. For V2X frequencies, the measured antenna efficiencies on GND and on the vehicle is higher than 55% across the band. The ECC and DG were also calculated in this MIMO configuration using equation 3.1 and 3.2 in a MATLAB script. Figure 3.22 shows these values. The worst value of ECC and DG exists in the low frequency band where the worst-case passive isolation exists between the two elements. Compared to the second configuration in Figure 3.8, using the wide-band monopole yields better ECC and DG values. The improved ECC and DG performance can be attributed to having two partial orthogonal currents (horizontal current from the PIFA and vertical current from the monopole).

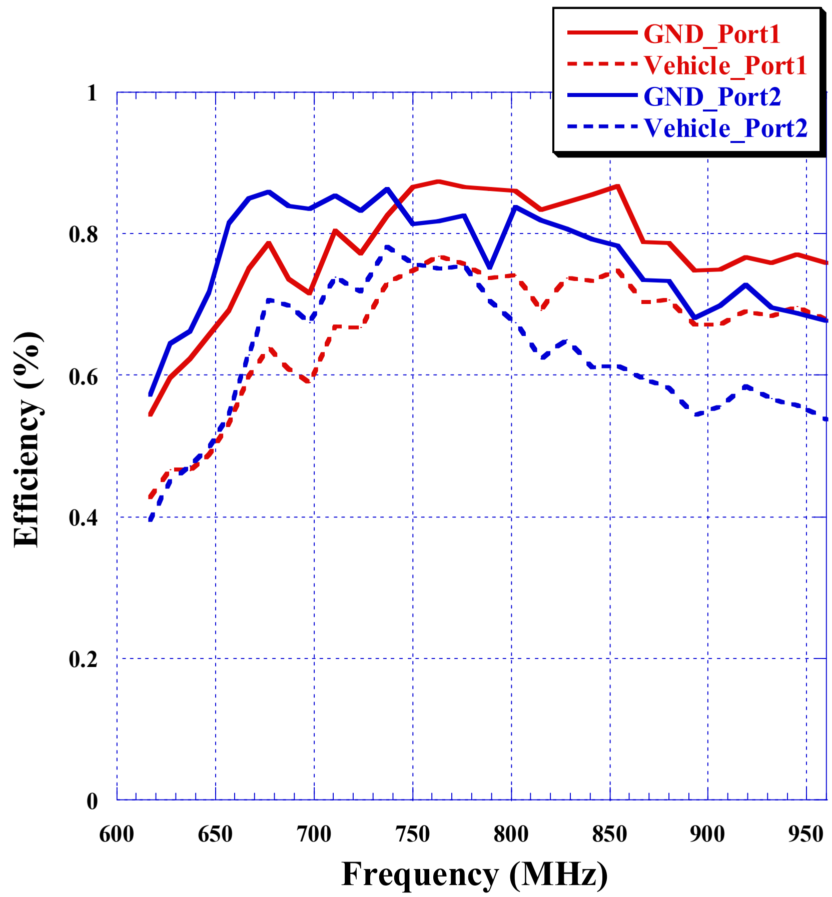

(a) 617 MHz-960 MHz

Figure 3.21. Antenna radiation efficiency for port 1 (monopole) and port 2 (PIFA) :(a) 617MHz-960MHz, (b) 1710MHz-2690MHz, (c) 3400MHz-5000MHz, (d) 5850MHz-5925MHz.

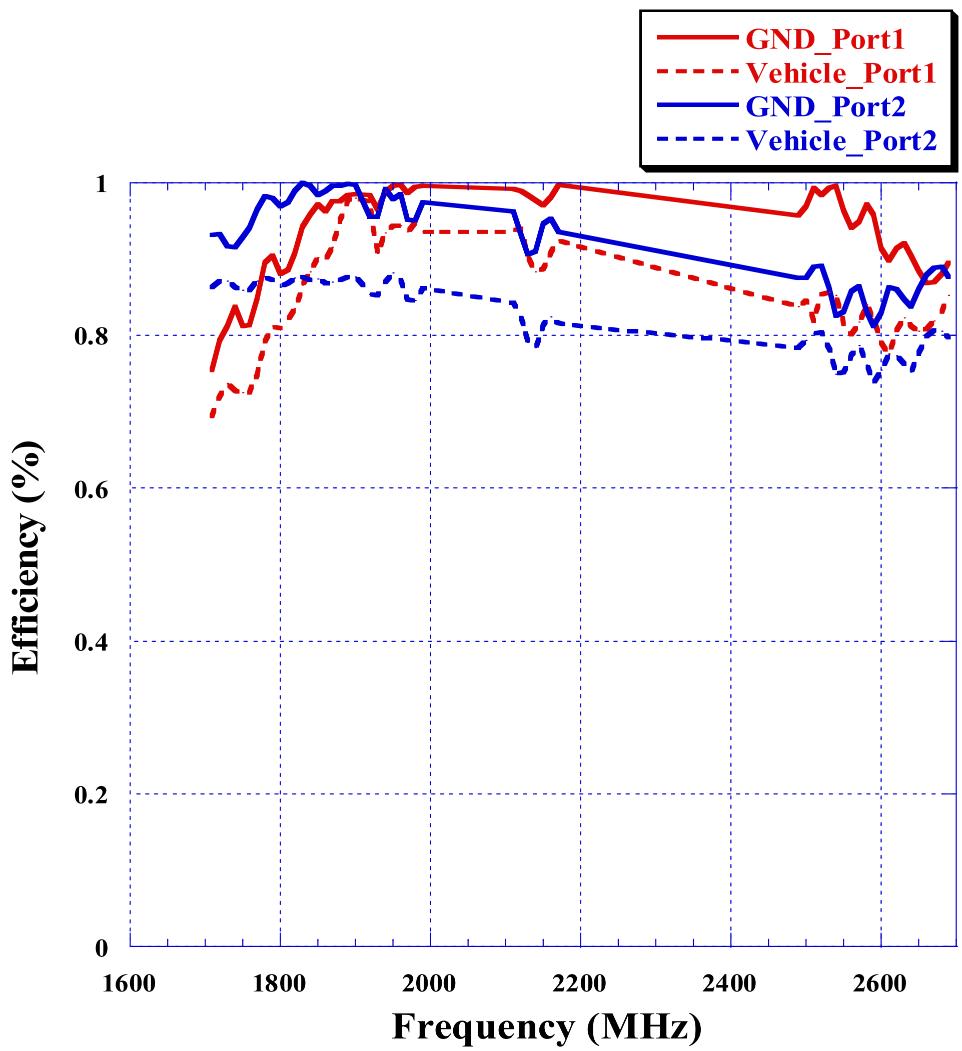

(b) 1710 MHz-2690 MHz

Figure 3.21. Continued.

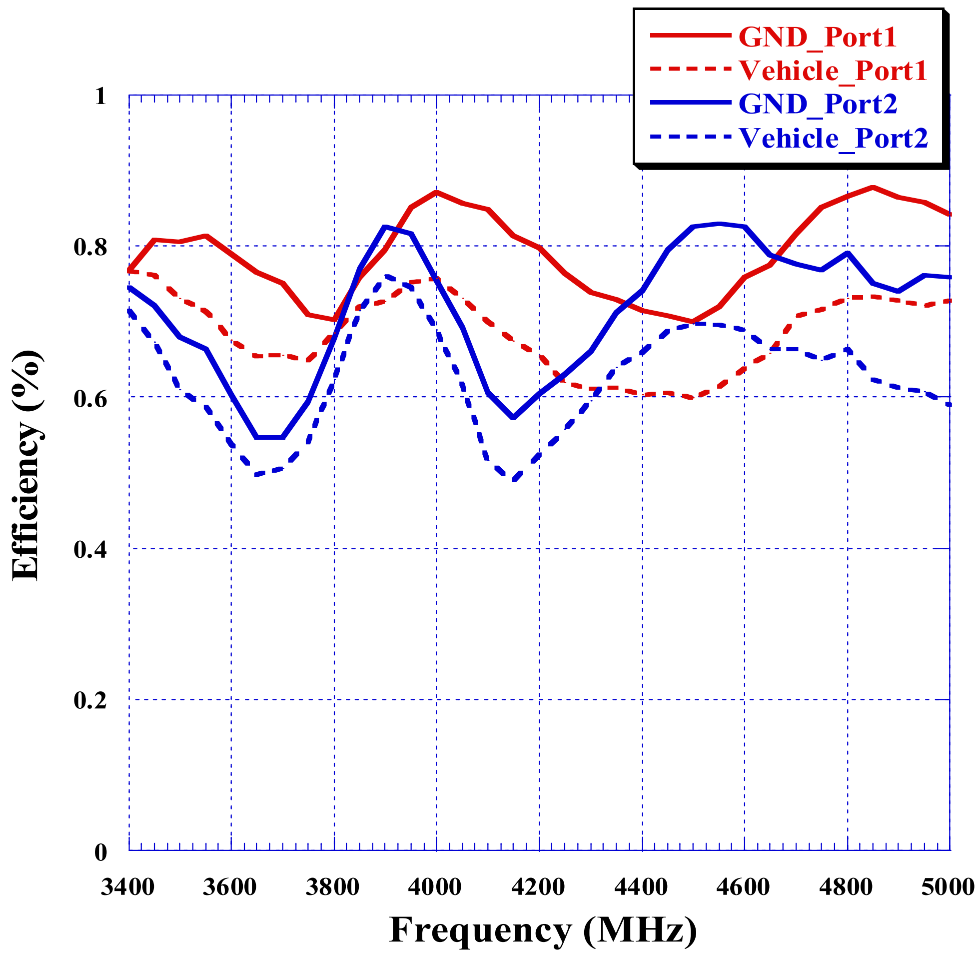

(c) 3400 MHz-5000 MHz

Figure 3.21. Continued.

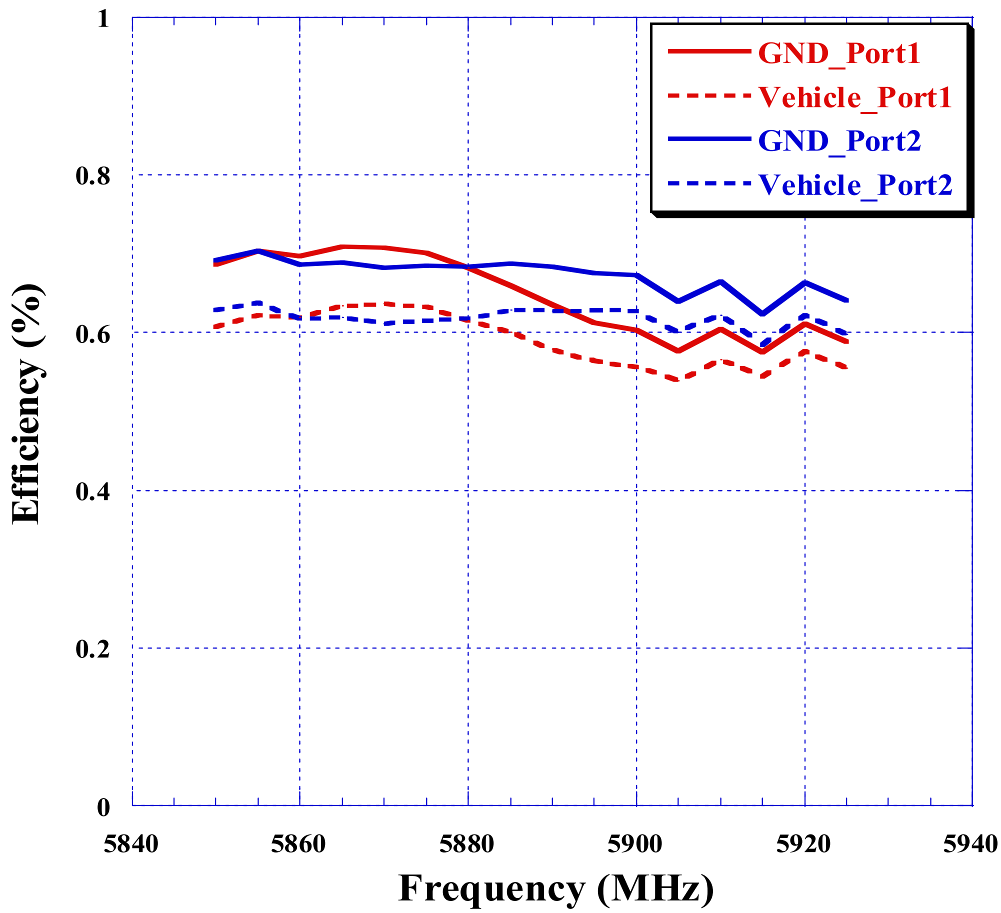

(d) 5850 MHz-5925 MHz

Figure 3.21. Continued.

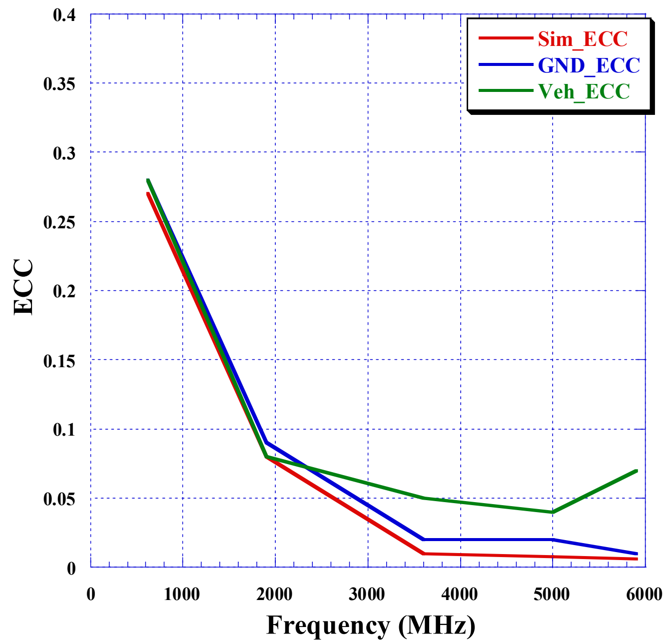

(a) ECC

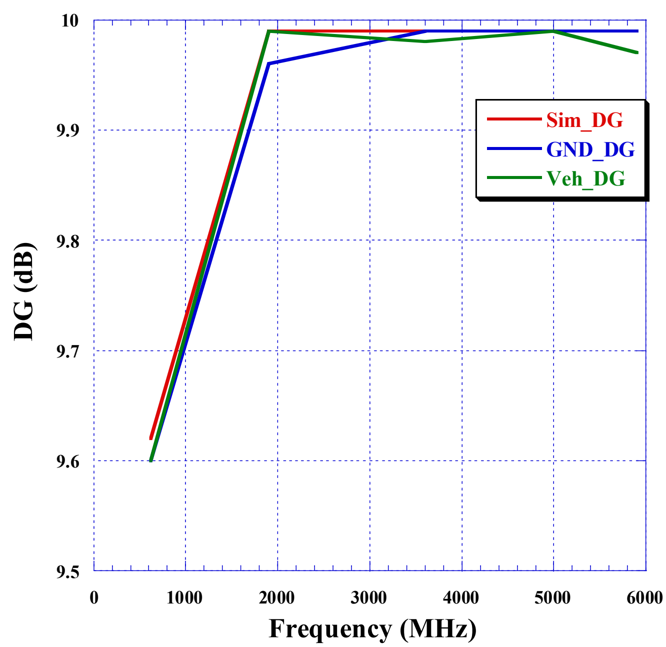

(b) DG

Figure 3.22. ECC and DG Values for PIFA-monopole MIMO system: (a) ECC, and (b) DG.

Next, a performance analysis is done via simulation by increasing the distance between the two elements by 40mm and rotating the PIFA by 90 degrees clockwise. First, the distance is changed to 160mm between the elements while keeping the same orientation. The electric field components are exported and then processed in MATLAB to see the effect on ECC and DG. Figure 3.23 shows the calculations done for ECC and DG at distance 160mm and it can be noticed that increasing the distance in this configuration improves the ECC and DG at the expense of package size.

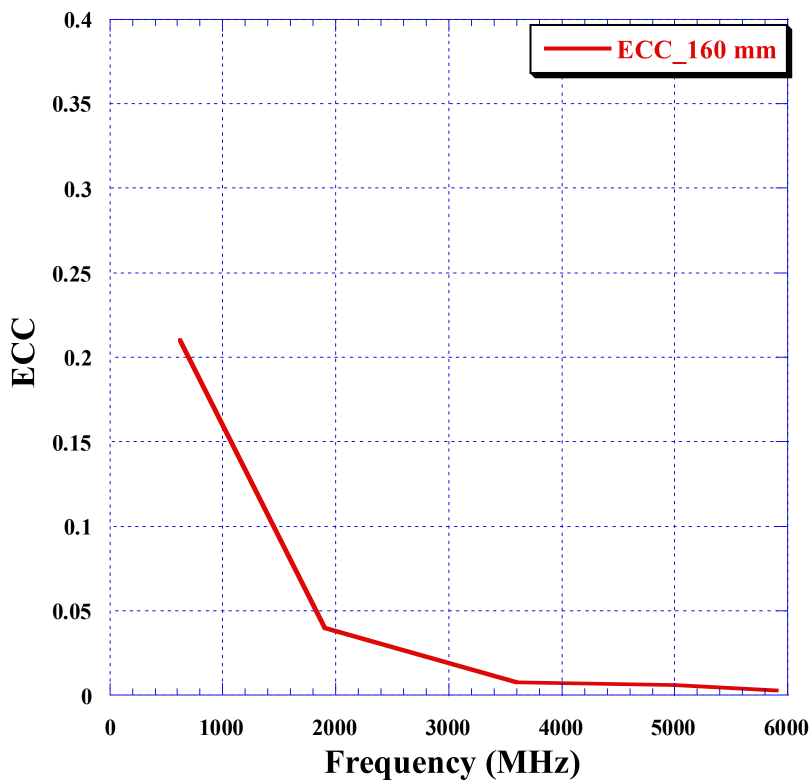

(a) ECC

Figure 3.23. ECC and DG Values for at distance 160mm: (a) ECC, and (b) DG.

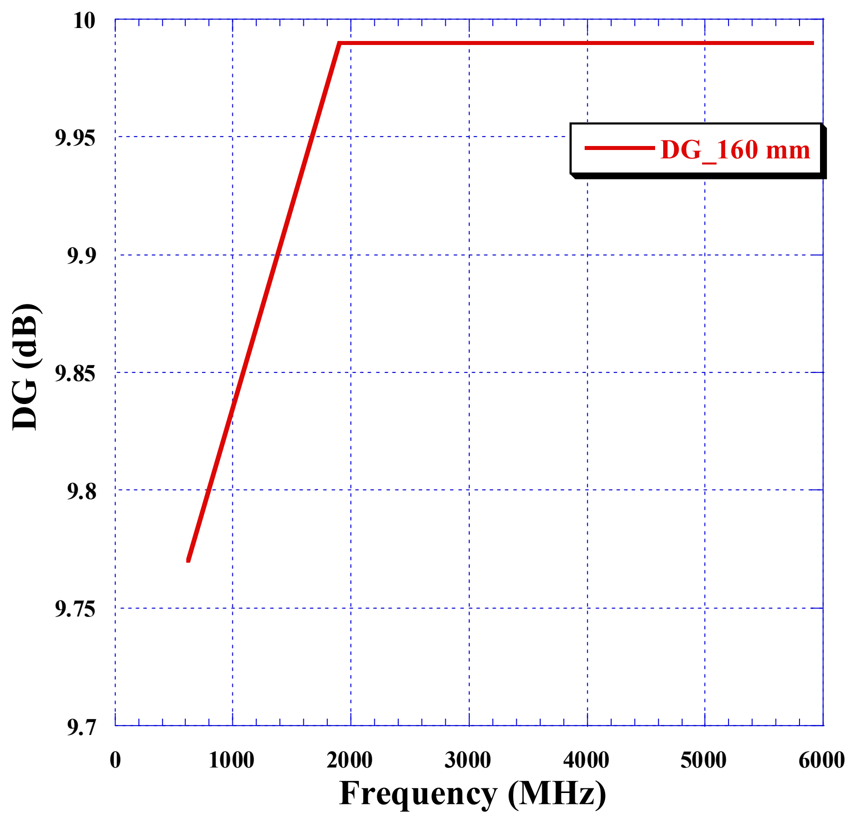

(b) DG

Figure 3.23. Continued.

Fig. 3.24 presents the values of ECC and DG when rotating the PIFA 90 degrees clockwise. There is a slight improvement in the low band frequency while the mid and high band increased for the ECC. This could be reasoned from rotating the PIFA, the shorting pin has moved further away from the monopole while the feeding pin gets closer to it, which might help in the low band isolation but not in the mid and high frequency bands.

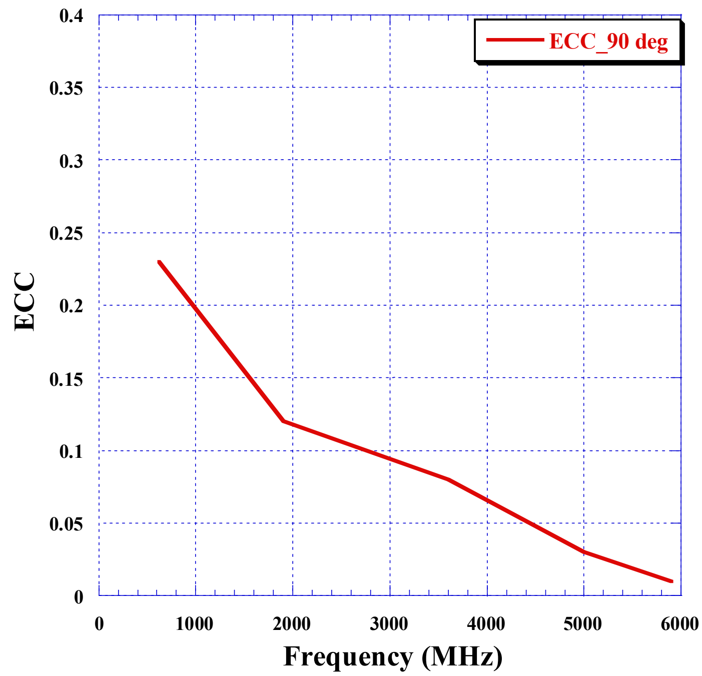

(a) ECC

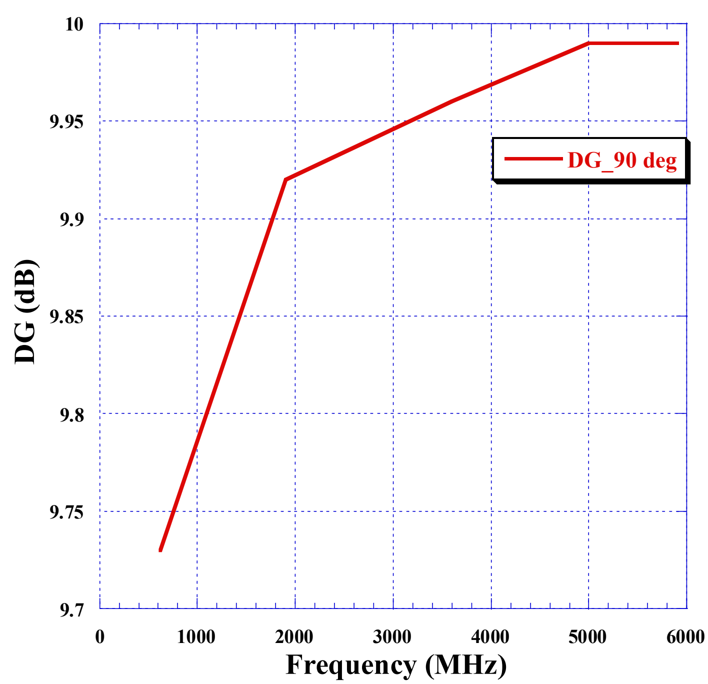

(b) DG

Figure 3.24. ECC and DG Values for at 90 degrees rotation: (a) ECC, and (b) DG.

3.4 Conclusions

Multiple two-element based MIMO antenna systems were presented in this paper for 5G and V2X bands to be used in automotive applications. The ECC and DG values were calculated in each MIMO configuration using electric field components (magnitude and phase) from the radiation patterns of each antenna element. The first MIMO system represents two low profile PIFAs separated by a given distance (600mm) on the vehicle's roof. The system achieves a passive isolation better than 26dB, ports efficiencies higher than 68% on vehicle across all bands, ECC lower than 0.10, and DG higher than 9.94dB. The second MIMO system consists of two PIFAs on the same PCB separated by a fixed distance and rotated in various positions. This MIMO system has a passive isolation better than 11dB, ports efficiencies higher than 60% on vehicle, ECC lower than 0.39, and DG higher than 9.20dB. Finally, the third MIMO configuration investigated the performance when having one element as a monopole and one as PIFA. It achieves passive isolation better than 10dB, ports efficiencies higher than 55% on vehicle, ECC lower than 0.28, and DG higher than 9.60dB. In general, each MIMO configuration has a satisfactory performance and can be used in the vehicular applications depending on the desired requirement, housing style, and physical dimensions.

CHAPTER FOUR

WIDE BAND RAISED PRINTED MONOPOLE FOR 5G COMMUNICATIONS

4.1 Introduction

To achieve the requirements for 5G and V2X autonomous communications, multiple input multiple output (MIMO) antenna system should be implemented. MIMO systems have many antenna elements placed at both receiver and transmitter that operate at the same frequency range which will increase the number of channels across the radio frequency (RF) link, and hence significantly improving the total data rate and throughput in the network without increasing the transmit power or enlarging the frequency band [26]-[27]. The RF performance of the MIMO system is very dependable on the efficient design of the antenna elements. The antennas should have good radiation efficiencies and high isolation or very low correlation between them, which will result in very reliable and low latency system even in a highly scattering electromagnetic environment [41]. The Envelope Correlation Coefficient (ECC) is an important parameter that is used to measure the correlation between the antenna elements. A low value of ECC (ideally zero) shows a high isolation (low correlation) between the antennas that results in independent RF channels in the system which is needed to achieve the required MIMO performance [43].

The MIMO antenna design in the automotive field has many limitations that affect its performance. Physical dimensions, size limitations, and interference (coupling) between different antennas are challenging issues especially if the antennas are placed in one housing. These challenges make it hard to meet the standards of MIMO performance in terms of radiation efficiency, isolation, and diversity especially when multiple applications are implemented in one single housing such as: AM/FM, Digital Audio Broadcast (DAB), cellular 5G, Satellite Digital Audio Radio System (SDARS), Dedicated Short Range Communications (DSRC), Global Navigation Satellite system (GNSS) [6].

In this study, a novel broad band raised printed monopole with partial ground plane for automotive applications has been designed. Its special shape and physical dimensions make it appropriate for installation inside a shark-fin module on the car's top. The suggested design's distinctive form, combined with the usage of slots and partial ground plane (PGP) structures, allows it to cover a large frequency range, from 1.71GHz to 5GHz, while maintaining relatively compact dimensions. To meet the high-performance needs of 5G communications, a 2x2 MIMO antenna system is also examined. The ground plane construction on the back of the monopole, which increases passive isolation without increasing the spatial distance between the components, allowed the suggested MIMO system to achieve good performance and isolation between elements. This is especially true at lower frequency bands.

4.2 Proposed Antenna Design and RF Performance Results

The design consists of raised monopole printed on FR4 material with dielectric constant (ϵ_r) of 4.4, permeability of 1, loss tangent of 0.025, and high mechanical strength and insulating characteristics with low cost which makes it an excellent candidate for a substrate material. Figure 4.1 and table 4.1 shows the antenna layout and its optimized geometrical parameters with total dimensions of 30mm (height) x 27mm (length) x 1mm (width or substrate thickness).

The monopole structure consists of a feeding line and a wide rectangular shape with two branches. The feed line has a height of 11mm (F_h) and a width of 3mm (F_L) that feeds the rectangular shape with RF signal. A reversed U-shape slot is constructed along the feed line to increase the travelling path of RF current which supports higher wavelengths and hence helps tune the antenna towards lower frequency bands. The wide rectangular shape is excited by the feed line, its height and length allow the antenna to operate across the whole frequency range from 1.71GHz to 5GHz in addition to two branches connected to the structure that will increase the total height of the element to make the element operate at lower frequency bands. As a guideline for the antenna design, the feed line, and the rectangular shape with two branches should be loaded at $\frac{\lambda_c}{4}$ distance from the ground plane where $\lambda_c$is the center frequency of the operating frequency range (f_c = 2.5GHz) to provide good impedance matching and radiation pattern values. The length of the wide rectangular shape increases the total volume of the antenna and hence allows it to cover a wide frequency range. The FR4 material and the reversed U-shape slot will load the antenna element and further increase the current path which enables the design to operate at lower frequencies.

The partial ground plane shape on the back side has a height of 8mm (Hg) and a length of 27mm (Lg). This structure has a significant effect on improving the VSWR of the antenna and provides a better isolation between the elements in the MIMO system as presented in the next section. The height and length of the PGP were optimized to improve the impedance bandwidth across the operating bands and to reduce the mutual coupling between the elements. Figure 4.2 shows the fabricated antenna prototype with front and back views [55].

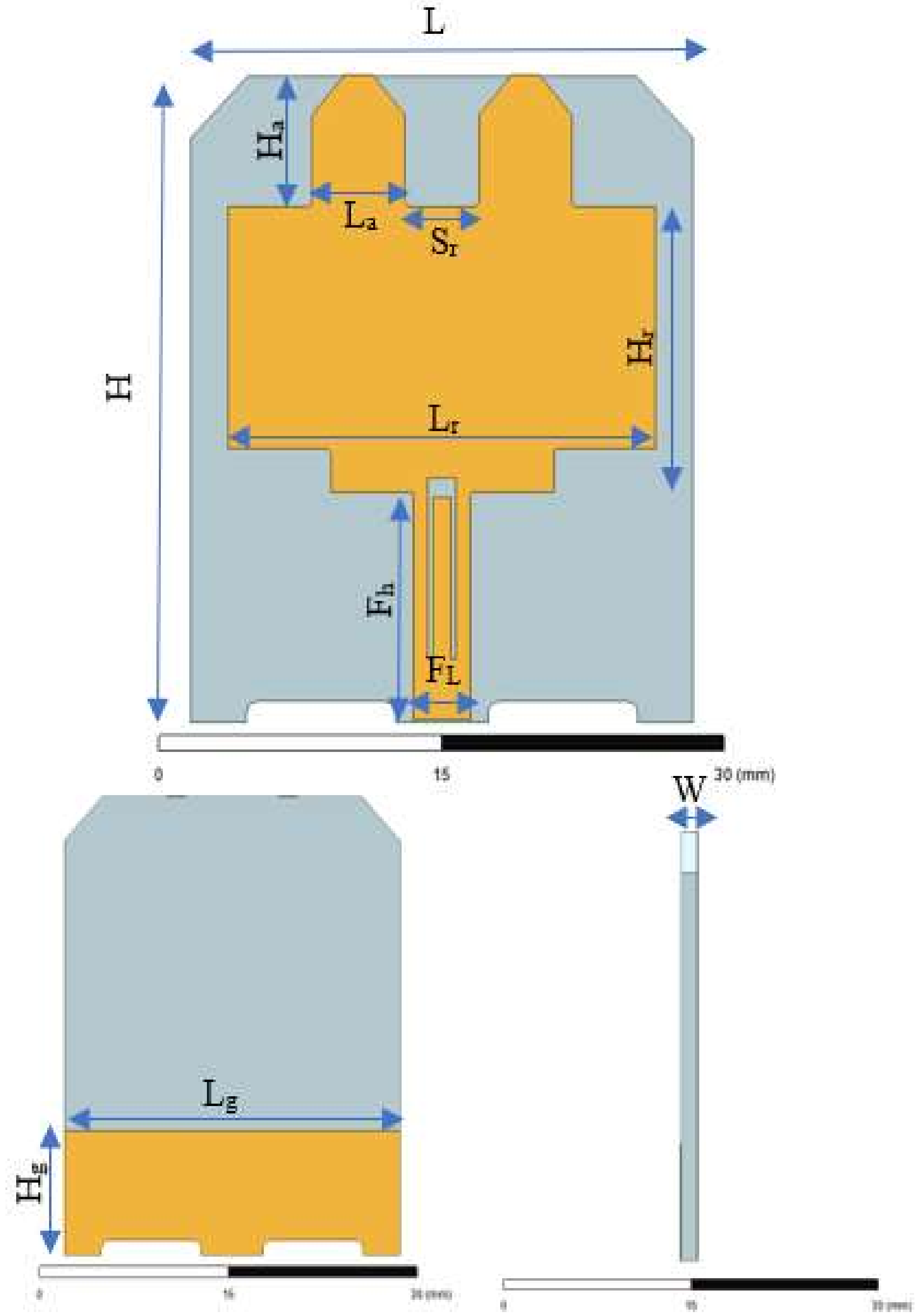

Figure 4.1. Simulated antenna with front, back and side views with its geometrical parameters.

(a) Front view

(b) Back view

Figure 4.2. Fabricated antenna prototype with front and back views: (a) front view, and (b) back view.

Table 4.1. Values of the optimized geometrical parameters of the proposed antenna.

Parameter	Value (mm)
H	30
L	27
W	1
H_a	6.25
L_a	5.25
F_h	11
L_{ge}	7.8
L_{re}	5.25
H_{te}	4.2
L_g	27
H_g	8
S_r	4
L_r	23
H_r	12.75
F_L	3
L_{te}	1.5
L_{fe}	4.25
S_h	9
H_{re}	1.85

The antenna is simulated using HFSS software that implements Finite Element Method (FEM) and then the fabricated prototype is measured on a one-meter rolled-edge ground plane in an anechoic chamber. The antenna setup inside the chamber is shown in Figure 4.3 where an SMA connector is being used to connect the antenna feed point with the chamber's measurement coaxial cable.

Figure 4.4 shows a comparison between the simulated and measured VSWR of the proposed design. It can be depicted from the results that the performance of VSWR is better than (2:1) across the whole frequency band (1.71GHz to 5GHz). Figure 4.4 also shows good agreement of antenna impedance between the simulated model and the fabricated prototype with minor differences due to antenna placement on ground plane and small cable loss across frequency bands. In addition, Figure 4.4 shows a reasonable rejection for GNSS and DSRC bands which makes the design suitable to be integrated with multiple applications in a single housing. Figure 4.5 shows the effect on bandwidth impedance of the PGP shape that is placed on the back side of the element. The VSWR gets better with around 2.5 across the entire 5G band when the rectangular ground plane is implemented, which is essential to meet the impedance matching requirement for the design.

The surface current distribution and electric field intensity on the front and back side of the element is shown in Figure 4.6. The magnitudes are shown in decibels (dB) which is acquired by obtaining the magnitude of magnetic field (H-field) measured in (A/m) and electric field (E-field) measured in (V/m) then applying the formulas (4.1) and (4.2):

$$\text{Surface Current (dB)} = 20 * \log (|H (A/m)|) \qquad (4.1)$$

$$\text{E-field (dB)} = 20 * \log (|E (V/m)|) \qquad (4.2)$$

It can be concluded that at low frequencies, the current distribution is more intense and spread across the entire structure of the antenna up to the two branches. However, when increasing the frequency band, the current supports shorter paths to radiate at higher frequencies. The effect of PGP on the current is also shown in Figure 4.6 across different frequencies. It can be concluded that a significant amount of in-phase current is going through the partial ground plane shape which helps improve the impedance bandwidth across the whole band.

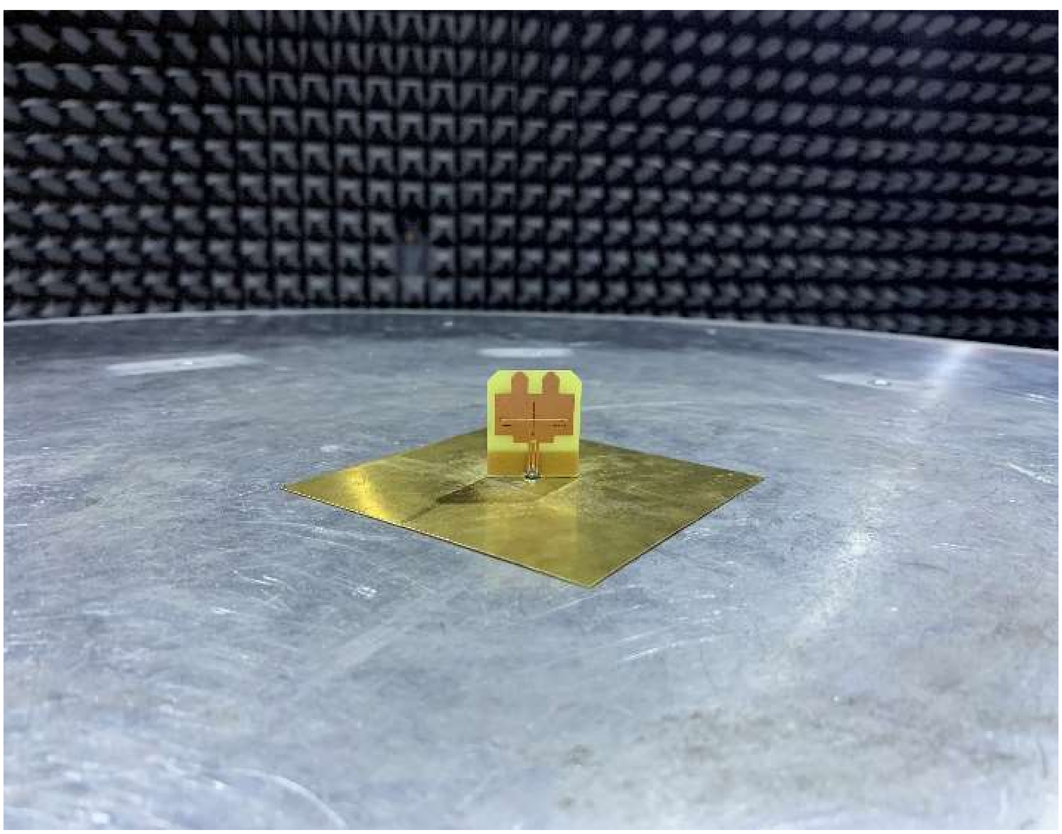

Figure 4.3. Antenna Setup on ground plane.

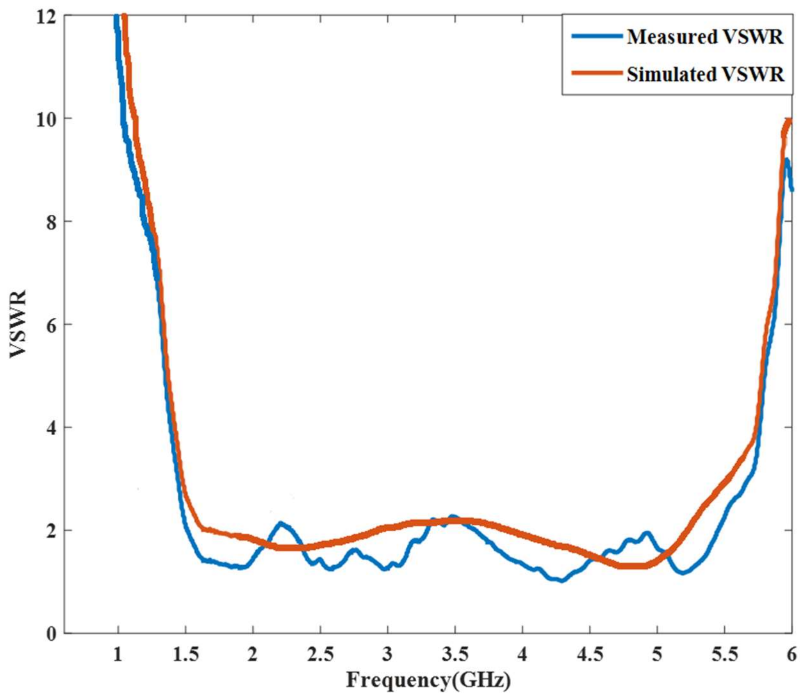

Figure 4.4. Measured and simulated VSWR on ground plane.

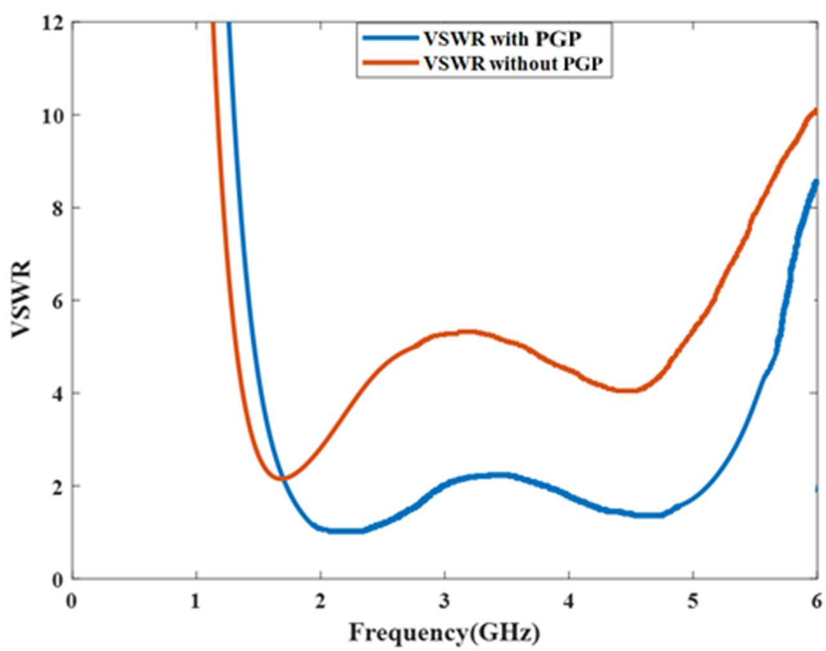

Figure 4.5. Comparison of simulated VSWR with and without partial ground plane structure on the back side of the element.

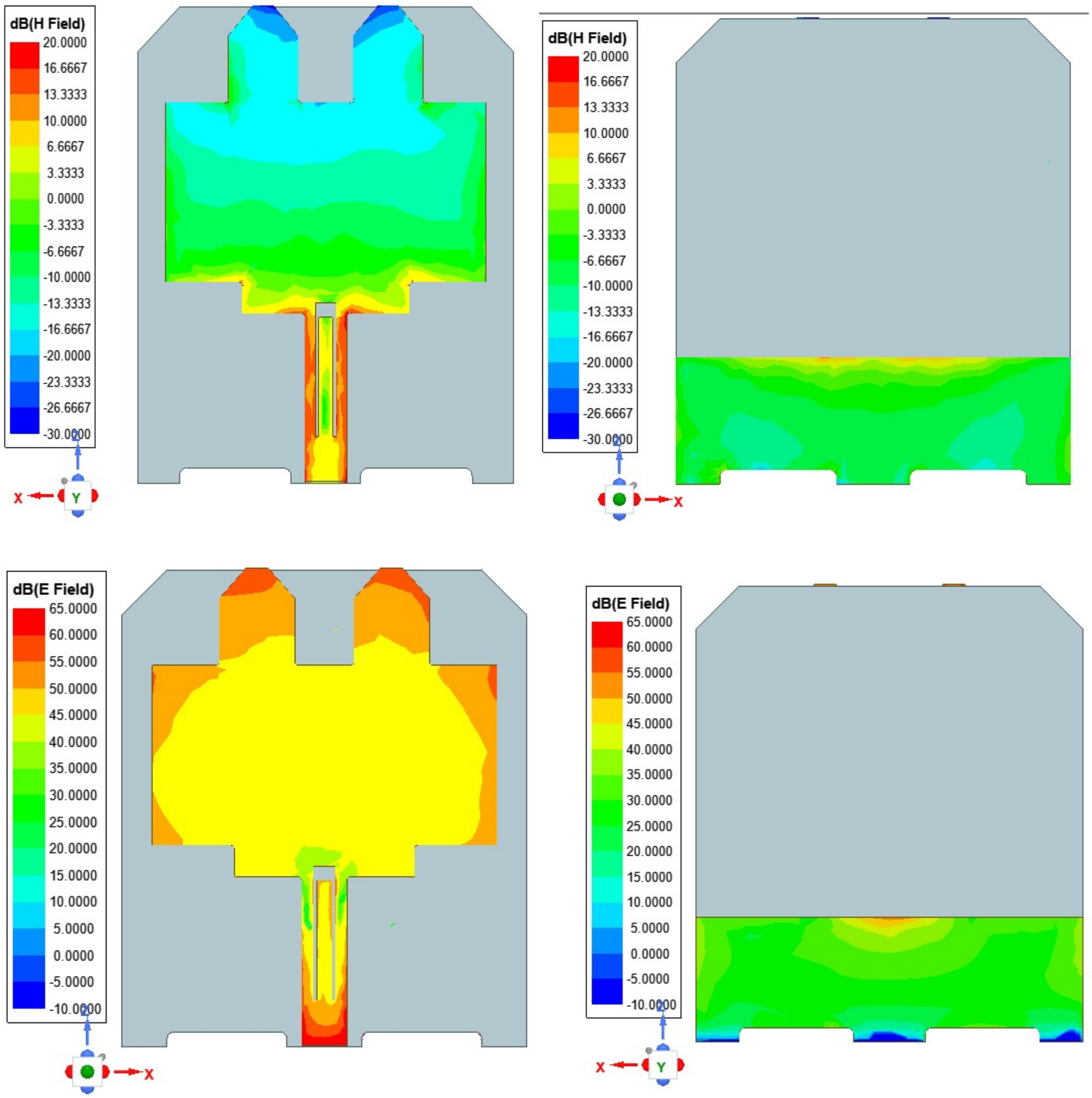

(a) 1710 MHz

Figure 4.6. Current distribution and electric field intensity measured in (dB) on the front and back side of the antenna: (a) 1710MHz, (b) 3600MHz, and (c) 5000MHz.

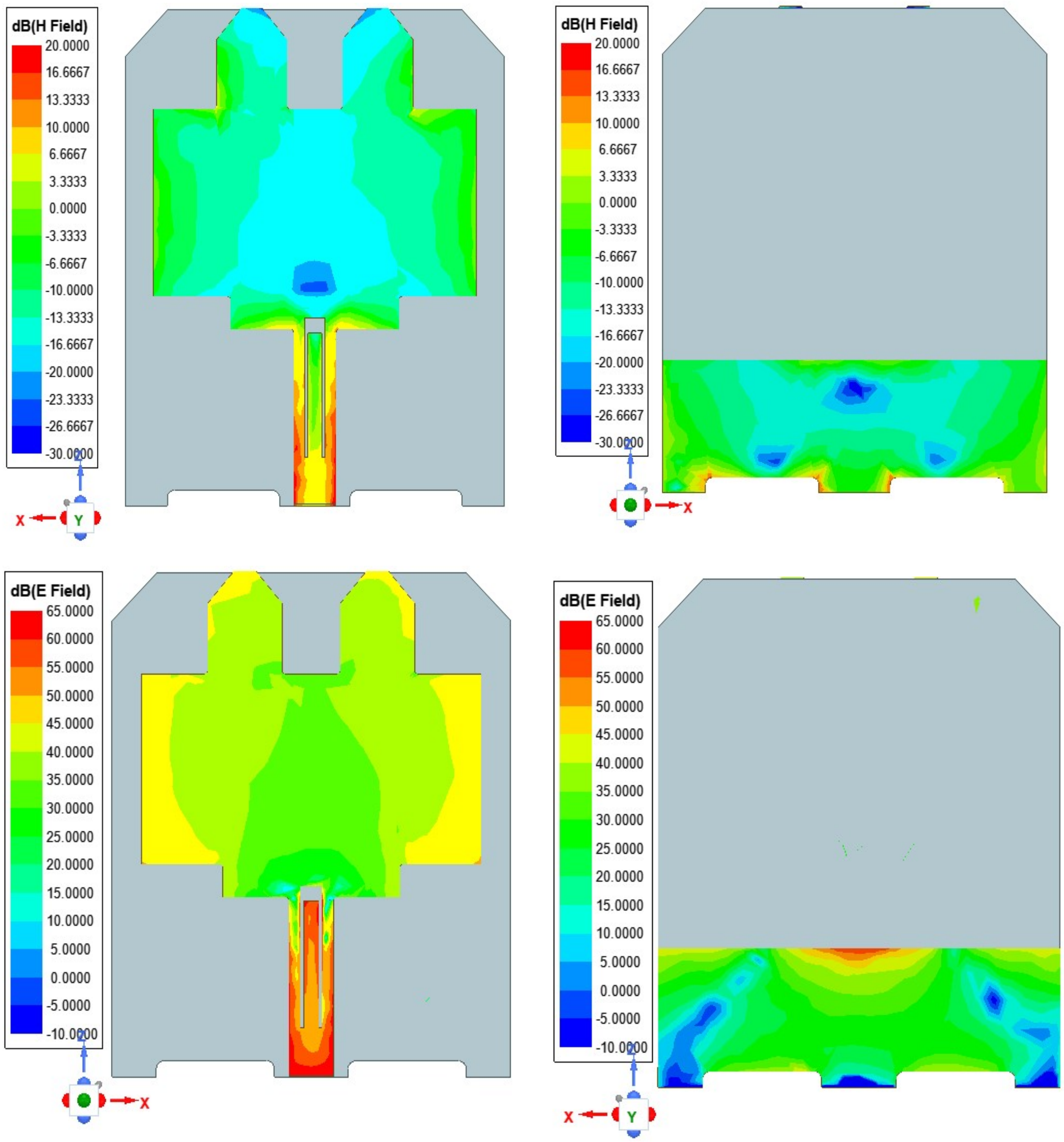

(b) 3600 MHz

Figure 4.6. Continued.

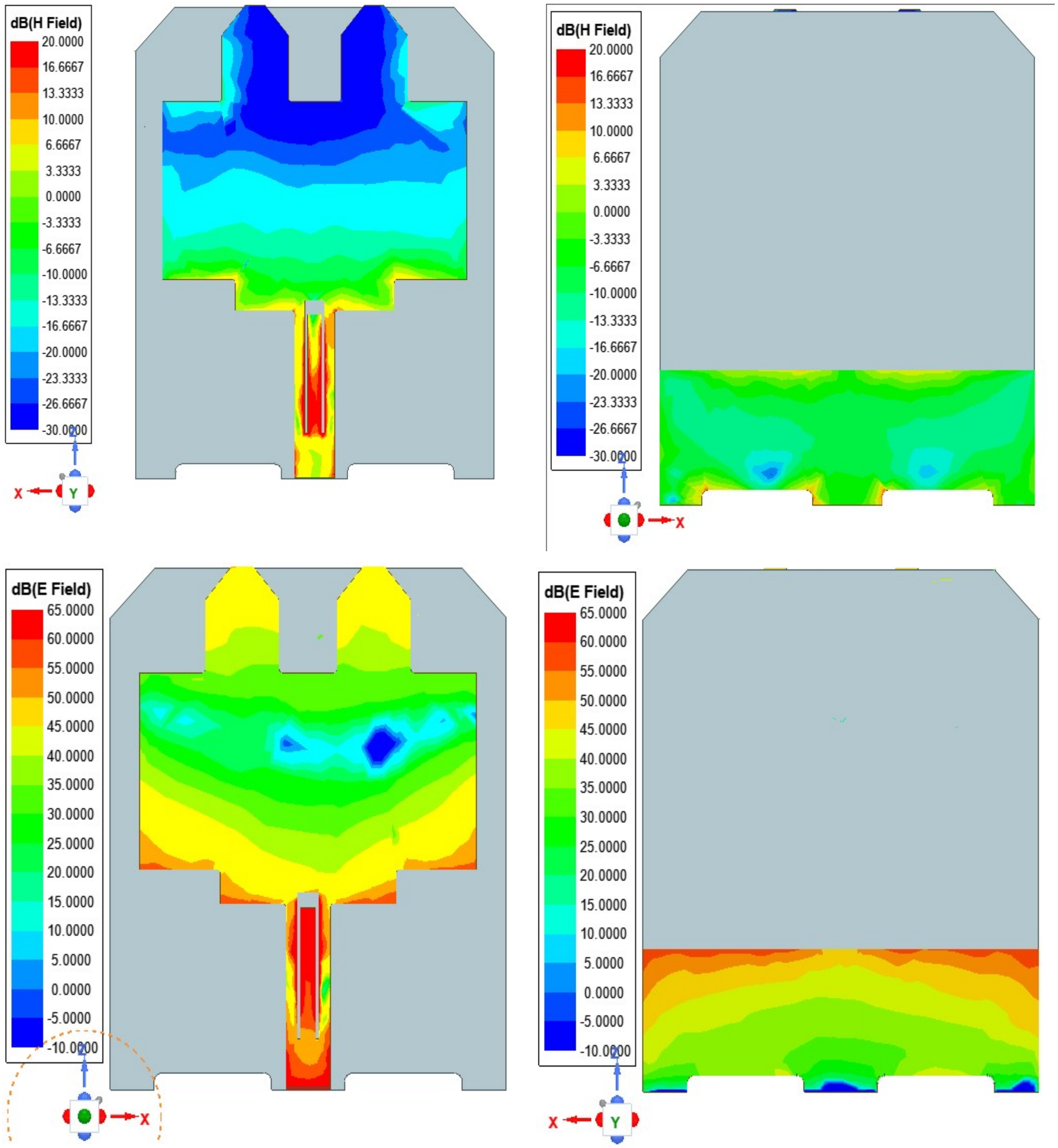

(c) 5000 MHz

Figure 4.6. Continued.

For optimal performance of 5G antenna on a vehicle, it is important to have an omni directional radiation pattern for theta between 75-87 degrees across the operating frequency bands. In Figure 4.7, horizontal cuts of the radiation patterns with vertical polarization at theta equals 80 degrees are plotted at multiple frequencies (1.71GHz, 3.6GHz, and 5GHz). The data traces present a comparison of radiation patterns of the simulated model on 1-meter ground plane against fabricated prototype radiation measurements on one-meter rolled-edge ground plane.

It can be noticed from Figure 4.7 plots that both simulation and measurement have a very good omni directional behavior across the whole operating bands, even though at high frequencies, the pattern shapes get a bit squinted at the sides (azimuth angles 90 and 270 degrees) but still have a very good omni directional shape across the entire azimuth angles with lowest gain value around 0dBi. Furthermore, the average gain obtained from ground plane measurements inside the chamber is found to be 1.75dBi, 3.20dBi, and 3.32dBi at frequencies 1.71GHz, 3.6GHz, and 5GHz, respectively, which indicates an excellent radiation performance of this antenna at 5G bands.

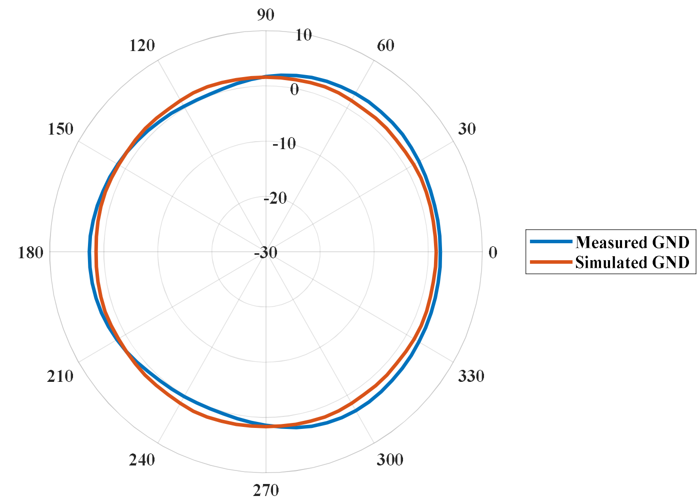

(a) 1710 MHz

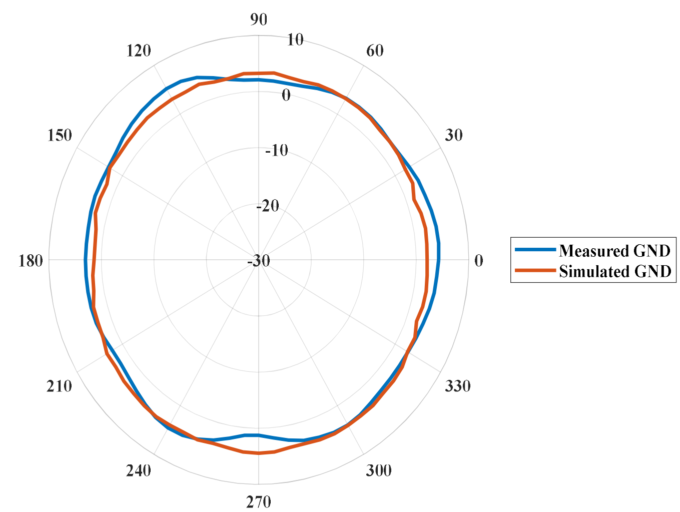

(b) 3600 MHz

Figure 4.7. Horizontal cuts of radiation patterns of simulated and measured on GND gain in (dBi) at theta equals 80 degrees: (a) 1.71GHz, (b) 3.6GHz, and (c) 5GHz

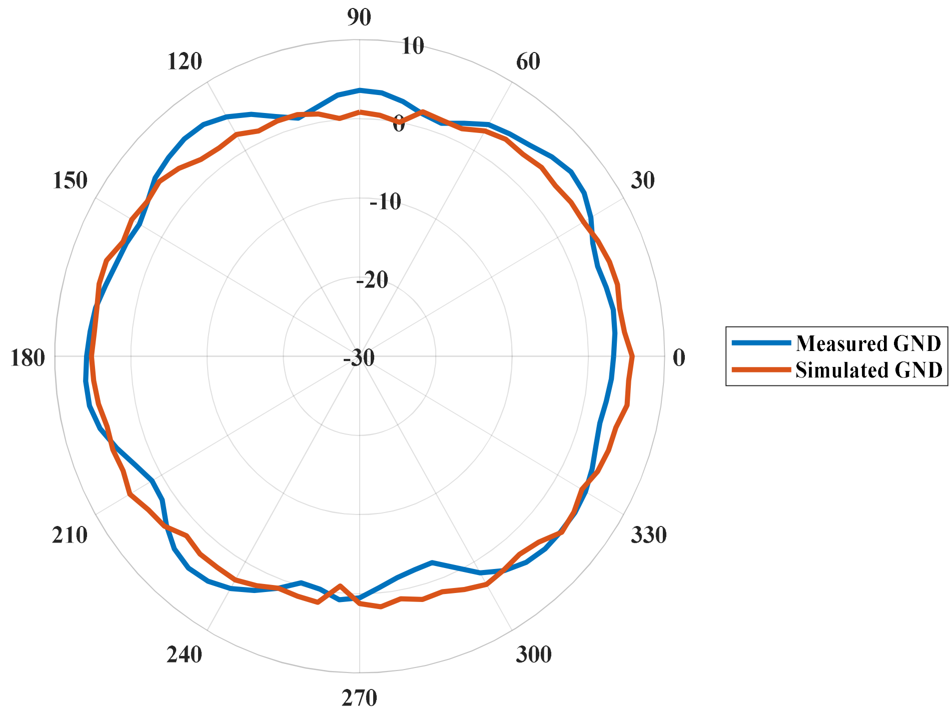

(c) 5000 MHz

Figure 4.7. Continued.

The measured antenna radiation efficiency is shown in Figure 4.8. It is obtained as a ratio of the power radiated from the antenna to the power delivered to the antenna's input. In another words, it describes how much of the delivered input power is being radiated by the antenna. It can be noticed from Figure 4.8 that the minimum radiation efficiency is about 65% with total average efficiency of 74.4% which shows very good radiation properties of the proposed design that makes it very suitable for 5G application in automotive industry.

The measured LAG of the antenna (in dBi) is shown in Figure 4.9. LAG is computed by calculating the average summation across the azimuth (phi) of linear average gain at every theta angle from 75 to 87 degrees across the whole frequency band than converting the results to dBi by using the formula (4.3):

$$LAG\ (dBi,f) = 10 * \log\ (\text{average gain across phi}) \qquad (4.3)$$

Figure 4.9 shows that minimum value of LAG is found to be 1.7dBi with most of the operating frequency range having better than 3dBi which gives an excellent gain performance for the proposed antenna.

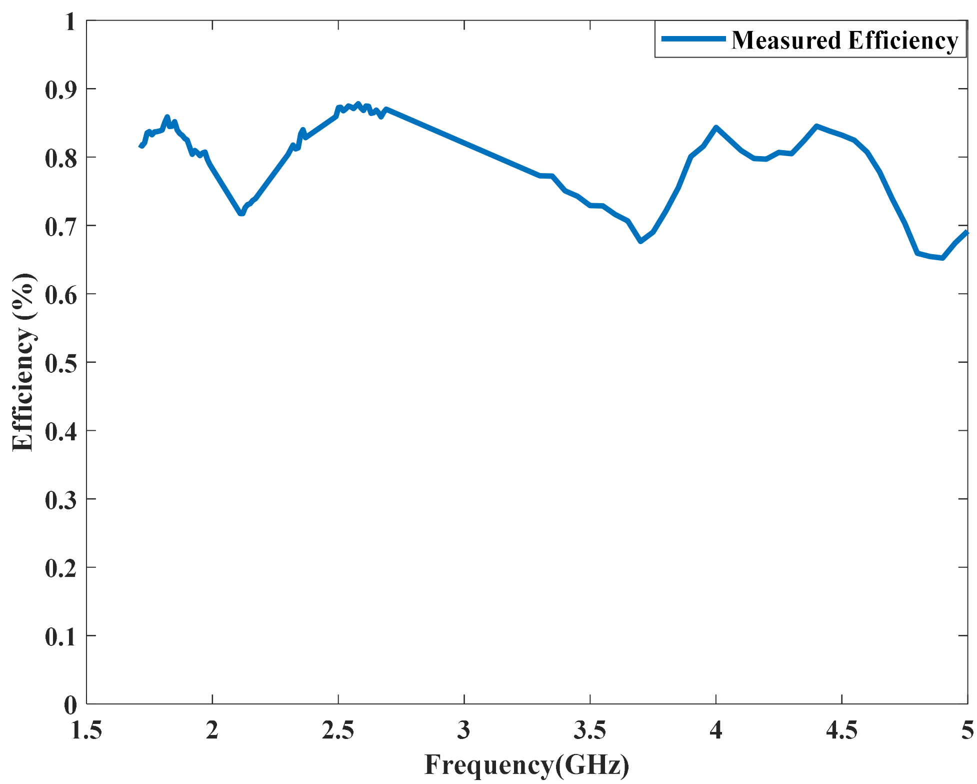

Figure 4.8. Measured antenna radiation efficiency on ground plane.

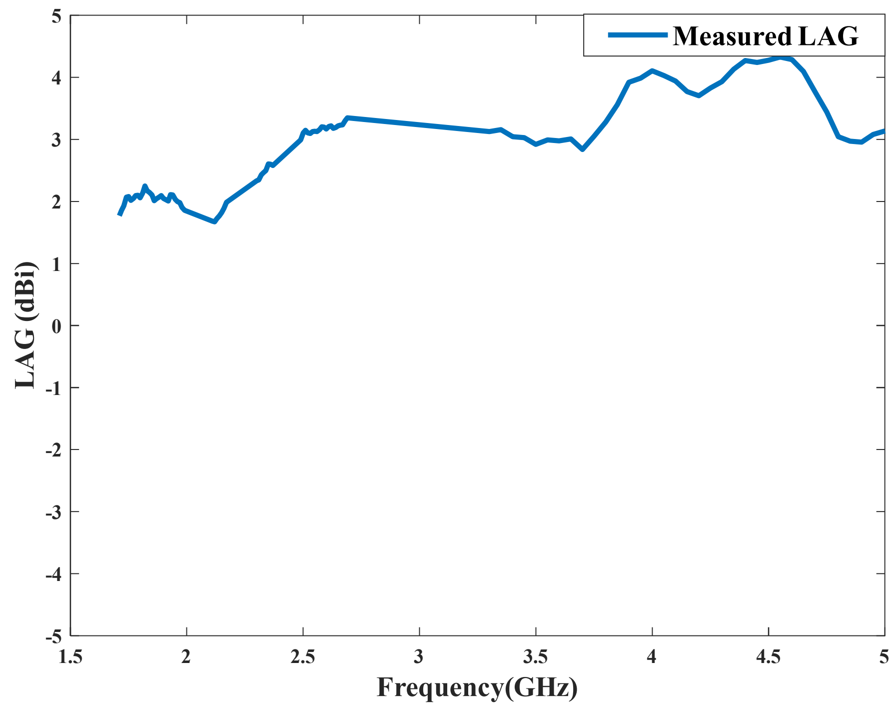

Figure 4.9. Measured LAG in dBi on ground plane across 5G band.

4.3 2x2 MIMO Antenna System Layout and Performance Results

In this section, two identical elements of the proposed antenna in the previous section are placed on the same Printed Circuit Board (PCB) with a spatial distance of 80mm (approximately 0.5 lambda of the smallest frequency in the band "1.71GHz"). Each antenna element is orientated on the opposite direction of each other (mirrored across z-axis) as shown in Figure 4.10 where the simulation and ground plane measurement setups for the proposed MIMO system is presented. The defected ground plane structure of each element is facing each other which is optimal for isolation improvement.

Figure 4.11 presents the passive isolation between the two antennas. Both measured and simulated isolation are in good agreement across the whole frequency band with minor differences due to antennas placement on PCB and small attenuation from RF cables at different frequencies. It can be noticed that the worst mutual coupling between the two antennas has passive isolation of 16 dB at the lower bands of the operating frequencies since the RF wavelengths are longer at these frequencies. However, most of the frequency points have better isolation than 20dB as shown in Figure 4.11 which shows a good isolation in the system. Figure 4.12 shows the difference in passive isolation on a simulation model with and without PGP shape on the back side of the element. The existence of the rectangular ground plane improves the isolation by approximately 3dB across the whole frequency bands.

In Figure 4.13, horizontal cuts of combined radiation patterns at theta 80 degrees are plotted for multiple frequencies 1.71GHz, 3.6 GHz, and 5GHz. The radiation patterns are measured by measuring one antenna while terminating the other antenna with 50 ohms then the two measurements are combined to get the total radiation pattern of the MIMO system. Figure 4.13 also shows very good omni directional behavior across the bands which is a significant requirement for the RF coverage around the MIMO system. Moreover, the combined average gain observed from the measured radiation patterns is found to be 3.15dBi, 5.12dBi, and 5.22dBi at frequency points 1.71GHz, 3.6GHz, and 5GHz, respectively.

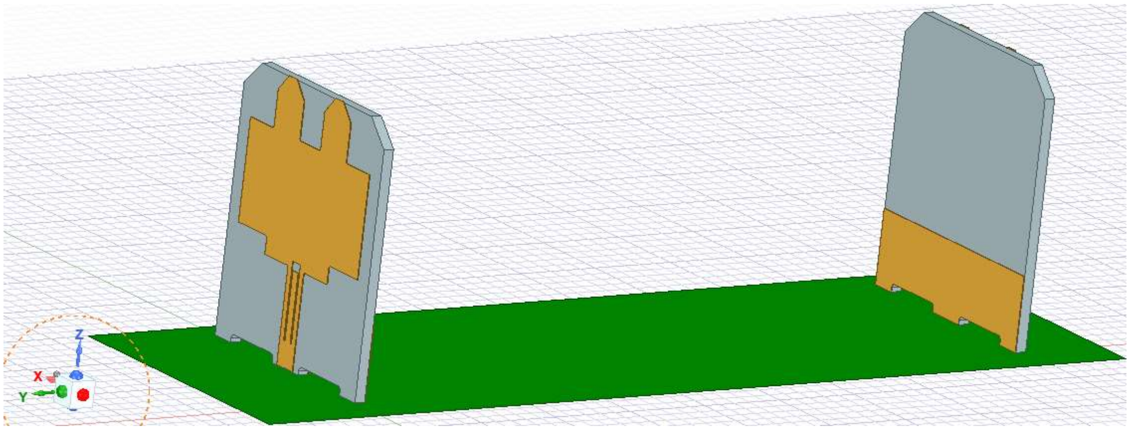

(a) Simulation model

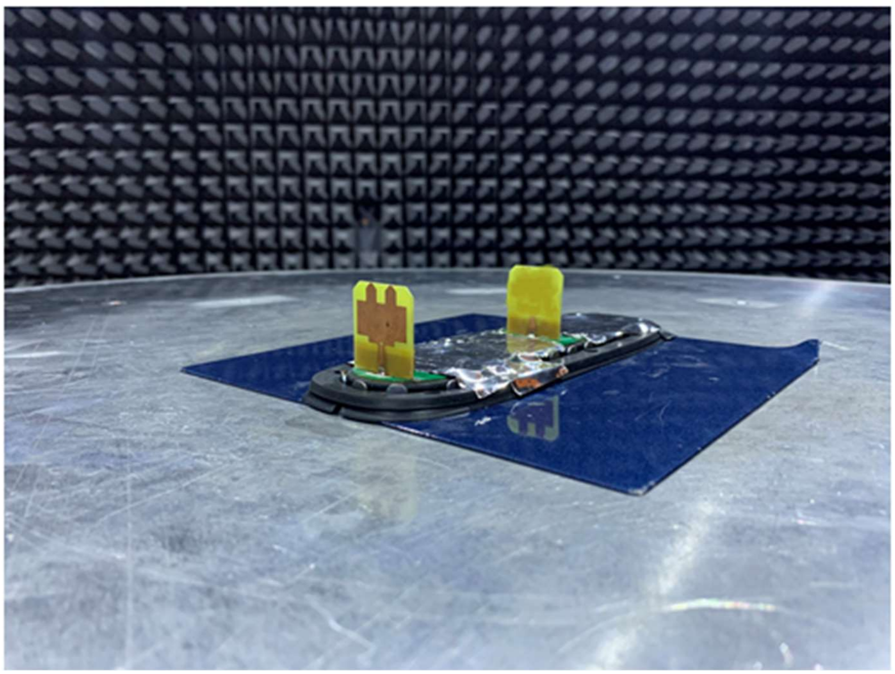

(b) Fabricated prototype.

Figure 4.10. Simulation model and prototype measurement setup for proposed MIMO system: (a) Simulation model. (b) Fabricated prototype.

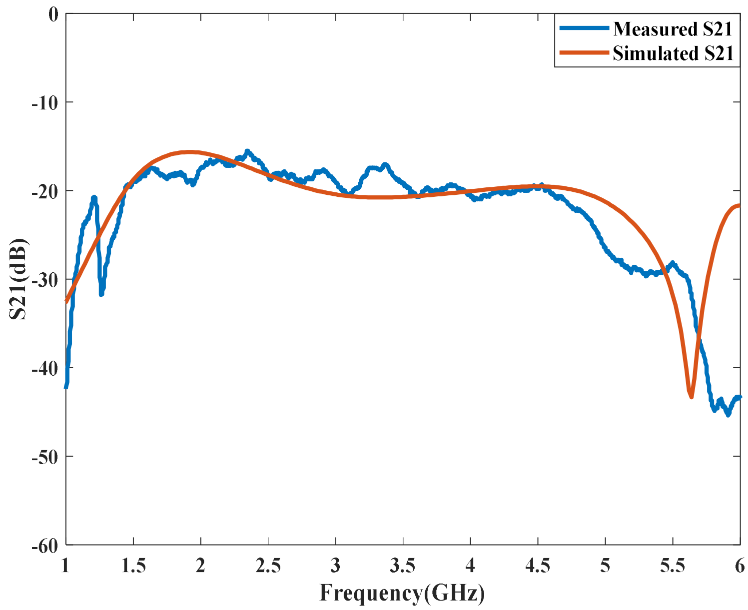

Figure 4.11. Passive isolation measured in dB of simulation model and prototype.

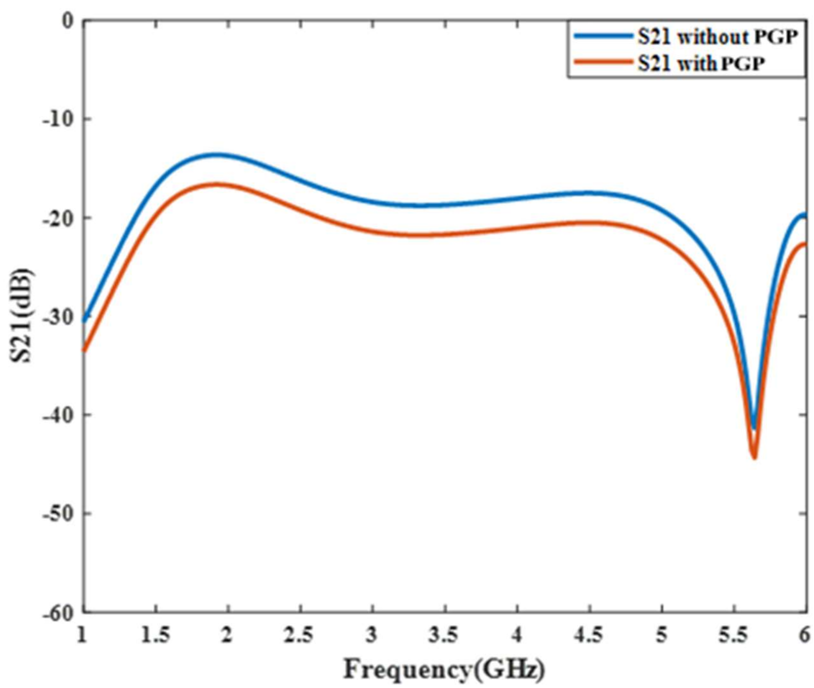

Figure 4.12. Passive isolation measured in dB with and without partial ground plane structure.

The ECC and DG of the proposed MIMO system is presented in Figure 4.14. and Figure 4.15. The ECC has been calculated using the electric field components formula (4.4):

$$\rho_{e,ij} = \left| \frac{\int_0^{2\pi}\int_0^{\pi}(XPR \,.\, E_{\theta i} \,.\, E^*_{\theta j} \,.\, P_\theta + XPR \,.\, E_{\phi i} \,.\, E^*_{\phi j} \,.\, P_\phi)\sin(\theta)\, d\theta d\phi}{\sqrt{\prod_{k=i,j}\int_0^{2\pi}\int_0^{\pi}\left(XPR \,.\, E_{\theta k} \,.\, E^*_{\theta k} \,.\, P_\theta + XPR \,.\, E_{\varphi k} \,.\, E^*_{\varphi k} \,.\, P_\phi\right)\sin(\theta) d\theta d\phi}} \right|^2 \quad (4.4)$$

Where $E_{\theta i}$ and $E_{\theta j}$ represent the E-field complex components in the theta direction for the first and second elements (i, and j). $E_{\varphi i}$ and $E_{\varphi j}$ are also the complex E-field components but in the phi direction. XPR is the cross-polarization factor that takes into account the difference in wave polarization (vertical or horizontal) of the received wave. P_θ and P_φ represent the power densities for theta and phi angles. To simply the calculations for equation (4.4), uniform power densities can be assumed across elevation and azimuth angles, and XPR could be equal to 1 to assume no polarization differences between the antennas.

The diversity gain which is known to be as the quantified improvement in signal-to-noise ratio when the antennas in the MIMO system receives the RF signal and is calculated by the formula (4.5):

$$\text{DG} = 10 * \sqrt{(1-\rho)} \quad (4.5)$$

The electric field components were extracted from the ground plane measurements which include the amplitude and phase of E-field in theta and phi planes, then a MATLAB script processes the electric field data using the above equations. It can be shown from Fig. 14 that the worst-case of ECC value is about 0.05 that corresponds to DG of 9.98dB which shows the antennas are highly uncorrelated across the 5G bands which is a crucial requirement for the MIMO performance.

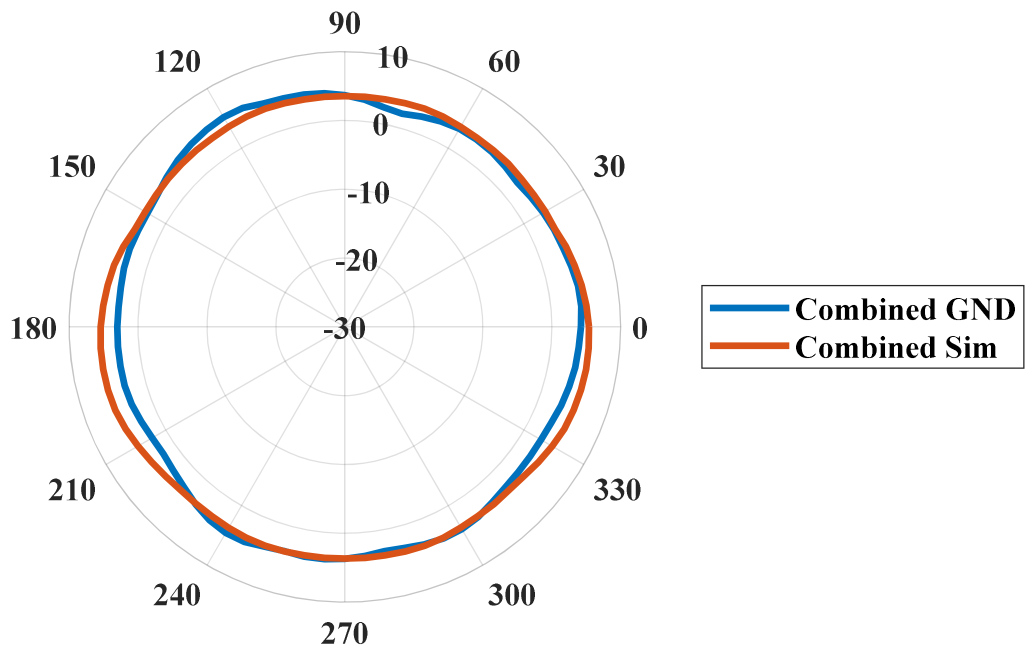

(a) 1710 MHz

Figure 4.13. Comparison of combined radiation patterns of simulation and ground plane measurements in (dBi) at theta equals 80 degrees: (a) 1.71GHz, (b) 3.6GHz, and (c) 5GHz.

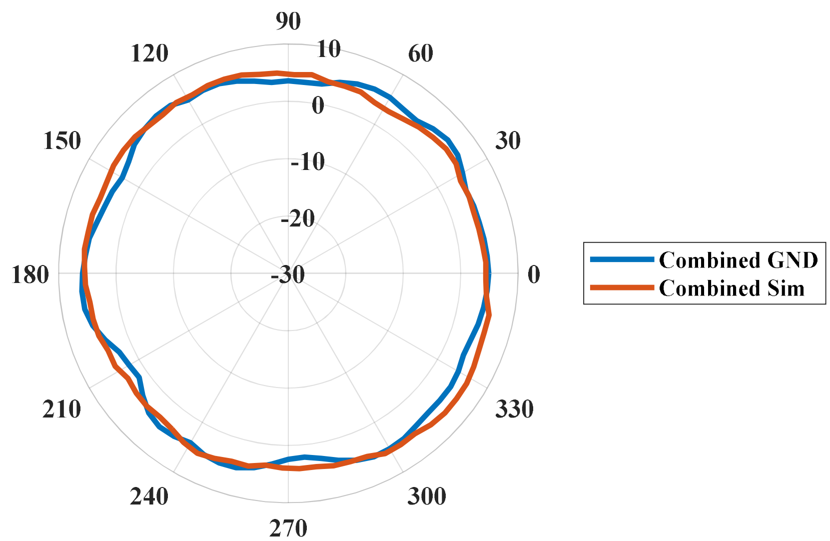

(b) 3600 MHz

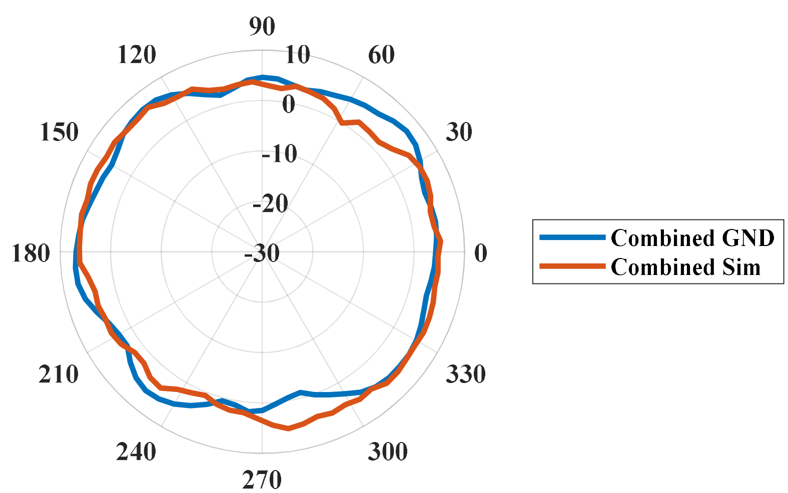

(c) 5000 MHz

Figure 4.13. Continued.

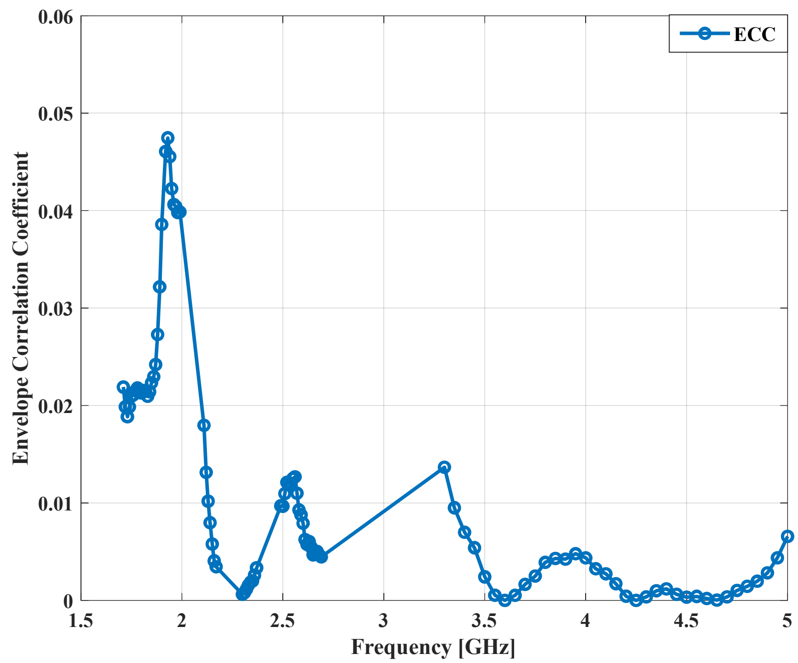

Figure 4.14. ECC values for ground plane measurements.

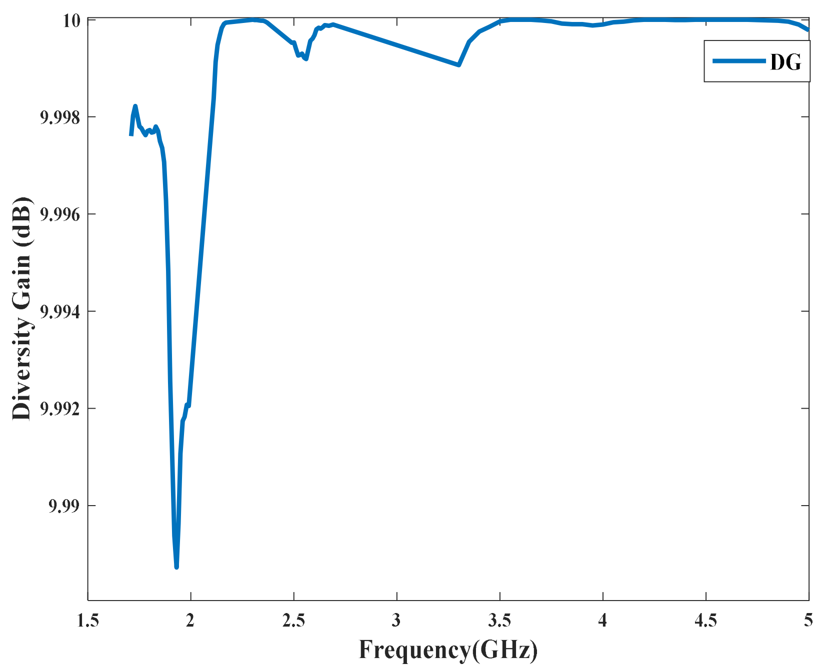

Figure 4.15. Diversity gain in dB for ground plane measurements.

4.4 Conclusions

A compact raised printed monopole antenna has been analyzed in this paper to be used in automotive applications that operates on the 5G middle and high frequency bands from 1.71GHz to 5GHz. The design consists of a slotted feed line exciting wide rectangular shape with two branches. The slot in the feed line, upper two branches and the dielectric material (FR4) are used to further tune the antenna towards lower frequency bands. PGP structure has been implemented on the back side of the antenna to provide higher isolation and improve bandwidth impedance. A simulation model was built using HFSS software and then a prototype was measured on one-meter rolled-edge ground plane in an anechoic chamber. The performance of the design shows VSWR performance better than 2:1 with average radiation efficiency of 74.4% on ground plane. LAG was measured from theta equals 75 to 87 degrees with minimum value of 1.7dBi while having higher than 3dBi across most frequency points. A 2x2 MIMO system was analyzed and presented using two identical elements of the proposed design but with different orientation. The MIMO system shows a passive isolation better than 16dB, ECC lower than 0.05, and DG higher than 9.98dB across the operating frequency bands. In general, the presented antenna design in this paper is suitable to be used for 5G vehicular applications inside shark-fin housing due to its reasonable dimensions and good RF performance.

CHAPTER FIVE

LOW-PROFILE MIMO 5G AND L1/L5 GNSS COMMUNICATIONS

5.1 Introduction

The global navigation satellite system (GNSS) is used in the automotive industry to compute three-dimensional position coordinates which can be used to navigate through different routes. The antenna design for vehicular GNSS system is getting more challenging since larger frequency bandwidth and harder requirements are presented to ensure receiving an acceptable signal level and obtaining an accurate physical location, especially for autonomous driving [52, 53].

In this section, fully integrated low-profile antenna systems have been developed for vehicular applications in the sub-6GHz 5G and L1/L5 GNSS frequency bands to be used in low-profile housing on the vehicle's roof. The first system integrates MIMO 5G with upper L-band from 1559MHz to 1610MHz (L1-band) while the second system covers the lower L5 band from 1164MHz to 1189MHz.

5.2 Antenna System Layout and Design

The proposed antenna design consists of two low-profile planar inverted F-antenna (PIFA) operating in the 5G cellular bands from 617MHz-5GHz and two ceramic patch antennas, one on each sample as shown in Figure 5.1. The first patch antenna covers L1 GNSS band from 1.56GHz-1.61GHz while the second one covers lower L5 band from 1164MHz-1189MHz. The distance between the two 5G elements is 120mm (which is approximately λ/4 of lowest frequency 617MHz) with the patches centered between the

PIFAs. The orientation and position of each element is important to get the best performance and isolation in each system.

The low-profile 5G antenna is based on a PIFA design with unique slots made on the horizontal plane that makes the antenna broader in bandwidth. A detailed description for the element design and its 5G MIMO performance is presented in the previous chapters.

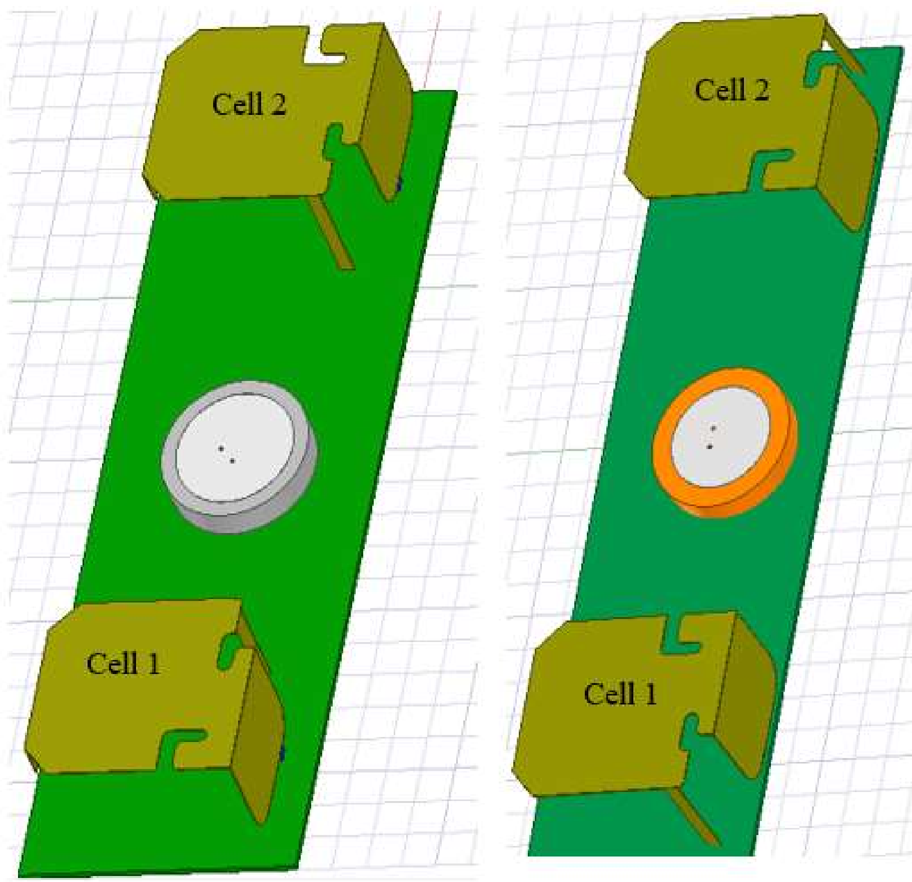

(a) (b)

Figure 5.1. Proposed antenna systems: (a) MIMO 5G with L1 patch, and (b) MIMO 5G with L5 patch.

The GNSS patches are designed with ceramic dielectric material with dual-pin feed combined for right hand circular polarization (RHCP) by creating a 90-degree phase shift between the two feed pins. The L1 GNSS patch presented in Fig. 1(a) has a dielectric constant of 10.5, patch radius of 16.8mm, and thickness of 8mm. The L5 patch has a dielectric constant of 20.5, patch radius of 15.2mm, and thickness of 8mm [54].

5.3 RF Performance Results and Analysis

Figure 5.2 and Figure 5.3 shows the VSWR for L1 and L5 respectively. The L5 patch has VSWR performance better than (2.5:1) across frequency range (1164MHz-1186MHz). And the L1 patch has a VSWR better than (3:1) across frequency range (1560MHz-1610MHz). Figure 5.4 shows the VSWR for the MIMO 5G cells which shows values better than (3.5:1) from 617MHz-6GHz with a reasonable rejection for L1/L5 GNSS bands. Cell 1 and cell 2 presents the front and back 5G elements respectively.

Figure 5.5 and Figure 5.6 show the isolation between the 5G elements and L1/L5 ceramic patches. The isolation on the L1 sample shows passive isolation better than 20dB while L5 sample has isolation better than 15dB.

The radiation patterns for L1 and L5 ceramic patches measured at theta equals 10 degrees are shown in Figure 5.7 and Figure 5.8. The average RHCP gain for L5 band is found to be 1.2dBi, 0.7dBi, and 0.5dBi at 1166MHz, 1176MHz, and 1186MHz, respectively. As for L1 band, the RHCP average gain is 3.4dBi, 4dBi, and 4.1dBi at 1560MHz, 1572MHz, and 1606MHz, respectively.

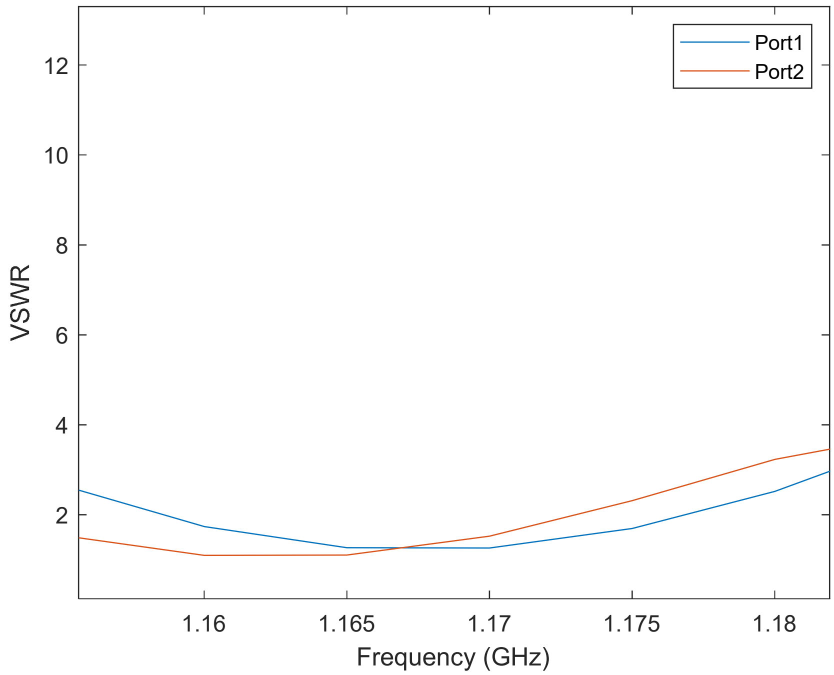

Figure 5.2. VSWR across L5 GNSS band.

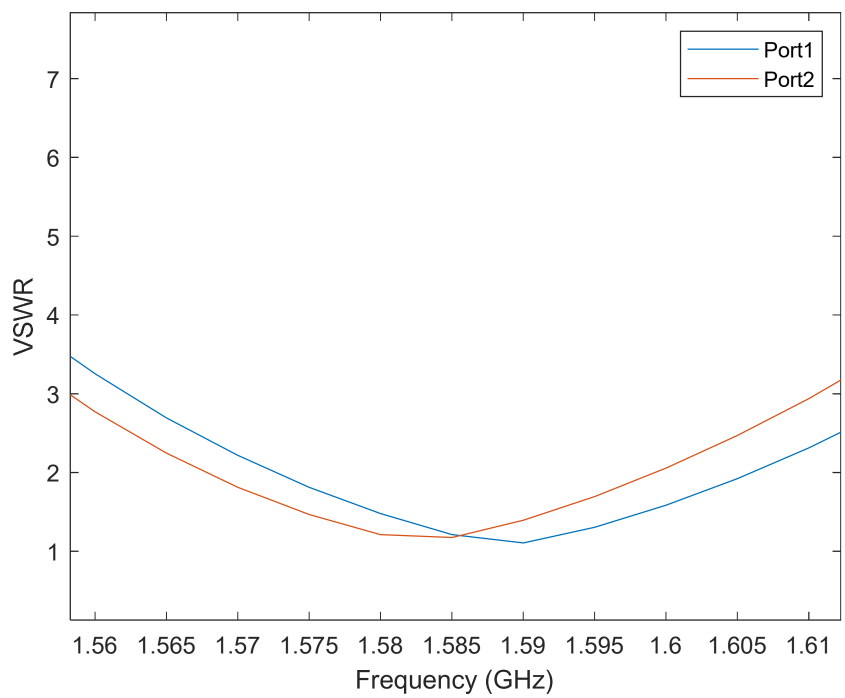

Figure 5.3. VSWR across L1 GNSS band.

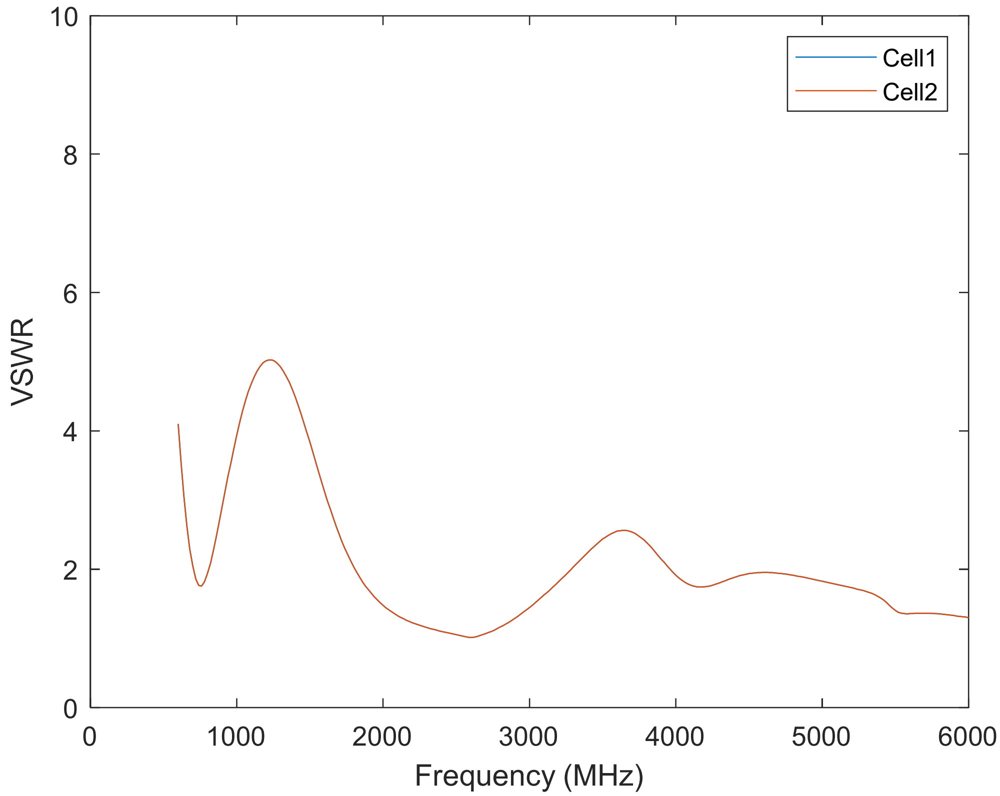

Figure 5.4. VSWR for 5G PIFAs.

The combined radiation patterns for the MIMO 5G elements at theta equals 80 degrees are shown in Figure 5.9. The combined average gain for vertical polarization is found to be -2.1dBi, 0.6dBi, 4.6dBi, and 3.1dBi at frequencies 617 MHz, 1.9 GHz, 3.6 GHz, and 5 GHz, respectively.

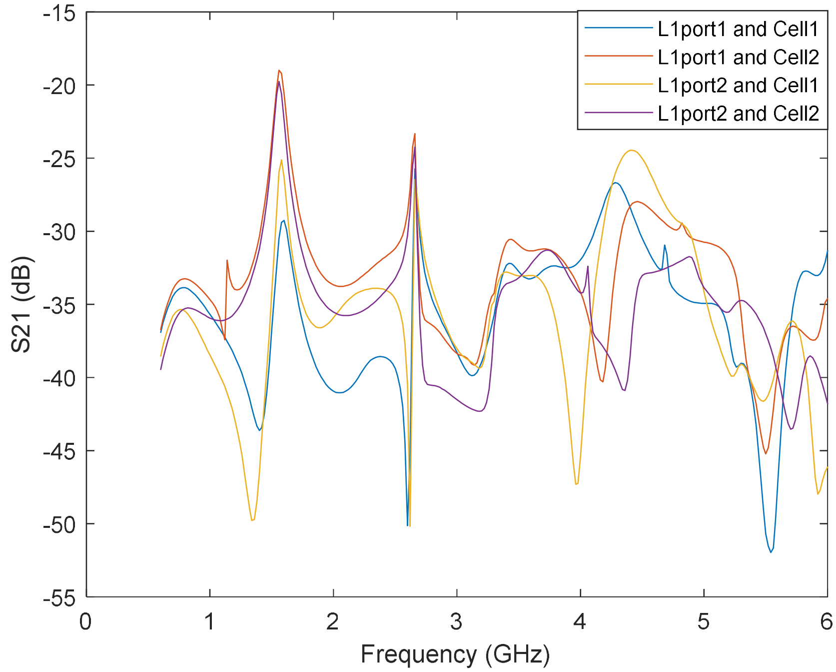

Figure 5.5. Isolation between L1 ports and Cell1/Cell2.

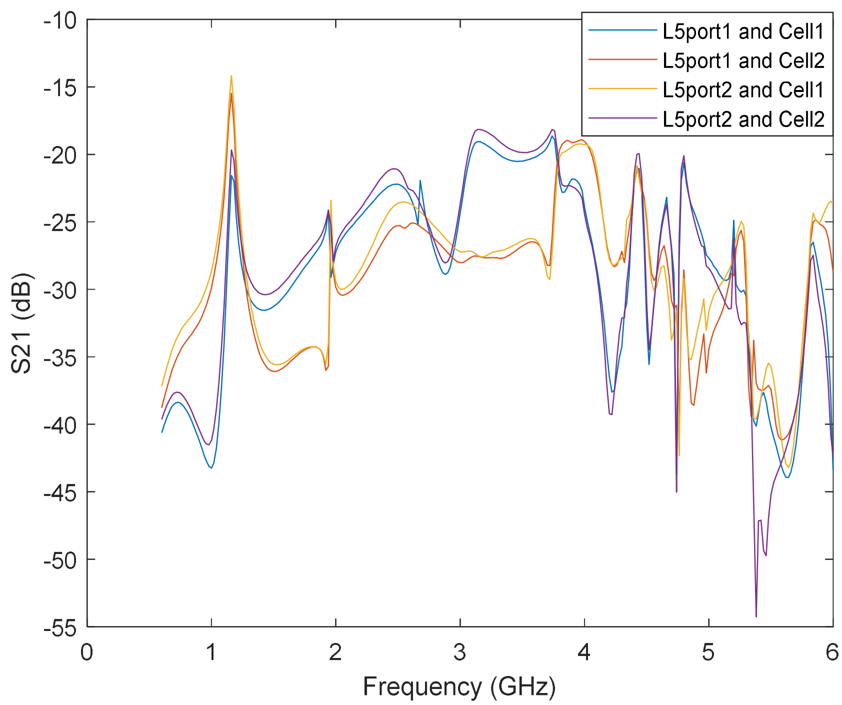

Figure 5.6. Isolation between L5 ports and Cell1/Cell2.

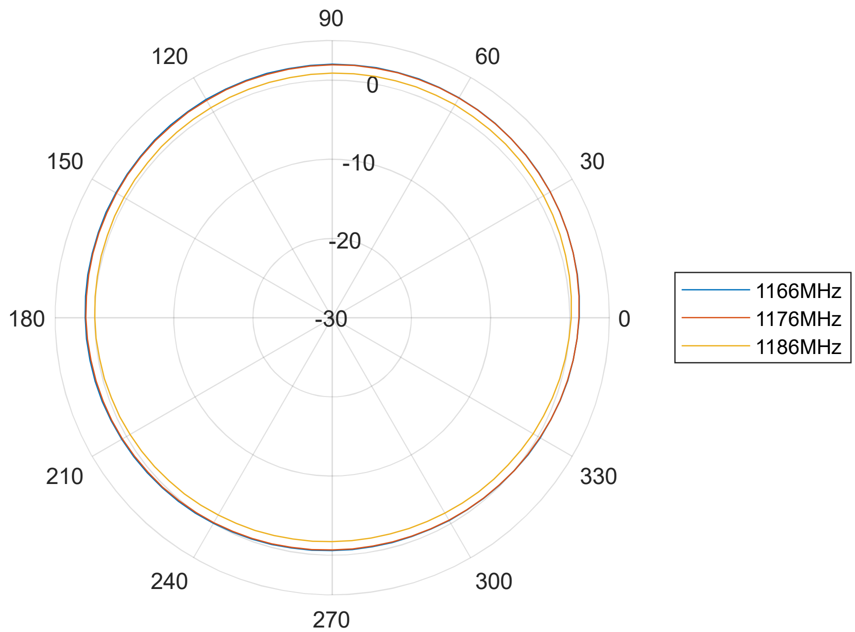

Figure 5.7. Radiation patterns across L5 frequencies at theta = 10 degrees for RHCP.

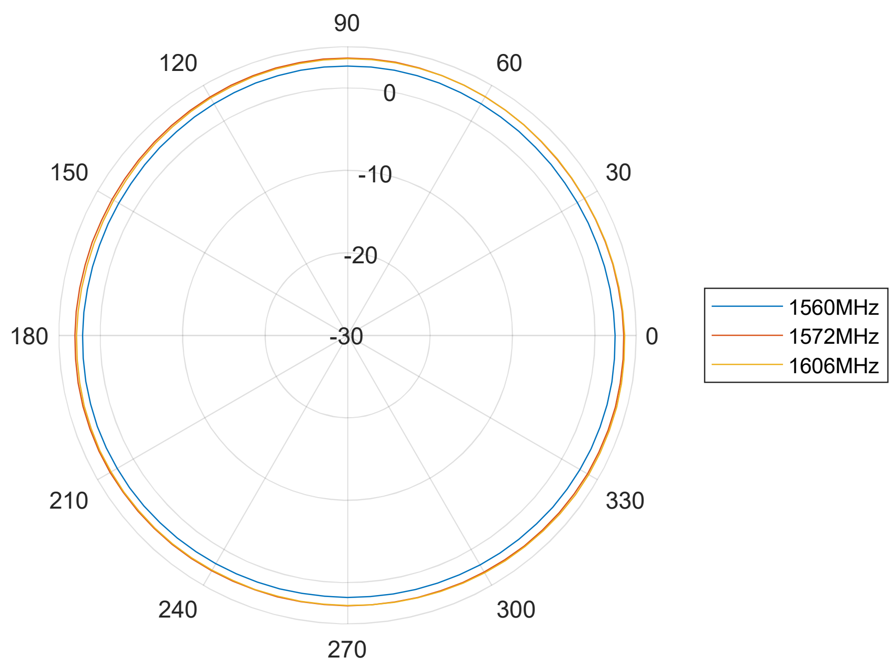

Figure 5.8. Radiation patterns across L1 frequencies at theta = 10 degrees for RHCP.

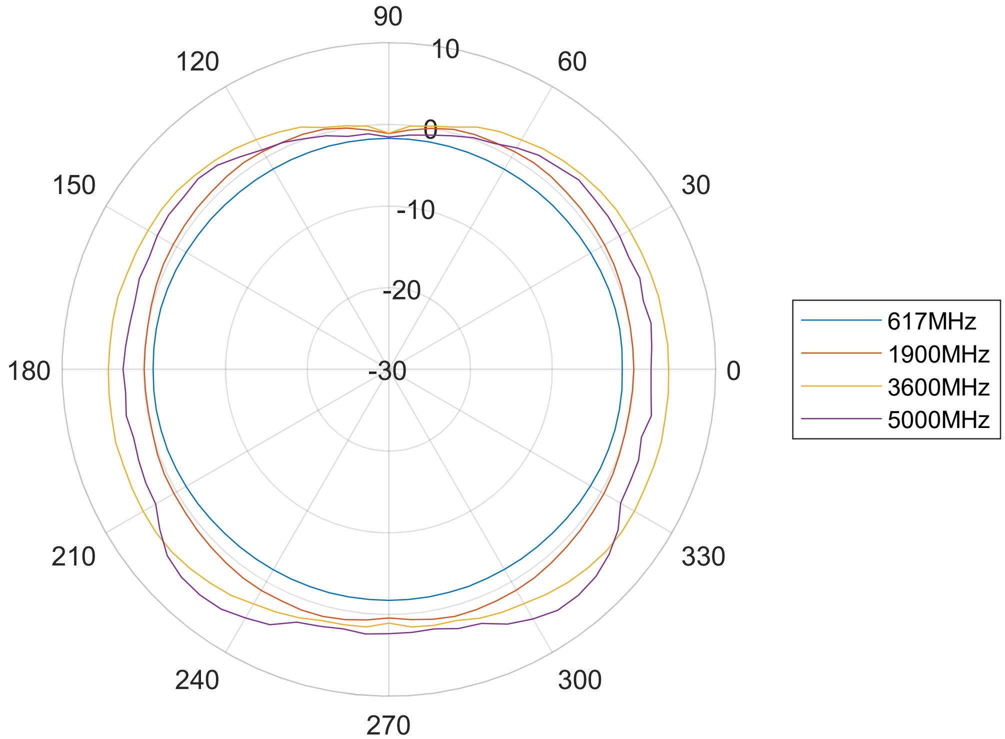

Figure 5.9. Combined radiation patterns for MIMO 5G elements at theta = 80 degrees for vertical polarization.

Figures 5.10, 5.11 and 5.12 show the radiation efficiency of L1 patch, L5 patch, and 5G cell respectively. The average efficiency for L1 element is found to be 55% while having a maximum efficiency of 69% at 1585MHz. L5 has an average efficiency of 43% and maximum efficiency of 55% at center frequency (1176MHz). each of the 5G elements has an average efficiency of 64% and a maximum efficiency of 91% at middle 5G bands.

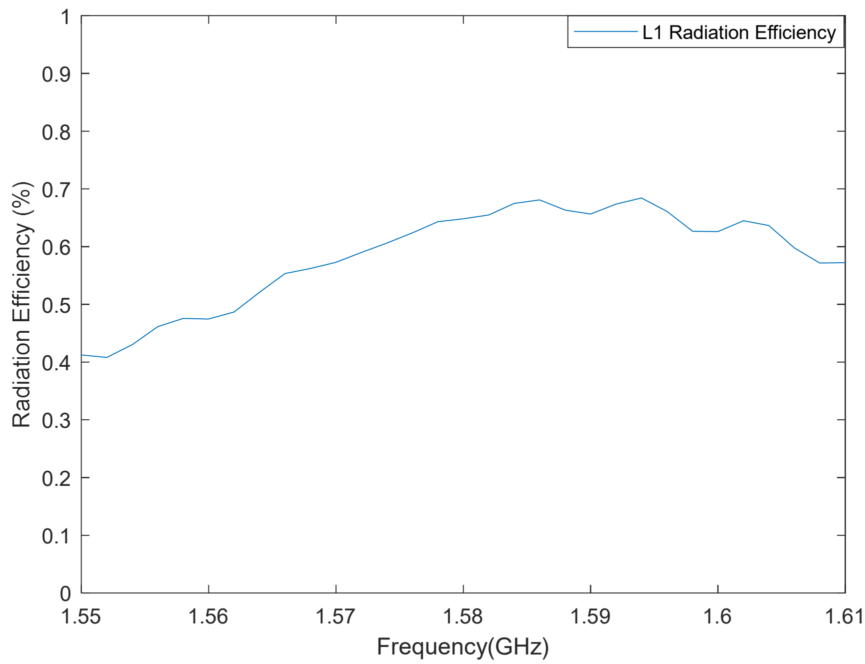

Figure 5.10. Antenna radiation efficiency for L1 patch.

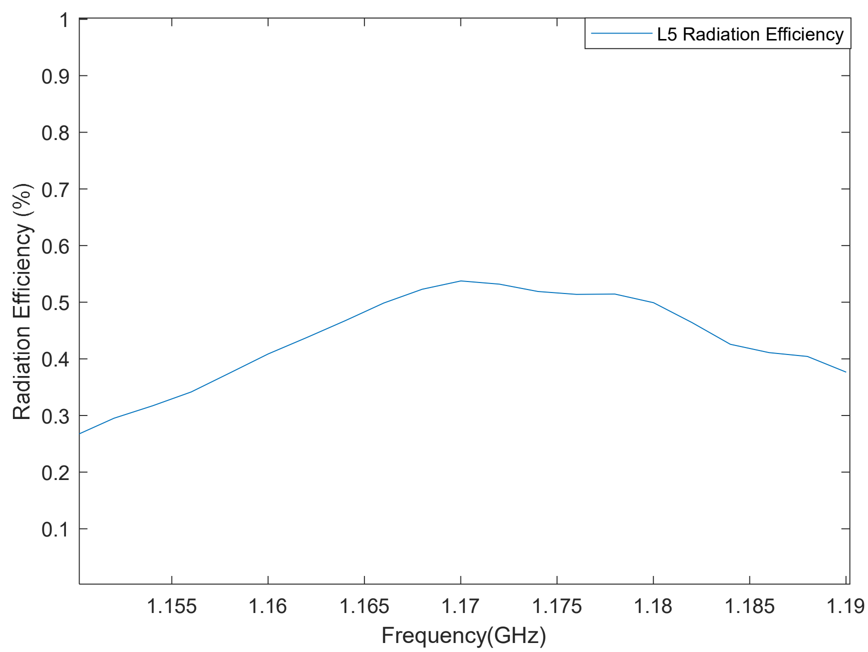

Figure 5.11. Antenna radiation efficiency for L5 patch.

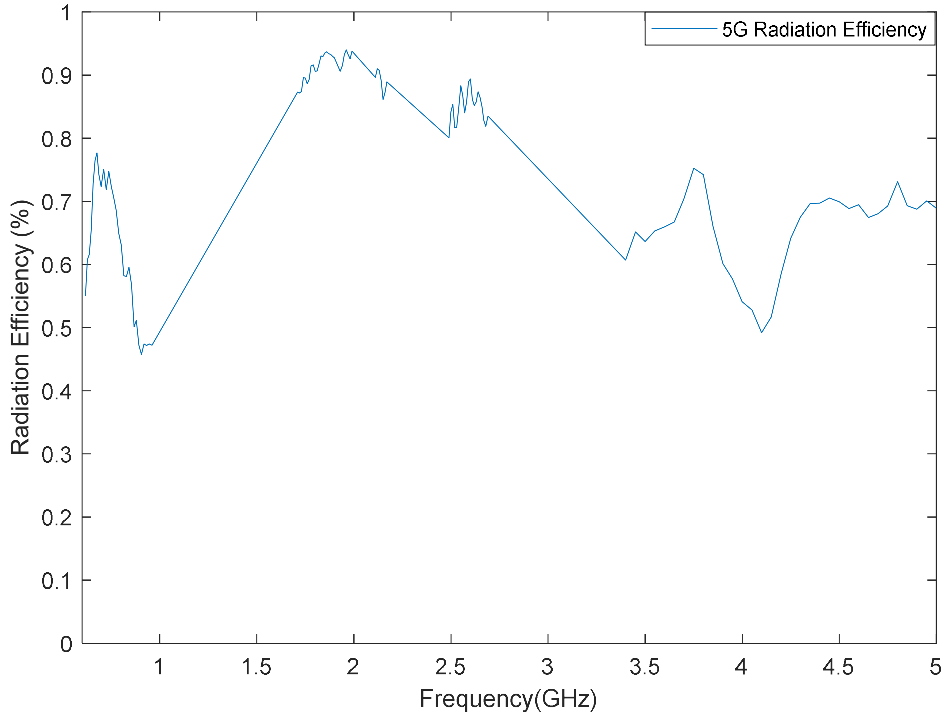

Figure 5.12. Antenna radiation efficiency for 5G cell elements.

5.4 Conclusions

Integrated 5G MIMO antenna systems with L1/L5 GNSS ceramic patch antennas are presented in this chapter to be used in a low-profile housing in the automotive industry. The systems cover the sub-6-GHz 5G bands from 617MHz-5GHz and L1/L5 bands (1164MHz-1186MHz and 1560MHz-1610MHz). The antennas were simulated using HFSS simulation software and the results show a VSWR better than 2.5:1 for L5 band, 3:1 for L1 band, and 3.5:1 for 5G bands. In general, the proposed designs are suitable for low-profile antenna applications on vehicle.

CHAPTER SIX

CONCLUSIONS AND FUTURE WORK

6.1 Conclusions

A topic of great interest to the automotive industry is the subject of the research described in this work. Modern automakers have begun to establish the fundamental guidelines and standards for autonomous driving. 5G/V2X antennas, high accuracy GNSS antennas, and 5G/V2X MIMO antenna systems all play a significant role in that effort. A low-profile wideband antenna has been presented in this work that functions across 5G frequency band from 617MHz to 5GHz and across DSRC band from 5850MHz to 5925MHz. It consists of a wide rectangular plate at the feeding pin with two cut slots to control high frequency bands and a shorting pin for low frequency bands. The antenna was simulated using an HFSS simulation tool and then measured on a 1-meter GND and on a testing vehicle inside an anechoic chamber. The measurements show a VSWR better than 3.3:1 and an average efficiency of 83% on a GND and 72% on the vehicle for 5G frequencies while DSRC frequencies has an average efficiency of 71% on GND and 69% on vehicle. In general, the proposed antenna design is a good candidate for low-profile antenna applications on a vehicle.

Multiple two-element based MIMO antenna systems were presented in this research for 5G and V2X bands to be used in automotive applications to provide diversity, increased capacity, and higher throughput. The ECC and DG values were calculated in each MIMO configuration using electric field components (magnitude and phase) from the radiation patterns of each antenna element. The first MIMO system represents two low profile PIFAs separated by a given distance (600mm) on the vehicle's roof. The system achieves a passive isolation better than 26dB, ports efficiencies higher than 68% on vehicle across all bands, ECC lower than 0.10, and DG higher than 9.94dB. The second MIMO system consists of two PIFAs on the same PCB separated by a fixed distance and rotated in various positions. This MIMO system has a passive isolation better than 11dB, ports efficiencies higher than 60% on vehicle, ECC lower than 0.39, and DG higher than 9.20dB. Finally, the third MIMO configuration investigated the performance when having one element as a monopole and one as PIFA. It achieves passive isolation better than 10dB, ports efficiencies higher than 55% on vehicle, ECC lower than 0.28, and DG higher than 9.60dB. In general, each MIMO configuration has a satisfactory performance and can be used in the vehicular applications depending on the desired requirement, housing style, and physical dimensions.

A compact raised printed monopole antenna has been analyzed in this work to be used in automotive applications that operates on the 5G middle and high frequency bands from 1.71GHz to 5GHz. The design consists of a slotted feed line exciting wide rectangular shape with two branches. The slot in the feed line, upper two branches, and the dielectric material (FR4) are used to further tune the antenna towards lower frequency bands. PGP structure has been implemented on the back side of the antenna to provide higher isolation and improve bandwidth impedance. A simulation model was built using HFSS software and then a prototype was measured on one-meter rolled-edge ground plane in an anechoic chamber. The performance of the design shows VSWR performance better than 2:1 with average radiation efficiency of 74.4% on ground plane. LAG was measured from theta equals 75 to 87 degrees with minimum value of 1.7dBi while having higher than 3dBi across most frequency points. A 2x2 MIMO system was analyzed and presented using two identical elements of the proposed design but with different orientation. The MIMO system shows a passive isolation better than 16dB, ECC lower than 0.05, and DG higher than 9.98dB across the operating frequency bands. In general, the presented printed antenna design in this work is also suitable to be used for 5G vehicular applications inside shark-fin housing due to its reasonable dimensions and good RF performance.

In chapter 5, Integrated 5G MIMO antenna systems with L1/L5 GNSS ceramic patch antennas are presented to be used in a low-profile housing in the automotive industry. The systems cover the sub-6-GHz 5G bands from (617MHz-5GHz) and L1/L5 bands (1164MHz-1186MHz and 1560MHz-1610MHz). The antennas were simulated using HFSS simulation software and the results show a VSWR better than (2.5:1) for L5 band, (3:1) for L1 band, and (3.5:1) for 5G bands. In general, the proposed integrated designs are suitable for low-profile antenna applications on vehicle.

The study presented in this research provides real-world examples of futuristic antennas that are geared toward preparing the vehicular industry for the future of autonomous driving. In addition to antenna performance, the work considers other crucial elements such as antenna volume, cost, and manufacturing ease including how well it will cohabit with other unavoidable technologies, and where it will be mounted on the automobile.

6.2 Future Work

Future research could focus on the following topics to further the work given in this dissertation:

- Investigate appropriate board-level filtering to separate 5G applications from V2X communications.
- To construct MIMO antenna systems for a 5G cellular antenna that is lower in volume, investigate the potential of adding dielectric to reduce antenna size and spatial MIMO separation.
- Investigate the possibility of designing a stacked L1/L5 patch antenna or one dual-band patch antenna that can be integrated with 5G/V2X MIMO system.

APPENDIX

TABULATED SUMMARY OF LITERATURE REVIEW

Table A.1. Comparison between proposed design and literature.

	Type	Bandwidth	Dimensions (LxWxH) (mm3)	Gain/ Efficiency
Proposed Antenna [23]	Compact PIFA	617MHz-6GHz	55x50x28	Average gain on vehicle -2.1 dBi @617MHz, -1 dBi @1.9GHz, 0dBi@3.6GHz and 0.9dBi@5GHz. Average efficiency 83% on GND, 72% on Vehicle.
11	Novel compact 3D antenna	790MHz-2.69GHz	50x50x30	Simulated Max. gain 1-2.5dB at low band, 6-8.5dB at higher bands.
12	Nefer Antenna	698MHz-6GHz	80x60x30	-3dB (High band gain is in driving direction) (70% 0.7-3.7GHz, 63% 3.7-6GHz on GND)
13	Top-loaded monopole	700MHz-3GHz	80x80x28	Average gain on GND -2 dBi @752MHz, -1.5 dBi @892MHz, -2dBi @1.755GHz and -1.5dBi @1.93GHz. (73.3% @752MHz, 76.4% @892MHz, 85% @ 1.755GHz, 95.3% @1.93GHz)
14	Printed monopole	698MHz-2690MHz	25x1.53x76	Measured gains are higher than 2 dB
15	Vivaldi monopole	698MHz-4GHz	69.1x0.86x 73	Max gain/ efficiency: 3.64dBi/97.83% @700MHz, 3.54dBi/91.29% @900MHz 5.21dBi/89.28% @1.8GHz 5.54dBi/80.58% @2.1GHz 6.42dBi/85.43% @2.5GHz)

16	T-Shape monopole	698MHz-960MHz 1.427GHz-2.7GHz	33x10x55	Max gain 2.8dBi @ 900MHz,5.2dBi @ 2.6 GHz. Average efficiency 70%.
17	3-port printed antenna	0.69GHz-0.96GHz 1.7GHz-2.7GHz / (2.4GHz/ 5GHz)/ DSRC (5.9GHz)	87x1.6x60	Gain at 2.4GHz varies from -10 to 2.4dBi. Average gain @0.69GHz -1dBi/ 0.96GHz -3dBi/ 1.7GHz, -2 dBi / 2.7GHz -5 dBi Max gain at 5.9GHz is 2dBi to the front and -0.5dBi to the back.
18	Printed PICA	800MHz - 10GHz	76.2x0.79x 76.2	Max gain: 4dBi @1GHz 6dBi@5GHz 8dBi@9GHz
19	Printed annular monopole	0.69GHz - 10GHz	140x1.524x 86	Gain from 0.6dBi to max of 4.2dBi

Table A.2 Literature Review Summary on Automotive 5G/V2X MIMO Systems.

Ref.	Type	Bandwidth	Antenna Dimension (LxWxH) (mm3)	ECC method / value
30	2x2 PIFA	775MHz-925HHz	59.5x12.4x21	S-parameter only / lower than 0.5
46	2x2 printed Yagi	Center frequency 3.5GHz, bandwidth 600MHz	60x1.6x55	Not reported/ lower than 0.5
31	2x2 PIFA	790MHz-2.69GHz	50x50x28	E field components / lower than 0.3
33	2x2 Nefer Antenna	700MHz-6GHz	70x70x29	S-parameters only / lower than 0.16
34	2x2 printed monopole	790MHz-3GHz	30x0.8x80	S-parameters only / lower than 0.05
35	2x2 printed monopole PIFA	698MHz-3GHz	PIFA 65x62x20 / Monopole height is 53.	Not reported
47	2x2 monopole	698MHz-2.69GHz	Back monopole height 55mm / Front monopole height 45mm	S-parameters only / lower than 0.5
32	2x2 PIFA	690MHz-2700MHz	PIFA length is 75.9mm /height 25.5mm	S-parameters only /lower than 0.5

48	2x2 monopole	700MHz-900MHz	Not reported	S-parameters only / lower than 0.02
36	2x2 printed planar monopoles	698MHz-2700MHz	52x1.6x65	S-parameters only/ lower than 0.5
49	4x4 sleeve monopoles	790MHz-5GHz	Not reported	Not reported / lower than 0.12
38	2x2 transparent semicircular slot-loaded monopoles	2.4GHz-11GHz	24x2.2x29	E-field components / lower than 0.02
37	2x2 printed monopoles	698MHz-2690MHz	25x2x55	Not reported / lower than 0.3

Table A.3 Literature Review Summary on Automotive 5G Printed antenna.

	Type	**Frequency Bandwidth**	**Dimensions (LxWxH) (mm3)**	**VSWR/Gain/ Efficiency**
Proposed Design [55]	Raised printed monopole	1.71GHz-5GHz	27x1x30	(2:1) VSWR from 1.71GHz-5GHz. Peak gain 3.7dBi @1.71GHz, 5.4dBi @3.6GHz, and 6.7dBi @5GHz. Avg. radiation efficiency 74.4% on GND
28	Patch antenna with slots and stubs	3.7GHz-5.05GHz	30x1.6x30	(2:1) VSWR. Peak gain 5dBi, Avg. gain 1.5dBi @3.6GHz, 2dBi @5GHz
29	Flagged shape printed antenna	3GHz-6GHz	36x1.6x66	(1.5:1) VSWR. Peak gain 3.28dBi @3.1GHz
36	Printed planar monopole	698MHz-2700MHz	52x1.6x65	(2.6:1) VSWR. Max gain 1.68dBi @700MHz, 5.95dBi @1.8GHz, 3,34dBi @2.3GHz, 3.76dBi @2.7GHz
37	Printed monopole	698MHz-2690MHz	25x2x55	(2.5:1) VSWR. Max gain -0.7 to 5dBi
50	printed antenna	3.34GHz-3.87GHz	20x1.6x35	(2:1) VSWR. Peak gain 2.34dBi
51	Printed monopole with two branches	720MHz-960MHz 1.6GHz-4GHz	30x1.6x70	(2:1) VSWR. Max gain 5.89dBi @2.4GHz, 3.52dBi @3.5GHz
46	Printed Yagi-Uda	2.9GHz-4.1GHz	60x1.6x55	(2.1:1) VSWR. Peak gain higher than 7dBi

REFERENCES

[1] Abboud, K., H. A. Omar, andW. Zhuang, “Interworking of DSRC and cellular network technologies for V2X communications: A survey,” IEEE Transactions on Vehicular Technology, Vol. 65, No. 12, 9457–9470, Dec. 2016.

[2] Wang, C., J. Bian, J. Sun, W. Zhang, and M. Zhang, “A survey of 5G channel measurements and models,” IEEE Communications Surveys & Tutorials, Vol. 20, No. 4, 3142–3168, Fourth quarter 2018.

[3] Ghafari, E., A. Fuchs, D. Eblenkamp, and D. N. Aloi, “A vehicular rooftop, shark-fin, multiband antenna for the GPS/LTE/cellular/DSRC systems,” 2014 IEEE-APS Topical Conference on Antennas and Propagation in Wireless Communications (APWC), 237–240, Palm Beach, 2014.

[4] https://www.its.dot.gov/research_archives/connected_vehicle/pdf/DSRCReportCongress_FINAL_23NOV2015.pdf.

[5] Arianos, S., G. Dassano, F. Vipiana, and M. Orefice, “Design of multi-frequency compact antennas for automotive communications,” IEEE Transactions on Antennas and Propagation, Vol. 60, No. 12, 5604–5612, Dec. 2012.

[6] Artner, G., W. Kotterman, G. Del Galdo, and M. A. Hein, “Automotive antenna roof for cooperative connected driving,” IEEE Access, Vol. 7, 20083–20090, 2019.

[7] https://www.nhtsa.gov/sites/nhtsa.gov/files/documents/v2v_pria_12-12-16_clean.pdf

[8] https://www.antenna-theory.com/antennas/patches/pifa.php

[9] https://www.intechopen.com/chapters/38164

[10] A. G. Domel, G. Domel, J. C. Weaver, M. Saadat, K. Bertoldi, and G. V. Lauder, “Hydrodynamic properties of biomimetic shark skin: effect of denticle size and swimming speed,” Bioinspiration & Biomimetics, vol. 13, 2018.

[11] Franchina, A. M., P. Nepa, R. Parolari, I. Moro, A. Polo Filisan, and D. Zamberlan, “A 3D LTE antenna for vehicular applications,” IEEE International Symposium on Antennas and Propagation & USNC/URSI National Radio Science Meeting, 637–638, San Diego, CA, Jul. 2017R.

[12] Hast¨urko˘glu, S. and S. Lindenmeier, “A wideband automotive antenna for actual and future mobilecommunication 5G/LTE/WLAN with low profile,” 11th European Conference on Antennas and Propagation (EUCAP), 602–605, Paris, Mar. 2017.

[13] Ghafari, E. and D. N. Aloi, “Top-loaded UWB monopole antenna for automotive applications,”Proceedings of the 2012 IEEE International Symposium on Antennas and Propagation, 1–2, Chicago, IL, Jul. 2012.

[14] Michel, A., P. Nepa, M. Gallo, I. Moro, A. Polo Filisan, and D. Zamberlan, “Printed wideband antenna for LTE-band automotive applications,” IEEE Antennas and Wireless Propagation Letters, Vol. 16, 1245–1248, Nov. 2016.

[15] Navarro-M´endez, D. V., et al., “Compact wideband vivaldi monopole for LTE mobile communications,” IEEE Antennas and Wireless Propagation Letters, Vol. 14, 1068–1071, 2015.

[16] Goncharova, I. and S. Lindenmeier, “A high efficient automotive roof-antenna concept for LTE, DAB-L, GNSS and SDARS with low mutual coupling,” 2013 9th European Conference on Antennas and Propagation (EuCAP), 1–5, Lisbon, Apr. 2015.

[17] Hua, Y., L. Huang, and Y. Lu, “A compact 3-port multiband antenna for V2X communication,”2017 IEEE International Symposium on Antennas and Propagation & USNC/URSI National Radio Science Meeting, 639–640, San Diego, CA, 2017.

[18] Suh, S.-Y., W. L. Stutzman, and W. A. Davis, “A new ultrawideband printed monopole antenna: the Planar Inverted Cone Antenna (PICA),” IEEE Transactions on Antennas and Propagation, Vol. 52, No. 5, 1361–1364, May 2004.

[19] Liang, X., S. Zhong, W. Wang, and F. Yao, “Printed annular monopole antenna for ultra-wideband applications,” Electronics Letters, Vol. 42, No. 2, 71–72, Jan. 19, 2006.

[20] Chen, L., X. Ren, Y.-Z. Yin, and Z. Wang, “Broadband CPW-fed circularly polarized antenna with an irregular slot for 2.45 GHz RFID reader,” Progress In Electromagnetics Research Letters, Vol. 41, 77–86, 2013.

[21] Chattha, H., Y. Huang, X. Zhu, and Y. Lu, “An empirical equation for predicting the resonant frequency of planar inverted-F antennas,” Antennas and Wireless Propagation Letters, Vol. 8, 856–860, IEEE, 10.1109/LAWP.2009.2027822, 2009.

[22] Sayidmarie, K. and L. Yahya, “Modeling of dual-band crescent-shape monopole antenna for WLAN applications,” International Journal of Electromagnetics and Applications, Vol. 4, 31–39, doi:10.5923/j.ijea.20140402.01, 2014.

[23] Ahmad Yacoub, Mohamed Khalifa, and Daniel N. Aloi, "Wide Bandwidth Low Profile PIFA Antenna for Vehicular Sub-6 GHz 5G and V2X Wireless Systems," Progress In Electromagnetics Research C, Vol. 109, 257-273, 2021.

[24] M. O. Khalifa, A. M. Yacoub and D. N. Aloi, "A Multiwideband Compact Antenna Design for Vehicular Sub-6 GHz 5G Wireless Systems," in IEEE Transactions on Antennas and Propagation, vol. 69, no. 12, pp. 8136-8142, Dec. 2021.

[25] Yacoub, A. and Aloi, D., “Low Profile PIFA Antenna for Vehicular 5G and DSRC Communication Systems,”SAE Technical Paper 2021-01-0150, 2021.

[26] Ahmad Yacoub, Mohamed Khalifa, and Daniel N. Aloi, "Compact 2 × 2 Automotive MIMO Antenna Systems for Sub-6 GHz 5G and V2X Communications," Progress In Electromagnetics Research B, Vol. 93, 23-46, 2021.

[27] Mohamed O. Khalifa, Ahmad M. Yacoub, and Daniel N. Aloi, “Compact 2x2 and 4x4 MIMO Antenna Systems for 5G Automotive Applications,” in The Applied Computational Electromagnetics Society (ACES), Vol. 36, 762-778, Number 6, 2021.

[28] Karthi, J. "A Novel UWB MIMO Antenna with High Isolation for Sub-6 GHz Band Application." Turkish Journal of Computer and Mathematics Education (TURCOMAT) Vol. 12.12 : 1934-1943, 2021.

[29] N. Supreeyatitikul, A. Phungasem and P. Aeimopas, "Design of Wideband Sub-6 GHz 5G MIMO Antenna with Isolation Enhancement Using an MTM-Inspired Resonators," 2021 Joint International Conference on Digital Arts, Media and Technology with ECTI Northern Section Conference on Electrical, Electronics, Computer and Telecommunication Engineering, pp. 206-209, 2021.

[30] Kwon, O., R. Song, and B. Kim, “A fully integrated shark-fin antenna for MIMO-LTE, GPS, WLAN, and WAVE applications," IEEE Antennas and Wireless Propagation Letters, Vol. 17, No. 4, 600-603, Apr. 2018.

[31] Franchina, V., et al., “A compact 3D antenna for automotive LTE MIMO applications," 2017 IEEE-APS Topical Conference on Antennas and Propagation in Wireless Communications (APWC), Verona, 326-329, 2017.

[32] C. Demien and R. Sarkis, "Design of Shark Fin Integrated Antenna Systems for Automotive Applications," 2019 PhotonIcs & Electromagnetics Research Symposium - Spring (PIERS-Spring), Rome, Italy, pp. 620-627, 2019.

[33] H S. Hastürkoğlu, M. Almarashli and S. Lindenmeier, "A Compact Wideband Terrestial MIMO-Antenna Set for 4G, 5G, WLAN and V2X and Evaluation of its LTE-Performance in an Urban Region," 2019 13th European Conference on Antennas and Propagation (EuCAP), Krakow, Poland, pp. 1-5, 2019.

[34] A. Heiman, A. Badescu and A. Saftoiu, "A new Multiple Input Multiple Output V2V automotive antenna for Long Term Evolution band applications," 2018 International Symposium on Fundamentals of Electrical Engineering (ISFEE), Bucharest, Romania, pp. 1-5, 2018.

[35] N. Guan, H. Tayama, M. Ueyama, Y. Yoshijima and H. Chiba, "A roof automobile module for LTE-MIMO antennas," 2015 IEEE-APS Topical Conference on Antennas and Propagation in Wireless Communications (APWC), Turin, pp. 387-391, 2015.

[36] D. Preradovic, D. N. Aloi, " Cross Polarized 2x2 LTE MIMO System for Automotive Shark Fin Application," The Applied Computational Electromagnetics Society (ACES), vol. 35, no. 10, pp. 1207-1216, October 2020.

[37] Y. Liu, Z. Ai, G. Liu and Y. Jia, "An Integrated Shark-Fin Antenna for MIMO-LTE, FM, and GPS Applications," in IEEE Antennas and Wireless Propagation Letters, vol. 18, no. 8, pp. 1666-1670, Aug. 2019.

[38] D. Potti et al., "A Novel Optically Transparent UWB Antenna for Automotive MIMO Communications," in IEEE Transactions on Antennas and Propagation, 2020.

[39] J. Malik, D. Nagpal and M. V. Kartikeyan, "MIMO antenna with omnidirectional pattern diversity," in Electronics Letters, vol. 52, no. 2, pp. 102-104, 21 1 2016.

[40] Y. A. S. Dama, R. A. Abd-Alhameed, S. M. R. Jones, D. Zhou, N. J. McEwan, M. B. Child, P. S. Excell, "An Envelope Correlation Formula for (N,N) MIMO Antenna Arrays Using Input Scattering Parameters, and Including Power Losses", International Journal of Antennas Propagation , vol. 2011, Article ID 421691, 7 pages, 2011.

[41] A. M. Elshirkasi, A. Abdullah Al-Hadi, M. F. Mansor, R. Khan, and P. J. Soh, "Envelope Correlation Coefficient of a Two-Port MIMO Terminal Antenna Under Uniform and Gaussian Angular Power Spectrum with User's Hand Effect," Progress In Electromagnetics Research C, Vol. 92, 123-136, 2019.

[42] Zhekov, S. S., A. Tatomirescu, E. Foroozanfard, and G. F. Pedersen, “Experimental investigation on the effect of user’s hand proximity on a compact ultrawideband MIMO antenna array,” IET Microwaves, Antennas Propag., Vol. 10, No. 13, 1402–1410, 2016.

[43] Sharawi, M., Hassan, A., & Khan, M. (2017). “Correlation coefficient calculations for MIMO antenna systems: A comparative study”. International Journal of Microwave and Wireless Technologies, 9(10), 1991-2004.

[44] Sainudeen Femina Beegum and Sanjeev Kumar Mishra, "Compact WLAN Band-Notched Printed Ultrawideband MIMO Antenna with Polarization Diversity," Progress In Electromagnetics Research C, Vol. 61, 149-159, 2016.

[45] Y. Gao, X. Chen, Z. Ying and C. Parini, "Design and Performance Investigation of a Dual-Element PIFA Array at 2.5 GHz for MIMO Terminal," in IEEE Transactions on Antennas and Propagation, vol. 55, no. 12, pp. 3433-3441, Dec. 2007.

[46] K. Sreelakshmi, Pronami Bora, Mona Mudaliar, Yuvraj Baburao Dhanade, B.T.P Madhav, “Linear array Yagi-Uda 5G antenna for vehicular application,” International Journal of Engineering & Technology, 7 (1.1), pp. 513-517, 2018.

[47] A. Thiel, L. Ekiz, O. Klemp and M. Schultz, "Automotive grade MIMO antenna setup and performance evaluation for LTE-communications," 2013 International Workshop on Antenna Technology (iWAT), Karlsruhe, pp. 171-174, 2013.

[48] H. J. Song et al., "Evaluation of vehicle-level MIMO antennas: Capacity, total embedded efficiency, and envelope correlation," 2014 IEEE-APS Topical Conference on Antennas and Propagation in Wireless Communications (APWC), Palm Beach, , pp. 89-92, 2014.

[49] O. Jonah, "5G Antenna for Automotive Applications," 2020 IEEE International Symposium on Antennas and Propagation and North American Radio Science Meeting, pp. 1493-1494, 2020.

[50] A.K. Saurabh and M.K.Meshram, ”Compact sub-6 GHz 5G-multiple-input-multiple-output antenna system with enhanced isolation,”Int J RW MicrowComput Aided Eng. vol.30, no. 8, e22246, Aug.2020.

[51] Yong Cheng , Jing Lu, and Can Wang, “Design of a Multiple Band Vehicle-Mounted Antenna,” International Journal of Antennas and Propagation, vol. 2019, Article ID 6098014, 11 pages, December 2019.

[52] Y. -. Zhang, X. Li, L. Yang and S. -. Gong, Dual-Band Circularly Polarized Annular-Ring Microstrip Antenna for GNSS Applications, in IEEE Antennas and Wireless Propagation Letters, vol. 12, pp. 615-618, 2013.

[53] S. Chae, B. Ahn, T. Yeo and J. Yu, An automotive stacked ceramic patch antenna with an integrated GNSS and SDARS antenna, 2017 International Symposium on Antennas and Propagation (ISAP), pp. 1-2, 2017.

[54] A. Yacoub and D. N. Aloi, "Low-Profile Automotive Antenna Systems for MIMO 5G and L1/L5 GNSS Communications," 2022 16th European Conference on Antennas and Propagation (EuCAP), 2022, pp. 1-4, doi: 10.23919/EuCAP53622.2022.9769623.

[55] A. M. Yacoub, M. O. Khalifa and D. N. Aloi, "Wide Band Raised Printed Monopole for Automotive 5G Wireless Communications," in IEEE Open Journal of Antennas and Propagation, vol. 3, pp. 502-510, 2022, doi: 10.1109/OJAP.2022.3170799.